UNIVERSITAT DE BARCELONA

Final Degree Project

Biomedical Engineernig Degree

Bioprinted gut-on-a-chip to mimic the intestinal mucosa

Barcelona, 14th of June 2021

Author: Adrià Díaz Ferrero

Director: Núria Torras

Co-Director: María García

Tutor: Elena Martínez

Acknowledgments

First of all, I would first like to express my deep and sincere gratitude to my director, Núria Torras as well as my co-Director, María García for their patience, motivation, enthusiasm, and immense knowledge and for providing guidance and feedback throughout this project. Without whom I would not have been able to complete this project. Further, I would like to thank my tutor, Elena Martínez, for giving me the opportunity to do this wonderful project in her group.

Secondly, I would like to say big thank you to all the Biomimetics systems for cell engineering group members for their energy and help throughout my project, especially to Oscar Castillo and Víctor Juarros who have supported me, for all the fun we have had in the last months and for their technical support during the project. It truly has been a very good time in this lab.

Many thanks to all of my friends and colleagues from university and outside for their time, advice, continuous encouragement and unfailing moral support. Thank you all for the strength you gave me.

Last but not the least, I cannot forget to thank my parents, brother and grandparents for all the unconditional support you have shown me in this very intense academic year and for their patience and encouragement during the last months. I simply could not have done this without you, special thanks.

Abstract

The search and development of technologies with the ability to replicate the complex characteristics of the human body has increased greatly in recent years. Organ-on-a-chip systems are clear examples, since they allow for the replication of a chosen organ including a representative population of cells and a controlled microenvironment with applied flow conditions, resulting in robust *in vitro* models that better recapitulate the *in vivo* tissue conditions, compared to standard 2D or 3D culture methods. The main aim of this final degree project is to develop a bioprinted gut-on-a-chip model to mimic the intestinal mucosa.

Firstly, the intestinal mucosa is composed of physical and immune elements and has protective functions. *In vitro* models that grown monolayers of epithelial cell lines provide a limited representation of the intestinal mucosa. The *in vitro* model reviewed will mimic the *in vivo* characteristics of the native tissue including its specific 3D topography, the main cellular components and flow conditions, allowing for a better understanding of its performance. In order to incorporate the intestinal mucosa in our model, a microenvironment must be created in which the cell can live and perform their functions. Hydrogel co-networks based on GelMA and PEGDA have been postulated as the best candidate. The incorporation of microstructured hydrogels, that mimic the three-dimensional structure of the intestine, and the cell environment on the present gut-on-a-chip model, better resemble the physiological conditions thus, having a strong impact on mucosal-related disease modelling and drug testing. The method used to carry out the structuring of the hydrogel has been bioprinting. Specifically, the most commonly used bioprinting methods for the generation of lab-on-chip systems have been analysed and compared, to evidence, the main advantages of the Digital light processing projector-based stereo-lithography printing method, reported in this project.

We have been able to optimize the geometry of the crypts, examine the swelling of the hydrogel and study the evolution of different microstructured hydrogels including the most representative stromal cell types embedded in the hydrogel. The main objective was to see if the cells were able to adapt to the three-dimensional topography of the hydrogel and, to determine, the compatibility of the printing method and of the gut-on-a-chip model. Finally, we found that the cells could grow and populate the microstructured hydrogel keeping high viability rates. Furthermore, it has been observed that the swelling of the hydrogel produces negative effects on the crypts, reducing considerable their size and causing them to have no physiological sense.

The first part of this thesis describes the state of the art of organ-on-a-chip technology, the main bioprinting techniques and gives a brief introduction to the intestinal mucosa main characteristics to help the reader to better understand the requirements of this project. Also, a concise analysis of the market for this technology, historical evolution and key players is presented. Straightaway, the Regulation and Legal Aspects behind the present application are discussed. The second part of the thesis gathers a comparison, highlighting the main advantages, limitations, and applications of each bioprinting technique; choosing the most appropriate one for this work. In addition, a complete description of the methodology and results obtained during the project are reviewed in this part. Finally, in the third part together with the Technical and Economic prefeasibility, the implementation schedule of the project, the conclusions and future improvements are also reviewed.

Keywords: *Organ-on-a-chip / Gut-on-a-chip / 3D Bioprinting / Microfluidics / Hydrogels / Photopolymerization*

"Our virtues and our
failures are inseparable,
like force and matter.
When they separate,
man is no more."

– Nikola Tesla

Table of Contents

ACKNOWLEDGMENTS II

ABSTRACT III

TABLE OF CONTENTS V

TABLE OF FIGURES VII

1. INTRODUCTION 1

1.1 STRUCTURE 2
1.2 AIM OF THE PROJECT 3
1.3 OBJECTIVES AND SCOPE OF THE PROJECT 3
1.4 METHODOLOGY 3

2. BACKGROUND OF THE PROJECT 5

2.1 STATE OF THE ART 5
2.2 THE INTESTINAL MUCOSA 8
2.3 HYDROGELS 9
2.4 3D BIOPRINTING TECHNIQUES 10

3. MARKET ANALYSIS 12

3.1 SECTORS LEADING THE MARKET 12
3.2 HISTORICAL EVOLUTION 12
3.3 FUTURE PERSPECTIVE 12
3.4 KEY PLAYERS 13

4. REGULATION AND LEGAL ASPECTS 15

4.1 REGULATORY CONTEXT 15
4.1.1 Standardization *16*
4.2 ETHICAL CONTEXT 16

5. CONCEPTION ENGINEERING 17

5.1 3D BIOPRINTING METHODOLOGY 17
5.1.1 Extrusion-Based Bioprinting *17*
5.1.2 Droplet-Based Bioprinting (Inkjet Printing) *18*
5.1.3 Photocuring-Based Bioprinting *19*
5.1.4 Method Selected *20*
5.2 MATERIALS AND METHODS 21
5.2.1 Preparation of the hydrogel pre-polymer solution *22*
5.2.2 Printing Methodology *22*
5.2.3 Microfluidic platform *22*
5.2.4 Volumetric Swelling *23*
5.2.5 Gut-on-a-chip assembly *23*

6. DETAILED ENGINEERING. RESULTS AND DISCUSSION 25

6.1 OPTIMIZATION OF THE STRUCTURAL PART OF THE CHIP 25
6.1.1 External casing *26*
6.1.2 PDMS layers *27*
6.2 BIOINK SELECTION 29

6.3 OPTIMIZATION OF THE CHANNEL DESIGN AND THE PRINTING PARAMETERS 30
6.3.1 Outer hydrogel dimensions *30*
6.3.2 Crypts geometry *32*
6.3.3 Hydrogel Characterization *34*
6.4 GUT-ON-A-CHIP MODEL 38

7. IMPLEMENTATION SCHEDULE 44

7.1 WORK-BREAKDOWN STRUCTURE (WBS) 44
7.1.1 WBS Dictionary *44*
7.2 TASK SEQUENCE MATRIX 45
7.2.1 PERT Diagram *46*
7.2.2 GANTT Diagram *47*

8. TECHNICAL PREVIABILITY 48

8.1 TECHNICAL CHALLENGES 48
8.1.1 Bioprinting *48*
8.1.2 PDMS *48*
8.2 SWOT ANALYSIS 49
8.2.1 Internal Analysis *49*
8.2.2 External Analysis *50*

9. ECONOMIC PREVIABILITY 51

10. CONCLUSIONS 54

10.1 FUTURE WORK 55

REFERENCES 56

11. ANNEXES 62

11.1 OPTIMIZATION OF THE RECTANGLE 62
11.2 HYDROGEL CHARACTERIZATION 63
11.3 ASSEMBLY OF THE MICROFLUIDIC CHIP 64

Table of Figures

FIGURE 2.1. EXAMPLE OF GUT-ON A CHIP MICROFLUIDIC PLATFORM CONTAINING INTESTINAL CRYPTS. ADAPTED FROM NIKOLAEV ET. AL. 2020. [25] 6
FIGURE 2.2. ILLUSTRATION OF THE CROSS-SECTION OF A MECHANICALLY ACTIVE HUMAN GUT-ON-A-CHIP WITH A CENTRAL CHAMBER AND TWO VACUUM CHAMBERS USED TO PERFORM MECHANICAL DEFORMATION. [2] 7
FIGURE 2.3. REPRESENTATION OF EPITHELIAL TISSUES, WITH THEIR NATIVE 3D ARCHITECTURE, CONVENTIONAL 2D CELL CULTURES AND NOVEL 3D APPROACHES OF CELL CULTURE. ADAPTED FROM TORRAS ET. AL. 2018. [44] 9
FIGURE 2.4. FOUR TYPICAL 3D PRINTING PROCESSES. FROM LEFT TO RIGHT: DIGITAL LIGHT PROCESSING (DLP), FUSED DEPOSITION MODELLING (FDM), INKJET PRINTING (IP) AND SELECTIVE LASER SINTERING (SLS). [6] 11
FIGURE 3.1. RISE IN ACADEMIC PUBLISHING IN OOC ON GOOGLE SCHOLAR. REPRESENTATION OF THE NUMBER OF PUBLICATIONS PER YEAR, WHERE THE TOPIC OF THE ARTICLE WAS DIRECTLY RELATED WITH THE KEY WORDS "MICROFLUIDICS" AND "ORGAN-ON-A-CHIP" FROM 2000 TO 2015. [51] 12
FIGURE 3.2. SOME OF THE PROMINENT KEY PLAYERS IN THE ORGAN-ON-A-CHIP AND BODY-ON-A-CHIP MARKET [51]. 14
FIGURE 5.1. ILLUSTRATION OF EXTRUSION-BASED BIOPRINTING. A) PNEUMATIC-DRIVEN BIOPRINTING. B) PISTON-DRIVEN BIOPRINTING. C) SCREW-DRIVEN BIOPRINTING. ADAPTED FROM ZEMING ET. AL. (2019). [6] 18
FIGURE 5.2. TWO EXAMPLES OF DROPLET-BASE BIOPRINTING. A) INKJET BIOPRINTING METHOD. B) LASER-ASSISTED METHOD. LOAI ET. AL. (2019). [65] 19
FIGURE 5.3. SIMPLIFIED SCHEMATIC DRAWING OF THE SLA AND DLP PRINCIPLES. A) SCHEMATIC DRAWING OF THE SLA BIOPRINTING SET-UP AND THE SCANNING SYSTEM. B) SCHEMATIC DRAWING OF THE DLP BIOPRINTING SET-UP, THE DIGITAL MICROMIRROR DEVICE AND THE LASER. ADAPTED FROM LONG NG, ET. AL. (2020). [8] 20
FIGURE 5.4. FROM LEFT TO RIGHT: COMMERCIAL SOLUS 3D PRINTER AND A VIVITEK PROJECTOR AND ILLUSTRATION OF A VISIBLE-LIGHT-BASED STEREOLITHOGRAPHY 3D BIOPRINTING SYSTEM [69]. 21
FIGURE 5.5. MODIFIED SOLUS 3D PRINTER USED TO PERFORM THE PRINTINGS. 22
FIGURE 5.6. FROM LEFT TO RIGHT: ILLUSTRATION OF THE RELEVANT PARAMETERS USED TO QUANTIFY THE SIZE OF THE CRYPTS AND ONE EXAMPLE OF THE METHOD. 23
FIGURE 5.7. GUT-ON-A-CHIP ASSEMBLY. THIS SCHEMATIC ILLUSTRATES THE STEPS DESCRIBED IN OUR METHODOLOGY. 24
FIGURE 6.1. LAYERS OF THE GUT-ON-CHIP FOR TWO-CHANNEL. 25
FIGURE 6.2. IMAGE OF THE TWO SECTIONS OF THE CASING. FROM RIGHT TO LEFT: BOTTOM PART AND COVER OF THE CASING. 26
FIGURE 6.3. FROM LEFT TO RIGHT: ILLUSTRATION OF THE INITIAL LID AND THE IMPROVEMENT MADE. 26
FIGURE 6.4. SCHEMATIC AND IMAGE OF THE FINAL LID IMPLEMENTED ON THE GUT-ON-CHIP. 27
FIGURE 6.5. A) IMAGE OF ONE PDMS BOTTOM LAYER. B) ILLUSTRATION OF THE PDMS LAYER FROM A SIDE VIEW. 27
FIGURE 6.6. IMAGE OF ONE PDMS TOP LAYER. 28
FIGURE 6.7. IMAGE OF THE DIFFERENT MOULDS USED DURING THE PROJECT. A) MOULD MADE WITH THE PHROZEN PRINTER. B) REPLICA OBTAINED WITH THE PHROZEN MOULDS. C) MOULD MADE WITH THE SOLUS PRINTER. 28
FIGURE 6.8. REPRESENTATION OF THE PDMS TOP AND THE MOULD USED. A) CHIP WITH ONE CHANNEL. B) CHIP WITH TWO CHANNELS. 29
FIGURE 6.9. SCHEMATICS OF THE GUT-ON-A-CHIP FOR THE HYDROGEL INCLUDING CRYPTS AND THE CHANNEL COMPRISED BETWEEN THE PRINTED HYDROGEL AND THE PDMS BOUNDARIES. 30

FIGURE 6.10. EVOLUTION OF THE THREE PARAMETERS STUDIED IN THIS EXPERIMENT AND THE CORRESPONDING ERROR FOR EACH MEASUREMENT. A) EVOLUTION OF THE THICKNESS FOR THE 3 SAMPLES, THE X-AXIS CORRESPONDS TO THE TIME IN MINUTES AND THE Y-AXIS TO THE THICKNESS IN MICROMETRES. B) EVOLUTION OF THE WIDTH FOR THE 3 SAMPLES, THE X-AXIS CORRESPONDS TO THE TIME IN MINUTES AND THE Y-AXIS TO THE WIDTH IN MICROMETRES. C) EVOLUTION OF THE LENGTH FOR THE 3 SAMPLES, THE X-AXIS CORRESPONDS TO THE TIME IN MINUTES AND THE Y-AXIS TO THE LENGTH IN MICROMETRES. D) EXAMPLE OF A RECTANGLE HYDROGEL PRINTED. 31
FIGURE 6.11. DIFFERENT VIEWS OF ONE OF THE 3D CAD DESIGNS USED FOR PRINTING THE HYDROGEL WITH CRYPTS: PERSPECTIVE (A), TOP VIEW (B) AND FRONT VIEW (C). 32
FIGURE 6.12. PARAMETERS A, B AND C MODIFIED IN THE OPTIMIZATION PROCESS. 33
FIGURE 6.13. PRINTING RESULTS FOR CRYPTS USING B = 150 MM. A) SKETCH OF THE 3D CAD MODEL. THE HIGHLIGHTED AREA CORRESPONDS TO THE REGIONS SHOWN IN IMAGES B AND C. B) CRYPTS IMMEDIATELY AFTER PRINTING WITH THE CRYPTS HIGHLIGHTED. C) CRYPTS AFTER PLACING A GLASS COVERSLIP ON TOP, MIMICKING THE CHIP ASSEMBLY. 34
FIGURE 6.14. PRINTING RESULTS FOR CRYPTS USING B = 200 MM. A) SKETCH OF THE 3D CAD MODEL. THE HIGHLIGHTED AREA CORRESPONDS TO THE REGIONS SHOWN IN IMAGES B AND C. B) CRYPTS IMMEDIATELY AFTER PRINTING. C) CRYPTS AFTER PLACING A GLASS COVERSLIP ON TOP, MIMICKING THE CHIP ASSEMBLY. 34
FIGURE 6.15. ILLUSTRATION OF THE TWO-CHANNEL CHIP DESIGN WITH THE HYDROGEL AFTER THE ASSEMBLY. 35
FIGURE 6.16. CHANGE IN LENGTH AND THICKNESS AFTER 96 HOURS OF SWELLING. 36
FIGURE 6.17. SCHEMATIC OF THE RELEVANT PARAMETERS USED TO QUANTIFY THE SIZE OF THE CRYPTS..... 36
FIGURE 6.18. CHANGE IN CRYPTS SIZE FOR THE TWO SAMPLES. 37
FIGURE 6.19. IMAGE OF THE HYDROGEL SAMPLES ONCE REMOVED FROM THE MICROFLUIDIC CHIP AFTER 96 HOURS. A) SAMPLE 1. B) SAMPLE 2. 38
FIGURE 6.20. A) ILLUSTRATION OF PDMS FOR 1-CHANNEL LAYOUT. B) ILLUSTRATION OF PDMS FOR 2-CHANNEL LAYOUT. C) SIDE VIEW OF THE CHIP IN WHICH WE CAN SEE THE CHANNEL FORMED BETWEEN BOTH PDMS LAYERS AND THE HYDROGEL. 39
FIGURE 6.21. A) CHIP PLACED INSIDE THE INCUBATOR. B) INFUSION PUMP OUTSIDE THE INCUBATOR TO INJECT DIRECT CURRENT FLOW. 39
FIGURE 6.22. DIMENSIONS OF THE FOUR SAMPLES AT INITIAL TIME FOR THE PARAMETERS A, A, B AND C. 40
FIGURE 6.23. DESIGN OF ONE CHANNEL CHIP AND THE CRYPTS AT DIFFERENT TIMEPOINTS (SAMPLE 2). A) CRYPTS AT THE INITIAL TIME, 0 HOURS AFTER THE BIOPRINTING. B) CRYPTS AFTER 72 HOURS AT THE INCUBATOR. IMAGES TAKEN WITH THE MICROSCOPY; WE CAN VISUALIZE EMBEDDED CELLS. C) CRYPTS AFTER 120 HOURS AT THE INCUBATOR. IMAGES TAKEN WITH THE MICROSCOPY; WE CAN VISUALIZE EMBEDDED CELLS. 41
FIGURE 6.24. MICROFLUIDIC CHIP WITH A HYDROGEL AFTER 120 HOURS. 42
FIGURE 6.25. DESIGN OF TWO-CHANNEL CHIP AND THE CRYPTS AT DIFFERENT TIMEPOINTS FOR SAMPLE 3 (A AND B) AND SAMPLE 4 (C AND D). A) CRYPTS AT THE INITIAL TIME, 0 HOURS AFTER THE BIOPRINTING (SAMPLE 3). B) CRYPTS AFTER 2 HOURS AT THE INCUBATOR. IMAGES TAKEN WITH THE MICROSCOPY; WE CAN VISUALIZE EMBEDDED CELLS (SAMPLE 3). C) CRYPTS AT THE INITIAL TIME, 0 HOURS AFTER THE BIOPRINTING (SAMPLE 4). D) CRYPTS AFTER 2 HOURS AT THE INCUBATOR. IMAGES TAKEN WITH THE MICROSCOPY; WE CAN VISUALIZE EMBEDDED CELLS (SAMPLE 4). 42
FIGURE 7.1. WORK-BREAKDOWN STRUCTURE OF OUR PROJECT. 44
FIGURE 7.2. PERT DIAGRAM ASSOCIATED WITH THE SEQUENCE MATRIX, WITH THE "EARLY" AND "LAST" TIMES INDICATED IN EACH NODE AND THE CRITICAL PATH MARKED IN RED. 46
FIGURE 7.3. GANTT DIAGRAM OF OUR PROJECT. 47
FIGURE 8.1. SCHEMATIC ADAPTED FROM VILA ET. AL. 2020, OF THE GELMA AND GELMA-PEGDA PHOTO-POLYMERIZATION REACTION AND CO-NETWORKS FORMED. [3] 48

1. INTRODUCTION

Over the last few decades, attention has increasingly focused on assay platforms involving human cells to study tissue development and regeneration, developing systems for disease modelling or for therapeutic screening. Current efforts in drug development, toxicology or tissue development are often challenging by a lack of predictive models to reliably assess the physiological reaction of the human body to certain drugs or toxins [1]. In this sense, research has been performed in the field of microfluidics, predominantly in biosciences, pursuing the miniaturization and automation of diagnostic tests, laboratory experiments, and (bio)chemical processes. These platforms, known as lab-on-a-chip devices, are microfluidic cell culture systems that combine biofabrication, miniaturization and tissue-engineering components to recapitulate tissue-like characteristics such as 3D structure, physiology, pathology, and function of organs in vitro [2,3].

Rather than pipetting discrete quantities of liquids from one container to another, currently, the liquid in a microfluidic system flows via the miniatured channels of a manifold, thus reducing the sample volumes for testing. Other advantages of this "on-chip" technology over conventional culture systems rely on the multiplexing screening capability providing information in a fast and easy manner, and the possibility of reusing the devices [2].

The liquid in these channels is normally moved by external pumps or pressure sources to which the fluidic chip is linked. In certain cases, to manage the applied pressures or balance the flow produced by the pump, the rate of flow is measured using different sensors. Reducing the size of the channels down to the micrometre range and liquid volumes to the range of microliters or even nanolitre, enable faster reactions [4]. Additionally, the smaller size of the complete system also means more feasible devices and lower costs of production.

Bioprinting is considered one of the most advanced technology for producing biomimetic cellular constructs assembling scaffolds for growing tissues. These constructs can be used as *in vitro* models for many applications and combined with *microfluidics* enable the creation of **Organ-on-a-chip** (OoC) devices simulating *in vivo* 3D microenvironmental constructions and colon architecture [5–7]. One of the most interesting examples is the human gut-on-a-chip technology to study disease development and progression with more accurate models, increase the efficacy of drug screening and development to overcome the main inconvenience of the conventional models that often rely on simple 2D culture systems. 3D bioprinting technology combined with microfluidics has gained interest in the last decade due to is high versatility and its highly automated fabrication system [8]. The aim of this technique is to fabricate 3D organized heterogeneous structures since this technology enables the precise patterning of a wide range of biomaterials with embedded living cells at pre-defined positions allowing for the development of on-chip models with high *printing resolution and uniformity*, *fast fabrication*, and *high reproducibility*, owing to the accurate control of the spatial distribution of biomaterials and cells during the printing process [8,9].

Concerning quality, resolution and generation of precise complex tissue structures, biofabrication technologies that use light for the polymerization of biomaterials have made relevant advances in recent years [10]. The development of new photocurable resins with bioactive properties and the improvement of biocompatible and biodegradable photoinitiators have led to the growth of these technologies [10]. Digital light processing (DLP)-SLA projector-based stereo-lithography printing method is a high-resolution technology based on a controlled light projection through a transparent

window over a cuvette filled with photocross-linkable bioink creating three-dimensional structures [10,11]. The stereolithography system works with a light-emitting device (DLP projector) that polymerizes a GelMA – PEGDA hydrogel containing cells combined with LAP (photoiniator) and tartrazine [3,12]. Photocross-linkable hydrogel exhibits bioactive properties including high biocompatibility and enhanced mechanical properties compared with pure GelMA hydrogels [13]. Gelatin-based hydrogels mimic the extracellular matrix and are widely used to make multicellular models due to their advantages, which allow us to make customized bioink according to the needs of our system [13].

The intestinal mucosal barrier is an example of one of the most studied tissue models from the human body. Divided into three distinct layers and located in our intestines, it plays a significant role to effectively absorb nutrients and drugs, and furthermore in the regulation of the immune response against microbes and pathogens, maintaining the intestinal homeostasis [2,14,15]. Thus, intestinal mucosal models can be used to better understand the mechanisms involved in the barrier function and to study its drug permeability in the early stages of drug discovery [3]. The intestinal epithelium is lined with a single layer of polarized cells that presents characteristic three-dimensional spatial features. Current *in vitro* models are 2D-based and therefore fail to capture the 3D microenvironment present on the intestinal mucosa, which has been shown to have a direct impact on the function of the intestinal barrier [16,17]. This lack of tridimensionality has been contemplated as the main reason for a poor correlation between *in vitro* and *in vivo* models [16]. In this sense, there are different groups that are working on the development of new models that include this three-dimensional topography [16,17].

The present project will combine concepts of tissue engineering, microfluidics, and diagnosis to validate a complex *in vitro* model of intestinal epithelium using a gut-on-a-chip. The aim is to create a model of the intestinal mucosa, specifically creating gelatin-based hydrogels models of the **colon** that includes the characteristic 3D topography of this tissue and that contains the principal cell types. The objective is to be able to integrate the model within a PDMS chip to study the viability and evolution of the model.

1.1 Structure

Chapter 1 presents the aim of the project, the main objectives, and the scope. The background as well as the state of the art and a brief introduction about 3D bioprinting and the intestinal mucosa can be found in chapter 2, whereas Chapter 3 is dedicated to the market analysis of the organ-on-a-chip devices. The regulatory context with the Legal Aspects is summarized in Chapter 4. Chapter 5 discuss the cell culture models and their 2D and 3D variants as well as the most used bioprinting techniques. In this section, the materials and methods used in this project are also described. A detailed review of the results obtained and its discussion are presented in chapter 6. The temporal implementation of the project with the different organizing diagrams can be found in chapter 7. In chapters 8 and 9, the technical, and economic previability of the project is discussed. Finally, the conclusions and future perspectives of the project are discussed in chapter 10. An annex with complementary information is also included.

1.2 Aim of the Project

The aim of this project is to optimize the fabrication of a hydrogel-based gut-on-chip model using an innovative 3D bioprinting technique. The system will combine a microstructured hydrogel together with an external casing containing the microfluidic connections, the fastener elements, and a transparent window. The microstructured hydrogel will be mimicking the intestinal stromal tissue present in the large intestine, taking into account both, its characteristic invaginations and its cellular compartment, including the most representative stromal cell types and the epithelial barrier surrounding a lumen-like central channel. This model will be used to better understand the mechanisms involved in the intestinal barrier function and its role regulating barrier dysfunction.

The development of this project will take place at the Institute of Bioengineering of Catalonia (*IBEC*) in the *Biomimetic systems for cell engineering* group. The project will include (i) the design of the chip and its casing, (ii) the fabrication of the microstructured hydrogel using 3D bioprinting which will contain some representative cells of the intestinal mucosa, (iii) the hydrogel assembly onto the microfluidic chip, and finally, (iv) the characterization of the whole system, evaluating its functionality as *in vitro* model.

1.3 Objectives and Scope of the Project

The project has been developed during the period between February and June 2021. The study covers the design, fabrication and optimization of a gut-on-a-chip device mimicking the large intestinal mucosa.

The objectives to be achieved in this project are the following:

(i) Design of the chip structure, both the outer part and the microstructured hydrogel.
(ii) Design the PDMS layers moulds that will contain the hydrogel. Find the accurate temperature and time to solidify the layers.
(iii) Optimization of the printing parameters to achieve proper 3D microfeatures in the hydrogels resembling the CAD model designed.
(iv) Design and testing of the external part of the microfluidic chip to allocate the 3D printed hydrogel. This casing will contain the microfluidic connections and should guarantee proper sealing of the hydrogel cavity.
(v) Optimize the fluidic conditions to guarantee proper microenvironmental conditions inside the chip, allowing cell media exchange.

1.4 Methodology

This section provides an outline of the research methodology used to develop the gut-on-a-chip device. This project has been carried out mostly by doing experimental research. In addition, a search has been done in scientific publications to find out the state of the art of bioprinting and OoC technology to determine how the current models could be improved. In the same way, information and data necessary for the development of the project have been obtained from previous work performed in the group.

The experiments consisted of developing the structural part of the chip. The chip consists of an external structural part that includes the casing, PDMS layers and cellular scaffold. First, the chip casing was designed and printed, which contained the PDMS layers. Secondly, the PDMS moulds

were designed and fabricated, their function was to house the hydrogel and form the microfluidic channel. Consequently, both the printing parameters to print the hydrogel and the three-dimensional design of the structures contained in the hydrogel were optimized. Finally, the three parts were combined to create the gut-on-a-chip and improvements corresponding to the initial design were also implemented.

2. BACKGROUND OF THE PROJECT

2.1 State of the Art

The main conceptual problem of the current cell-based assays is that they rely on two-dimensional monolayer cellular cultures. The lack of tridimensionality (3D) implies that the results obtained with these tests do not represent what is happening in the organs (3D complex structures). Moreover, the development of microarchitectures resembling the human physiology is necessary to study, in a more reliable manner, the processes taking place in native tissues and organs [18]. In addition, the standard assays to replicate organs and tissues require a considerable volume of cells, reagents, nutrients, etc. The complexity of the standard cell-based assays is not enough to recreate the real intricacy of the living systems, so most of the current examples in literature lack of proper 3D cell microenvironment [2,19,20]. The integration of cell culture models on microfluidic platforms, often known as Organ-on-a-chip (OoC) devices, offers new capabilities for analysing individual contributions of either cellular, physical or chemical parameters, allowing for the development of human-relevant disease models [2]. The success of the chip depends on how close their architectures are to the anatomical features [21]. The creation of OoC is useful in personalized drug screening and pathological studies since it is a platform that recapitulates the physiology of the patient much closer than other conventional methods [22]. OoC technology aims to replicate the structural, microenvironmental and physiological functions of the human organs building a specific human model and mimicking their mechanical and physiological cellular responses [7].

The applications of the OoC technology are wide and varied, depending on the tissue or organ to study. In the case of gut-on-a-chip systems, the main interest is focused on drug screening for pharma applications, creating relevant disease models [23]. In this way, *Nikolaev et. al. 2020* developed a biomimetic hydrogel scaffold recapitulating the relevant 3D geometry present in the small intestinal tissue (*Figure 2.1*) [24]. The platform consists of a hydrogel chamber flanked by two reservoirs and two external tubing to allow fluid irrigation and continuous perfusion. Through the seeding of cells to coat the surface of the hydrogel and continuous irrigation, they were able to prolong the survival of the artificial intestines up to 30 days. Additionally, they were able to study various phenomena and demonstrate that the chips shared many characteristics with real tissue, even seeing that there was a production of mucus [25]. Finally, the organoids were infected with a protozoan to study how infected cells active the inflammatory defence response against this pathogen, validating their use as a model for the development of effective therapies [25].

Even though the use of *Bioprinting* to build scaffolds for growing tissues is recent, the last articles about this topic show that this technology is the most advanced technology for producing biomimetic cellular constructs [5]. Recent advancements in bioprinting techniques promoted the creation of novel OoC systems. The main advantage of 3D bioprinting in front of the conventional soft lithography techniques used for the fabrication of microfluidics is its *versatility*, allowing for combining multiple materials, biomolecules and cell types simultaneously, reaching prints in a *faster* and *highly reproducible* manner [26,27].

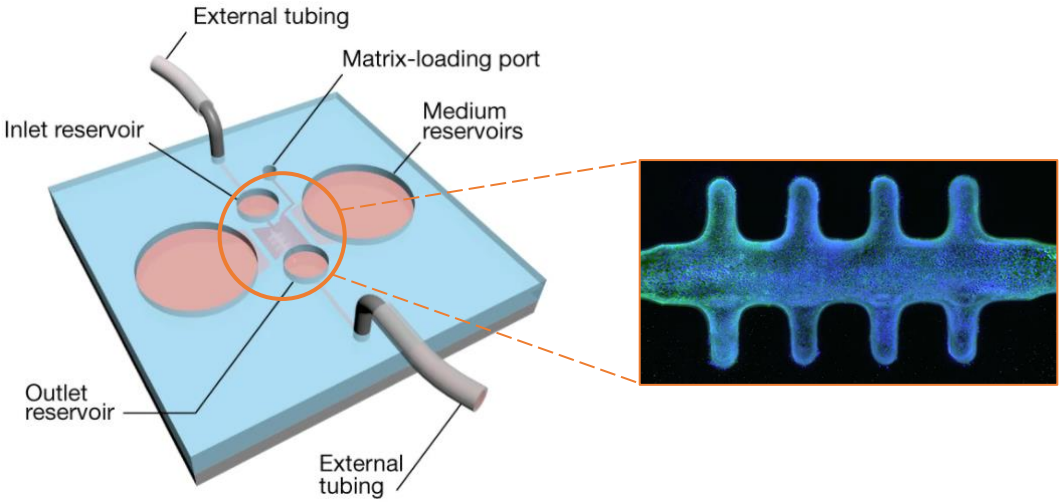

***Figure 2.1**. Example of gut-on a chip microfluidic platform containing intestinal crypts. Adapted from Nikolaev et. al. 2020.* [25]

Culturing human cells on chips enables studies of pharmacokinetics in specific individuals, facilitating personalized medicine. Different possibilities for OoC technology can be implemented for different applications such as models for disease and cancer, studies of specific biological mechanisms, drug discovery and toxicity tests, and regenerative medicine [28]. Considering the conventional solutions in which the tests were mostly performed on animals, it raises a big controversy on the ethical front in addition to providing results that cannot always be applied to humans [29]. Despite some characteristics of the human gut are remarkably different from that in mice, such as the gut microbiome where the *85% that colonizes in humans* does not exist in mice, animals models are used for testing before performing clinical trials with human beings, which usually fail to predict efficacy and safety of novel drugs [2,30].

Modelling physiological and pathophysiological processes in the intestinal tract outside the human body is a huge challenge. Despite several published works in the field, most researchers and clinicians base their studies on simplistic 2D cell culture models where only static conditions can be applied [31]. Systems based on bioreactors and microfluidic devices have been developed as alternative culture methods to better mimic the cellular microenvironment, allowing for the application of dynamic flow conditions inducing gradients of shear stress on the cells in the luminal cavity as occurs *in vivo*.

Great progress has been made in advancing *in vitro* models through 3D and microfluidic models. Gijzen et. al. 2020 introduced a microfluidic platform applicable for studying inflammatory processes called **OrganoPlate** [32]. The developed chip comprises three adjacent culture channels and its corresponding inlet and outlet. The chip consists of two medium perfusion channels and one gel channel separated by capillary pressure barriers called *phaseguides*. The three channels join in the centre of the chip, where they are separated by two phaseguides. The central channel serves as an observation window to monitor cells, readout, and see their progression. Firstly, a collagen-I extracellular matrix (ECM) is patterned into the middle channel of the chip. After this, the epithelial cells are seeded on the top perfusion channel, facilitating the cells to settle against the ECM. After some days, differentiated cells are added to the bottom channel. In addition, in order to better recapitulate intestinal physiology and increase the complexity of the model, various cell types were added [32].

On the other hand, Shim et. al. 2017, reported *in vitro* gut model incorporating a collagen scaffold that mimics the human intestinal villi [33]. The topography of the intestine was modelled by combining different fabrication techniques, using positive moulds of PDMS the hydrogel scaffold was developed. Cells were seeded on the top of the collagen scaffold, where they formed a uniform monolayer across the collagen villi surface. This structure was integrated into a microfluidic system that consists of three layers of PDMS, a glass and a polyester membrane. The basolateral reservoir was connected below the scaffold and the apical one above [33,34].

Last of all, one of the most recent examples of these complex systems is the gut-on-a-chip model developed by Donald Ingber and co-workers [2]. They present a microfluidic chip with two microchannels separated by a porous and flexible membrane, where they seed human intestinal cells on top of 3D structures that mimic intestinal villi and crypts (*Figure 2.2*) to study features of the barrier and transport functions [20,35]. Moreover, they include an endothelial barrier on the lower surface of the same membrane mimicking vasculature to study the tissue-tissue interface [2]. These characteristics offer relative advantages to use these models to simulate the barrier between the intestinal lumen and vasculature. Some devices more sophisticated integrate multiple chambers with different types of cells. The *Wyss Institute* at Harvard University recently designs a mechanically active gut-on-a-chip based on the models previously reviewed, where two chambers on both sides of the principal channel replicate the *peristalsis* using vacuum. According to the results obtained, the use of microfluidics and replication of the peristaltic movement allows the development of more complex disease models, drug development and personalized medicine [2,36]. Specifically, cells in this OoC interact with the membrane while experiencing peristalsis-like deformation *in vitro* similar to those experienced by the intestinal tissues.

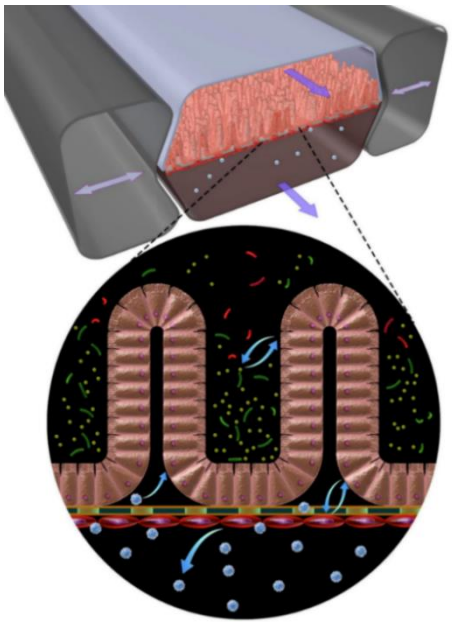

Figure 2.2. *Illustration of the cross-section of a mechanically active human gut-on-a-chip with a central chamber and two vacuum chambers used to perform mechanical deformation.* [2]

Different studies suggest that current *in vitro* intestinal models lack physiological relevance features that might play a critical role in some disorders [2,33]. The models previously reviewed present various approaches to mimic the three-dimensional structure of the intestine and to create human-relevant disease models [2]. However, in all these models the **intestinal mucosa** is not present.

This structure and composition constitutes a *critical immunological barrier* and is responsible for regulating inflammatory processes, preventing the passage of undesirable luminal content while preserving the ability to absorb nutrients [37,38].

2.2 The Intestinal Mucosa

The intestinal epithelium is part of the intestinal mucosal barrier which is composed of physical, biochemical and immune elements and has protective functions separating the digestive environment and the body [2]. In addition, this barrier is actively involved in processes of drug absorption and metabolization [14]. The dysfunction of the intestinal mucosal barrier is involved in numerous health problems and diseases, such as intestinal bowel diseases (IBDs) and Chron's, resulting in variations in its permeability that can alter the pass of microbes, microbial products, or foreign antigens into the body [14].

The intestine is a highly complex organ not only for its structure which is not easy to replicate using the traditional methods. This was first studied by March's group [39] who construct a 3D hydrogel structure on-chip and saw that this structure was closer to the intestine in shape and distribution density than the conventional methods used to mimic the intestine [23]. For these reasons, the development of alternate intestinal *in vitro* models is crucial for the gastroenterology field of research [40].

The complete simulation of the microenvironment mimicking the intestinal mucosa requires 3D models capable to reproduce the intestinal mucosa tissues. These systems provide a 3D architecture for cell growth and interactions cell-cell and cell-ECM making them better to mimic *in vitro* intestine microenvironment [15]. Few studies focus on the necessity or creation of 3D models for improving the actual models of drug absorption reconstructing the intestinal mucosa tissue through 3D models.

The objective of bioprinting is to develop OoC that should reflect different functionalities and structures of the human organs on microfluidic chips. This is widely used to validate the therapeutic efficacy of drugs, the study of disease mechanisms, regenerative medicine, etc. [41] Over the past five years, the complexity of the engineered intestine is increasing, which favours a better development OoC models and therefore more complex disease models, improved results in drug development and facilitates personalized medicine [2].

In vitro models that grown monolayers of epithelial cell lines provide a limited representation of the intestinal mucosa, only doing a simplistic representation of the epithelial component [3]. However, Bosman et. al. 1993 demonstrate that interactions between the epithelium and the stroma are important to maintain the integrity of the intestinal mucosa [3,42]. Therefore, according to Vila et. al. 2020, to reduce the difference between *in vitro* epithelial cell-based models and *in vivo* experiments is necessary the development of more physiologically relevant 3D intestinal mucosa-like models *in vitro* models able to represent the epithelial and stromal compartments [3,15,43].

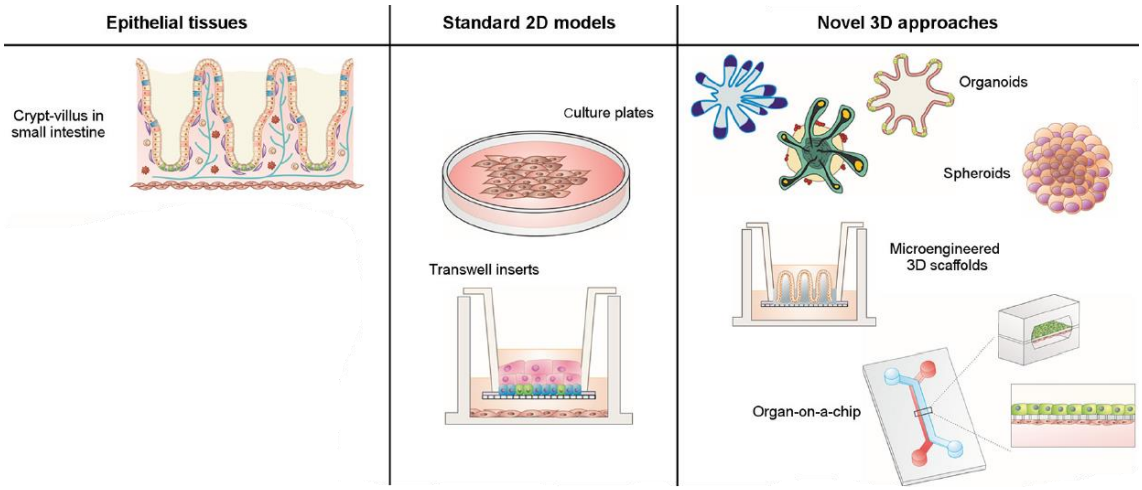

Figure 2.3. *Representation of epithelial tissues, with their native 3D architecture, conventional 2D cell cultures and novel 3D approaches of cell culture. Adapted from Torras et. al. 2018.* [44]

In conclusion, given the importance of the mucosa in regulating the functioning of the intestine, it is necessary to incorporate it into these gut-on-a-chip systems. However, in order to incorporate these structures, a microenvironment should be created in which cells can live and perform their functions. For this reason, with the aim of developing these functions, a biocompatible and biodegradable material that can be remodelled by cells should be created. In this sense, **hydrogels** have been postulated as potential candidates.

2.3 Hydrogels

To build the 3D scaffolds we have chosen **hydrogels**, polymeric materials with a high water content. Both of natural or synthetic origin, hydrogels can mimic a large variety of tissues due to their excellent characteristics, as high biocompatibility and tuneable physicochemical properties; which are strongly dependent on their composition and fabrication technologies [45]. Alginate, gelatine, agarose, chitosan, collagen, hyaluronic acid, poly (vinyl alcohol) and poly (ethylene glycol) are some examples of the most widely used materials to form hydrogels for tissue engineering scaffolds.

During the last five years, the *biomimetic systems for cell engineering* group at IBEC has developed hydrogel co-networks based on gelatin methacryloil (GelMA) and poly(ethylene glycol) diacrylate (PEGDA) that photopolymerize in the presence of either UV or visible light, with the main objective of creating 3D functional *in vitro* models of the intestinal mucosa [3], approaching the *in vivo* tissue composition and architecture. The resulting GelMA-PEGDA hydrogel co-network provides the required features of both the epithelial and stromal compartments [3]. On one hand, **GelMA** is a natural polymer that resembles some essential properties of the native ECM, providing biodegradation and cell adhesion sequences. Its composition is mechanically and biochemically tuneable according to the required properties, but lacks long-term mechanical stability. On the other hand, **PEGDA** is a synthetic (non-biodegradable) and highly stable polymer that does not present cell adhesion motifs; but it has good mechanical properties [17,45–47]. PEGDA is acquired by the derivation of PEG, a hydrophilic and biocompatible polymer that is a non-cell adhesive. Substituting terminal hydroxyl groups of PEG with acrylates PEGDA can be fabricated [46]. To perform this work, a hydrogel composed by GelMA-PEGDA co-network has been used. However, its composition has been tuned to adapt the mixture to the bioprinting process.

The main requirements the hydrogel used in this project should fulfil are: (i) to be consistent enough to sustain the culture on top forming a mature epithelial monolayer, but at the same time (ii) be porous and soft enough allowing the cells embedded in (the ones mimicking the stromal compartment) a proper growth rate and functioning [3,16,48].

GelMA-PEGDA hydrogel co-network should be crosslinked chemically forming covalent bonds resulting in a permanent, stable, and strong hydrogel network [3,15,49]. In our case, a photocrosslinkable hydrogel was developed in which biocompatible photosensitive compounds were added to the polymer mixture. The photoinitiator used was Lithium phenyl-2,4,6-trimethylbenzoylphosphinate (**LAP**) which in presence of visible a light source induces the photo-crosslinking of the hydrogel. The hydrogel co-network should be consistent enough to sustain the culture on top forming a mature epithelial monolayer, but porous and soft enough to allow the cells embedded in (stromal compartment) a proper growth rate and functioning [3,16,48].

Finally, it is necessary to structure the hydrogels to give them the 3D geometry that characterizes the intestine. For this, it is necessary to polymerize the hydrogel using 3D bioprinting techniques with the aim of polymerizing the hydrogel with a specific microstructure.

2.4 3D Bioprinting Techniques

3D bioprinting techniques offer the possibility to reproduce complex three-dimensional structures in a controlled and reproducible manner, due to its high versatility [5,7]. Moreover, aspects such as the porosity of the printed material and the interconnectivity of the printed network, which are difficult parameters to control using conventional fabrication methods, can be controlled and tunned in demand. Based on automated dispensing systems, these group of techniques allows via the controlled precipitation of biomaterials and cells to assemble *tissue scaffolds*, orchestrating a fully integrated and functional biological microenvironment [7]. However, before starting with the printing it is very important to investigate certain aspects that will influence the printing results, such as the *printing parameters*, the *composition of the bioink to be used (including or not cells)*, and the *main properties of the resulting scaffolds*, to choose the most suitable printing technique for the chosen application.

Basically, there are four main 3D bioprinting techniques (*Figure 2.4*): [6]

a) *Digital light processing* (DLP), based on planar pattern projection. A more detailed study of this technique is done in sections 5.1.3 and 5.1.4.
b) *Fused deposition modelling* (FDM), based on the local and continuous deposition of a material on a filament. This technique is reviewed in section 5.1.1.
c) *Inkjet printing* (IP) based on the controlled deposition of material using microspheres. More information of this technique can be found in section 5.1.2.
d) *Selective laser sintering* (SLS), based on the local and in-situ sintering of different material powders.

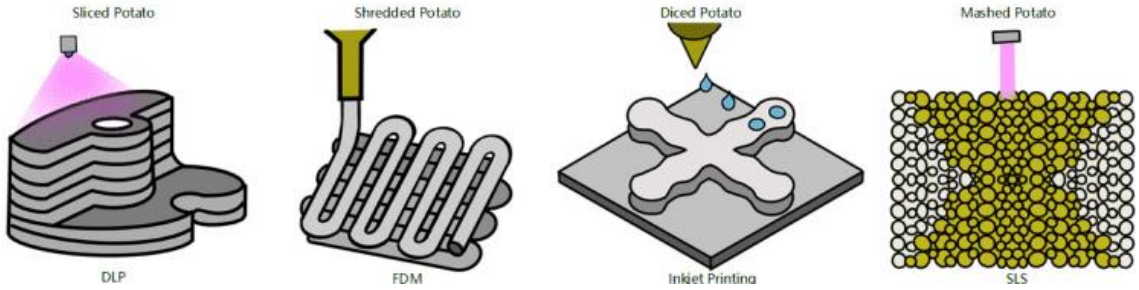

Figure 2.4. *Four typical 3D printing processes. From left to right: Digital Light Processing (DLP), Fused deposition modelling (FDM), Inkjet printing (IP) and Selective laser sintering (SLS).* [6]

All the above-mentioned bioprinting processes involve the same preparation steps, which should be performed following the order described below: [6]

1. *Data acquisition*: The data used to build the model can be obtained using different imaging techniques such as X-ray, microscopy and computed tomography (CT), or directly created by using dedicated software for 3D. When the 3D model is ready, its volume should be divided onto 2D horizontal slices. One on top of the other will recreate the full 3D model.
2. *Material selection*: this step includes the selection of the material to be printed, which can be composed of different types of polymers and include cells, growth factors and other chemical compounds. The combination of all these factors is what it is known as **bioink**. Its proper selection is a key aspect to guarantee the integrity of the prints, providing good biocompatibility and mechanical properties.
3. *Bioprinting*: the process of bioprinting needs an appropriate configuration of the parameters and observation during all the process. These parameters may vary as a function of the technique chosen and also the bioink used.
4. *Print validation*: final step in which the quality of the prints and their functionality is checked.

3. MARKET ANALYSIS

According to one of the latest market analyses report published on *Values Reports* and fulfilled at the beginning of the year, the OoC market is segmented by type, application, regions and key players [50]. Despite the economic situation derived from the pandemics, the market size is projected to reach 303.6 Million USD by 2026 and increase the Compound Annual Growth Rate (CAGR) of 39.9% during the period 2021-2026 [51].

3.1 Sectors leading the market

In the last 20 years, it has been observed an increasing expense in the development of drugs, while the number of drugs approved annually for commercialization decreases. This is one of the factors that has made **pharmaceutical companies** the leading sector in the OoC technology market [51]. The total costs to develop a drug are estimated nearly 2.5 billion dollars on average and, two-thirds of the total cost correspond to the *clinical trial stage*. Improving the *predictive power* of preclinical screening using on-chip technology would allow early detection of ineffective drugs, facilitating their discarding earlier and avoiding unnecessary spending [51].

On the other hand, the growing emphasis on developing reliable alternatives for *animal testing* models had increased the number of partnerships and collaborations between pharmaceutical companies and OoC manufacturers [52].

3.2 Historical evolution

As shown in Figure 3.1, according to *Zhang & Radisic* (2017), the number of articles per year about the organ-on-a-chip is growing with an exponential shape [51]. The topics related to *Organ-on-a-chip* and *Microfluidics* are being investigated in recent years and it is likely that the curve will continue to grow in the coming years [51]. The excitement over OoC technology rise in 2015 after the publication of a Lung-on-a-chip device mimicking the interface between endothelial and alveolar cells and aspects such as pulmonary inflammation or infections [53].

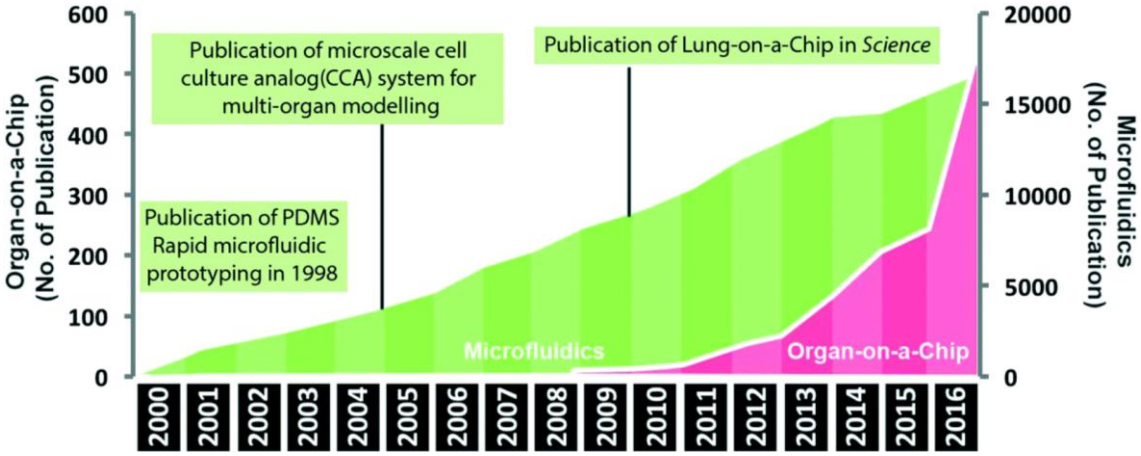

Figure 3.1. *Rise in academic publishing in OoC on Google Scholar. Representation of the number of publications per year, where the topic of the article was directly related with the key words "Microfluidics" and "Organ-on-a-chip" from 2000 to 2015.* [51]

3.3 Future Perspective

Nowadays, the market of organs-on-chips is emerging and is expected to reach 303.6 Million USD by 2026 while in 2020 the market was of 41 Million USD with a CAGR of between 35% and 40%

[50,54]. This growth in the market is mainly driven by the fact that this type of technology has many advantages with respect to the conventional ones and also an important future. In addition, the search for **alternatives for the animal testing** models and the increase of capital in research which develops organs-on-chips has favoured this market rise [30]. Furthermore, the growing need for early detection of drug toxicity with the objective to minimize the financial losses due to drug failure, causes significant investments by pharmaceuticals. To drug testing and development, OoC technology represents a good platform to study certain disease processes, using cells taken from patients. This makes it possible to develop personalized medicine in the future using samples taken from the patients [55].

That is the reason why the end-user of this technology can be segmented into: pharmaceutical and biotechnological, companies, and academic and research institutions. The OoC market can be divided into the following aspects:

- *Type*: the market can be segmented into different organs the most important **are liver, lung, heart, intestine and kidney**, among others [54]. The more interest in studying the organ, the more investment and therefore, the more market there is.
- *Application*: Depending on the objective of the model the market can be divided into different sectors of use. The most important applications are physiological development, personalized medicine, drug discovery and toxicology research, among others [51,55].
- *Region*: North America is expected to have the highest market growth and therefore, the highest CAGR grow of the market, followed by Europe. The continent that will experience the greatest market increase over 2010 will be Asia but will not reach the market size of Europe or North America [54].

3.4 Key Players

According to Low et. al. 2021, the market is emerging, and the market concentration is in the middle point between a consolidated market (dominated by one to five major players), and a fragmented and highly competitive market (without dominant players) [50,56]. Nowadays there are some companies that are prominent key players in this global market, most of them are in the United States. Some examples of these companies are: *Emulate Bio*, *Hurel Corporation*, *Nortis* and *Ascendance Biotechnology* in the United States, *CN Bio Innovations* in the United Kingdom and *Insphero AG* in Switzerland.

In Section 4.1 is reviewed part of the regulation developed in the UK by the *Medicines and Healthcare products Regulatory Agency* since it is one of the first countries in Europe that is developing new regulations about OoC devices [57]. Figure 3.2 shows the two main types of companies developing organs-on-a-chip systems: those that develop *body-on-a-chip models*, which include more than one organ per chip, and those that are focused on only one organ, what is known as *Tissue interface-on-a-chip*). Within this last group, we find Emulate bio which is developing gut-on-a-chip models, among other organs [51].

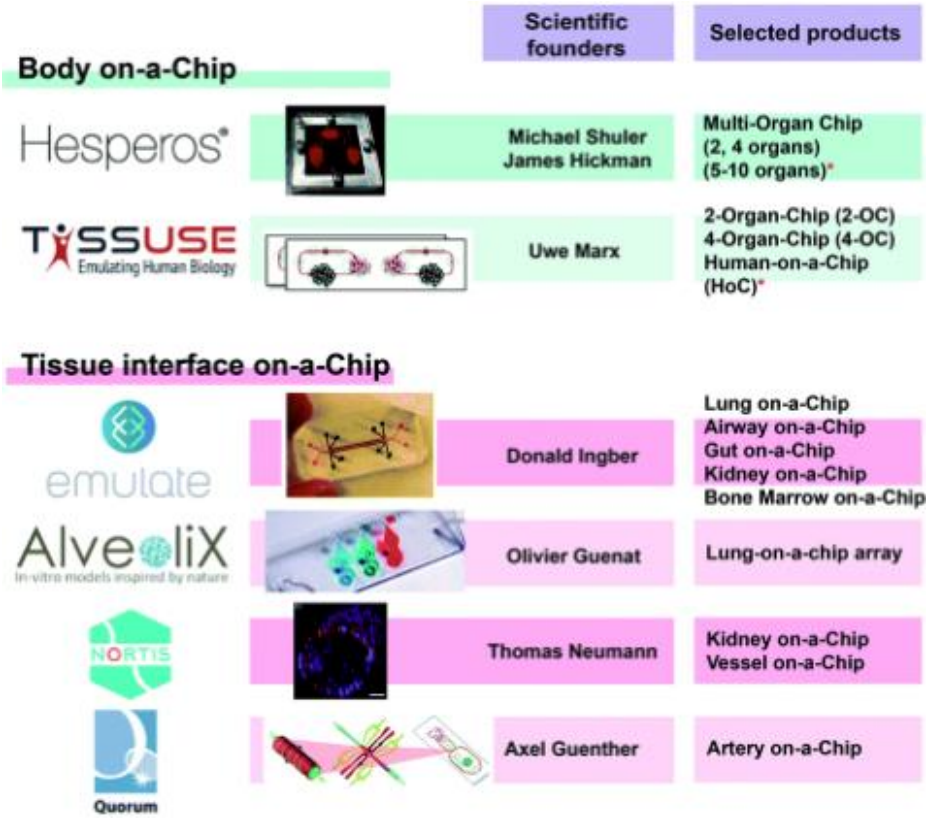

Figure 3.2. *Some of the prominent key players in the organ-on-a-chip and body-on-a-chip market* [51].

The most important finding of the global OoC market is that the Lung-on-a-chip organ type is expected to have the largest market share. In the last years, the interest and investment in gut-on-a-chip, is increasing, the drug development and drug discovery is the application that is growing faster. Finally, the pharmaceutical and biotechnological companies are expected to be the major end-user of the OoC devices [51,52].

4. REGULATION AND LEGAL ASPECTS

As we have reviewed during this project the organ-on-a-chip technology presents many advantages, and they are designed to be able to replace the experiments with animals and to obtain a better model of diseases [30]. That is the reason why the regulatory processes on the different agencies are speeding up. One example is the US Food and Drug Administration (FDA), which have set up a program to develop the regulation of human tissue chips to replicate the function of the structure of human organs [58]. The lack of harmonization between the FDA and the EU European Medicines Agency (EMA) increases the absence of clear regulation and legislation for 3D bioprinted tissue-engineered constructs [8]. The key regulatory considerations involved aspects such as the materials used, processes performed and the products obtained [8].

4.1 Regulatory Context

The Regulatory context in the OoC field is complex since the regulation depends on the final use of the device. In the case of drug screening the regulatory framework would be focused on the drug approval. That means that the OoC should approve the regulation for a specific purpose, usually for the purpose for which it was designed. There is no generic regulation for this type of technology. Regulatory can represent a significant barrier in the OoC implementation. The early stage of the technology involved in this project causes an early stage of the regulation. It is expected that in the next years more regulation will be accepted [54]. The Medicines and Healthcare products Regulatory Agency (MHRA) in the United Kingdom, where is located CN Bio Innovations one of the most important companies of OoC technologies, is studying the regulation of these technologies and wants to improve the regulatory routes to validate it. The method used by regulators is that they encourage the companies to share the data of the models to demonstrate the potential utility [59].

Along this project, the use of cells has been necessary, especially in later stages, and for their use different authorization and licensing were required. The regulation in Europe is defined by three directives: 2004/23/EC, 2006/86/EC and 2006/17/EC [60]. The directives define the regulation and legal aspects of the donation, procurement, testing of human tissue, and cells. The implementation is mandatory for all the state members of the European Union. Also, the directive 2003/94/EC is important since legal aspects of Good Manufacturing Practices for advanced therapies are specified [60].

In Europe, October 1, 2017, began a project called ORCHID (Organ-on-a-chip Development), it includes 6 universities from Spain, Germany, France, Netherlands, and Belgium. All these universities were coordinated by the Stichting Institute for Human Organ and Disease Model Technologies in the Netherlands to study the development of this technology. The total contribution was more than 520.000 €, and the main objectives were [54,61,62]:

- **Evaluation of the technology**, a complete study of the state of the art and unmet needs.
- Identification of **ethical issues**, establishing standards and identifying measures for a regulatory implementation.
- Analysis of **economic and societal impact**, training, and education.
- **Developing a roadmap** that will guide the required R&D efforts.
- Raising awareness and building the ecosystem for OoC technology through a digital reference platform

With nearly two years of research, the project ended on September 30, 2019 [61], and the results show that a similar effort than in US should be done by the European Medicine Agency (EMA) in EU. In US the FDA help the independent testing centres and do active contribution to help the development of the OoC technology [61].

4.1.1 Standardization

The standardization process is also a heavy barrier that should be overcome. As is reviewed in the (Mastrangeli, Mar. 2019) [54] one of the problems of the OoC technology is the absence of standardization. Aspects as the shape, interfaces, sizes, quality, tissue types, or ways of use, can change in different companies or institutes and it may cause compatibility problems. This process of regulation may take years before these technologies are accepted by regulatory agencies.

4.2 Ethical Context

The absence of any ethical concern regarding animal studies is introducing *new* ethics in science. The objective is to introduce the Animal welfare and change the use of animals in research. One of the first fields in which the use of animals was banned is in the process of testing cosmetics since it is banned in the European Union, United Kingdom, India, Israel, and Norway [50,52,54].

The use of OoC is considered as a replacement alternative for big part of the remaining animal studies since the ethical issues presented by the OoC are less than the use of animals in research and experimentation. Meanwhile, during clinical studies and testing compounds, innumerable animal lives are lost and often the results demonstrate a lack of accuracy to mimic human pathophysiology and fail to predict the response of the organ [52]. A better reproducibility of the experiments and a more balanced and accurate drug discovery process can be performed using human models *in vitro* in order to accelerate and advance personalized medicine and the development of new drugs [52,60].

5. CONCEPTION ENGINEERING

Given the initial specifications of the project, a chip was designed in order to store the hydrogel, which contained the microstructure that mimicked the large intestine and various specific cell types of the intestinal mucosa. At the beginning of the project, it was decided that the polymerization and structuring of the hydrogel would be performed by 3D bioprinting. We hypothesize that the combined effect of the 3D structure of the hydrogel acquired with the bioprinting technique, and the fluidic shear can provide the cells with the appropriate stimulus to induce further differentiation and improve physiological relevance.

5.1 3D Bioprinting Methodology

To develop the initial objectives that have been considered in this project, a series of bioprinting technologies/techniques have been identified that could be used (individually or in combination with other techniques) for the development of the *in vitro* model. On one hand, there are the standard culture models, which basically consist of seeding cells on 2D flat and hard substrates [7]. Culture uniformity is their main advantage, but they lack 3D topography and the possibility to recreate the stromal compartment in a controlled manner. On the other hand, 3D bioprinting offers the ability to construct microstructured tissues layer-by-layer with high precision and allows the inclusion of complex physiological structures [63].

5.1.1 Extrusion-Based Bioprinting

Extrusion-based bioprinting has been employed in recent years by researchers as a good cost-effective alternative to OoC fabrication [6]. The most important advantages presented by this method are its versatility, inexpensive equipment (good affordability) and the possibility to print a wide range of biomaterials. The technique is based on the extrusion of the bioink to form a continuous micro-filament which is deposited on a substrate that can be solid, liquid or a material derived from gel [6]. The different methodology used to extrude the material is the main difference between the 3 types of methods that can be applied to do this category of bioprinting:

- *Pneumatic-driven extrusion*: this method utilizes **compressed air** to extrude the material.
- *Piston-driven extrusion*: this method utilizes a mechanical system to extrude the material. A **piston-driven extrusion** is the most common. This method is highly recommended for extruding biomaterials with a high viscosity.
- *Screw-driven extrusion*: this method also used a mechanical system to extrude the material but in this case, a **screw-driven extrusion** is used. This system is similar to the Piston-driven system but using a screw, more pressure is provided which might damage the cell in the bioink.

In general, the Piston and Screw-driven methods provide a good printability and higher resolution using semi-solid or solid-state biomaterials. The main disadvantages of both techniques are that the volume of impression is limited and the process of cleaning and disinfection is more complicated [6]. Also, the cost of the equipment is higher than the Pneumatic-driven method. Finally, the three principles are represented in Figure 5.1.

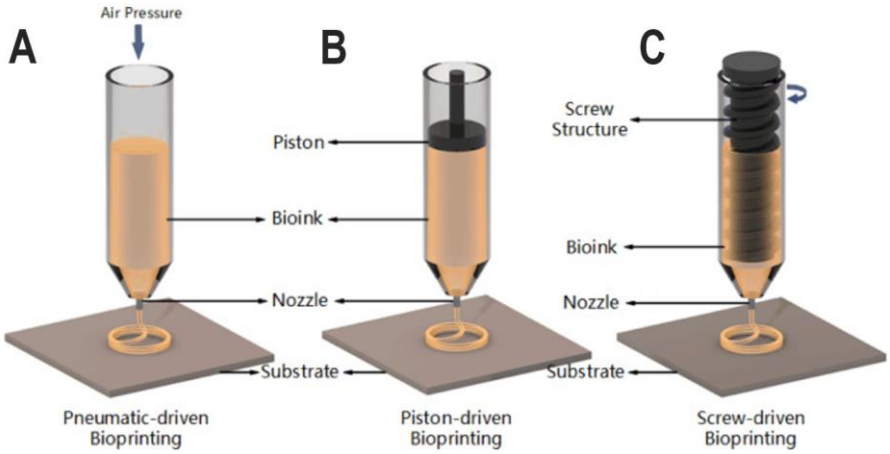

***Figure 5.1**. Illustration of extrusion-based bioprinting. A) Pneumatic-driven bioprinting. B) Piston-driven bioprinting. C) Screw-driven bioprinting. Adapted from Zeming et. al. (2019). [6]*

The main reason why the extrusion bioprinting method is not used in this project is because it presents problems with the cells. The cells suffer a high level of shear stress when passing through the extrusion system (syringe). In all three principles, the pressure is enough to reduce the viability of the cells within the printed matrix, falling in values by 50%.

5.1.2 Droplet-Based Bioprinting (Inkjet Printing)

To obtain a higher resolution we can use this technology based on droplets as the basic unit. The basic principle is the use of droplets which makes it a very simple model and with high control of biologic, including cells, growth factors, biomaterials, etc. In the same way, as the Section 5.1.1, the difference in the principles depends on the method used to form and release the droplets, which in this case will be the bioink [6]. There are three different principles to print using this technology:

- *Inkjet bioprinting*: Can be divided into two types of printing, continuous inkjet and drop-on-demand. The continuous inkjet has higher frequencies but achieves smaller volumes while the drop-on-demand has lower frequencies and volumes but higher spatial resolution [6].
- *Electrohydrodynamic jetting* (EHDJ): is based on electromagnetic fields. Placing two electrodes with a differential of potential is possible to form and release the droplets [6].
- *Laser-assisted bioprinting*: The most complex using droplets, is necessary a Pulsed Laser to excite the layers and three layers; one must be a glass/quartz layer, the second one must be the absorbing layer and finally the bioink. The excitation of the Glass/Quartz layer will cause the formation and release of the droplets [6].

The most common methods are the inkjet bioprinting (*Figure 5.2*) and the Laser-assisted bioprinting (*Figure 5.2*). The main disadvantage of this category is the lack of precision in the size and placement of the droplet. Also, requires a low viscosity bioink, which rejects several bioinks used for bioprinting [6,48,64].

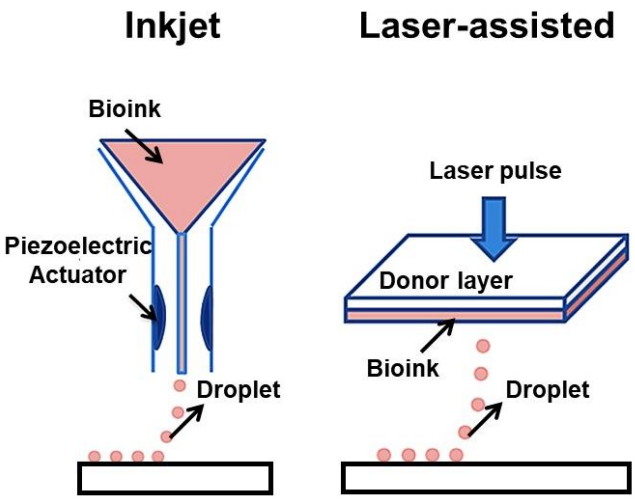

***Figure 5.2**. Two examples of Droplet-base bioprinting. A) Inkjet bioprinting method. B) Laser-Assisted method. Loai et. al. (2019).* [65]

5.1.3 Photocuring-Based Bioprinting

The photocuring-based bioprinting also named *vat polymerization* can be divided into **stereolithography** (SLA) and **digital light processing** (DLP).

- *SLA*: using this method a laser provided the energy to form the covalent bonds between adjacent polymer chains in bioink solution. The laser is reflected in a mirror and does an appropriate point by point moving in X and Y directions [6]. (Figure 5.3)
- *DLP*: however, during the DLP it solidifies a complete layer at once instead of point by point. It prints the bottom layer first, and each new layer is above the previous one [6]. (Figure 5.3)

This technique is based on the solidification of photosensitive polymers to form structures under a precisely controlled lighting with high precision [64]. The most common uses of these technologies are the creation of cell-free scaffolds, but in recent years cell-laden scaffolds have been created. As it is highlighted in (Zeming Gu et. al, 2019) [6] this technology compared to other methods of bioprinting, usually has significant improvement on printing resolution and printing speed which makes a good method for bioprinting.

Unlike the previous methods, this one works by polymerizing the bioink with light, patterns of light and dark pixels are projected and therefore it is necessary that this one contains light-curing material [66]. It should polymerize at the same wavelength of the light source coupled to the printer. Typically, the light source is a projector (visible, white light spectra) or an array of LEDs (of a specific wavelength). One advantage of these systems is that most of them use an open-source programming code coupled to Arduino platform, that can be easily modified to reach the end user's requirements. Its lower price together with the possibility of using custom resins as bioink [49]. Make this approach one of the most widely adopted by research groups worldwide.

Finally according to *Yong He et. al. 2020*, this technique has some inefficiencies such as its non-ideal density and uniformity of loaded cells [64]. The light exposure used to polymerize the bioink can negatively affect the cells and nontoxic photoinitiators should be used to non-affect the activity of the cells [64]. It is expected that DLP-SLA replaces the extrusion-based bioprinting as the most used method in the near future [64].

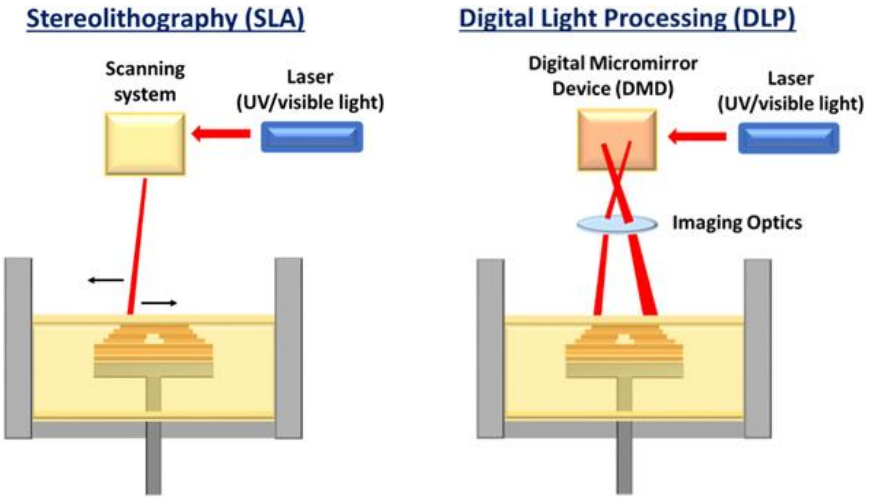

***Figure 5.3**. Simplified schematic drawing of the SLA and DLP principles. A) Schematic drawing of the SLA bioprinting set-up and the scanning system. B) Schematic drawing of the DLP bioprinting set-up, the digital micromirror device and the laser. Adapted from Long Ng, et. al. (2020).* [8]

Table 5.1 summarizes the most relevant parameters of the above-mentioned 3D bioprinting methods. In the first column, different parameters are analyzed and the three methods have been classified between the levels, *Low*, *Medium* and *High*.

***Table 5.1.** Comparison of the common bioprinting categories. Adapted from Miri et.al. 20219, Murphy & Atala 2014 and Ji & Guvendiren 2017.* [21,67,68]

Parameter	***Extrusion***	***Inkjet***	***Photocuring***
Speed	Medium	Low	High
Cost	Low	Low	Medium
Resolution	100-500 µm	100-500 µm	20-100 µm
Flexibility	Low	High	High
Commercialization	Medium	High	Low

5.1.4 Method Selected

Analysing all the features and parameters of the three common bioprinting categories, the best method for this project is the **digital light processing - stereolithography** (DLP-SLA) 3D bioprinting technique. In addition to being a technique that can be used for the fabrication of structured hydrogels with embedded cells, the same technique will allow for the fabrication of pieces and moulds for the development of the platform that would contain both the hydrogel with the cells and the microfluidic connections. This method allows the crosslinking of soft polymers using visible light, for that is required a special bioink containing light-curing materials. A more extensive explanation about this bioink can be found in sections 5.2.1 and 6.2.

As we have reviewed in section 5.1.3 a good way to obtain this type of bioprinter is by modifying a commercially available printer. In this way, we can avoid the problem of low commercialization of these printers presented in Table 5.1. In this project, a Solus 3D printing equipment (Junction3D) has been used (Figure 5.4). It was previously adapted by lab members for printing scaffolds with embedded cells using reduced bioink volumes and increasing cell viability.

The system consists of the following main components: a facing-down printing support coupled to a Z-axis motor, a resin vat with a transparent window, and a beam projector. Also, a customized aluminium printing support and aluminium vat were designed for printing small scaffolds (Figure 5.4). The objective is to illuminate the mirror under the printer and allow the process of photocuring (Figure 5.4).

An important parameter to consider is the cell damage due to **infrared radiation** (IR) exposure, to avoid it a short pass heat protection filter (*Schott*) was added to the output of the projector (*Vivitek*). The structure of the 3D printed pattern is in the vertical direction, layer by layer. Printing parameters such as the thicknesses of the printed layers, the brightness of the light and exposure times can be adjusted as a function of the print design and the bioink composition, to get the proper results, the optimization of these parameters is reviewed in Section 6.3.2.

The gut-on-a-chip should replicate different parts of the intestine to perform a good replication of the physiology of the human gut. The need to perfuse the hydrogel with cell culture medium, force the integration of the hydrogels with the embedded cells in a perfusable platform. This platform is composed of different layers of poly(dimethylsiloxane) (PDMS), (Section 6.1.2), and through an instrument and microfluidics, we can introduce cell culture medium to the hydrogel to be able to perfuse the chip correctly so that the cells can survive inside the gel (Section 6.4).

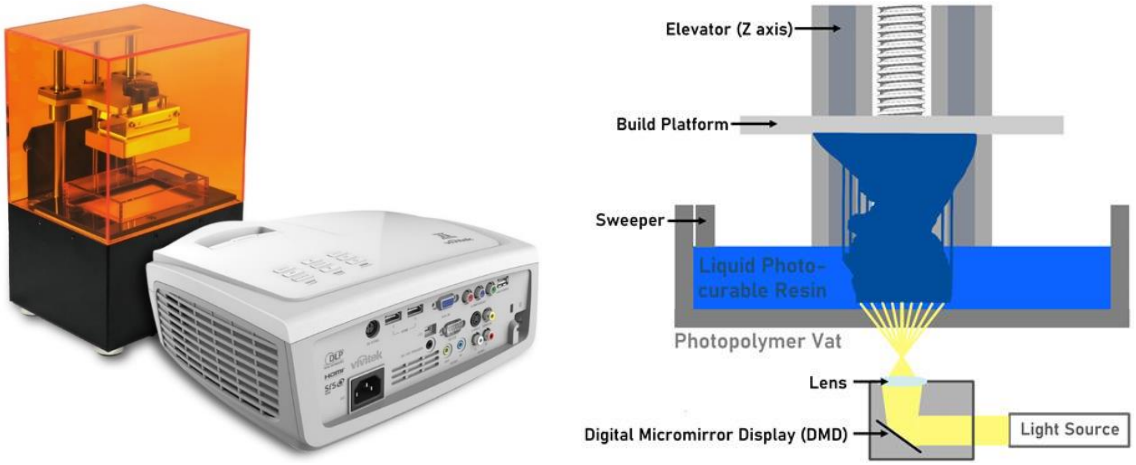

Figure 5.4. *From left to right: Commercial Solus 3D printer and a Vivitek projector and illustration of a visible-light-based stereolithography 3D bioprinting system* [69].

5.2 Materials and Methods

Materials

Gelatin from porcine origin (type A), Tartrazine and trichlorofluoro-silane were purchased from Sigma. Poly (ethylene glycol) diacrylate with a molecular weight of 4000 kDa was purchased from Polysciences and Lithium phenyl-2,4,6-trimethylbenzoylphosphinate (LAP) from TCI chemicals. Hanks Balanced Salt Solution and Phosphate Buffered Saline Solution were from Life technologies, and both complete Dubbelco's cell culture medium and penicillin-streptomycin, together with Normocin were purchased from Gibco. Sylgard 184 elastomeric kit was purchased from Dow Corning and isopropanol from Panreac.

SolusProto and ABS-like grey resins for both Solus and Phrozen 3D printers, respectively, were purchased from FEP shop.

5.2.1 Preparation of the hydrogel pre-polymer solution

The prepolymer solution for the printing of hydrogels was prepared using the following reagents. First, gelatin methacryloyl was made by following the method described elsewhere [70], and mixed in the proper concentration with PEGDA, LAP and tartrazine. The mixture was dissolved in HBSS supplemented with 1% v/v of P/S at 65 ºC in stirring conditions. Once completely dissolved, it can be stored at 4ºC for later use or directly poured into the bioprinter cuvette to start the printing. In the case of embedding cells in the hydrogel, cells should be detached from the culture flask and resuspend in the proper concentration in the prepolymer solution just before being added to the cuvette for printing. All the system, including the bioink should be at 37ºC to guarantee high cell viability.

5.2.2 Printing Methodology

The printing process was carried out in a customized ***Solus 3D Printer***. The works with a DLP projector reaching an XY resolution of 25 microns and a layer thickness down to 10 microns.

First, the build platform was adapted to be able to place 13 mm diameter glass slides on it, as new supports for the prints. In the same way, the cuvette for the bioink (also referred to as vat) was redesigned to reduce the amount of solution required for printing (see Figure 5.5). In addition, a heater was coupled to the system to keep the bioink solution at 37ºC, avoiding bioink gelation and, at the same time reducing cell death.

Before printing, the design to be printed has been created with CAD tools, specifically with FreeCAD and Autodesk Fusion 360. The designs were exported to ***.stl** format to be able to do the slicing of the design and print it layer by layer. In addition, *printing parameters* such as layer thickness and exposure time, among others, have also been adjusted to obtain the desired results.

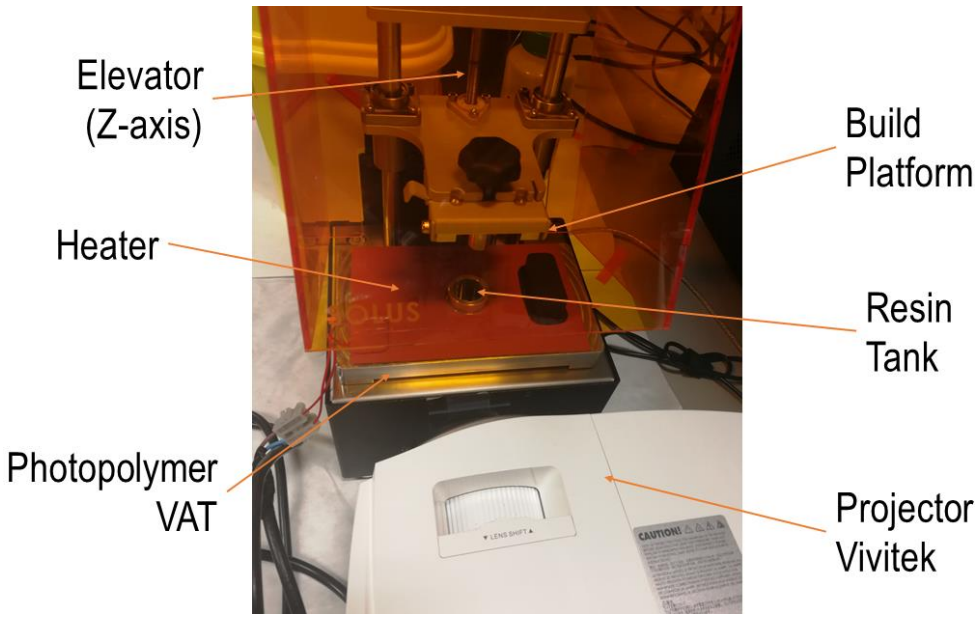

***Figure 5.5**. Modified Solus 3D printer used to perform the printings.*

5.2.3 Microfluidic platform

The microfluidic platform is compromised of the **microfluidic device** and the **casing** (see Figure 6.1). For the fabrication of the *microfluidic device*, PDMS was used. Briefly, PDMS prepolymer

solution was mixed in 10:1 (w/w) ratio with the cross-linking agent and poured into different sets of microstructured moulds (or masters) previously designed and 3D printed using a standard BSA-like photocuring resin. Previously, the 3D-printed masters were treated with oxygen plasma for 15 minutes and later with a vapor phase silane for 1 hour using. After a degassing step, the PDMS parts were cured at 85 ºC for 3 hours or 48 hours at room temperature to obtain the final elastomeric replicas.

For the *outer casing*, a high-resolution LCD printer called **Phrozen** was used. With this printer, the different pieces compromising the outer casing of our microfluidic system were fabricated. After printing, they were cleaned with isopropanol and cured under UV for 2 minutes and let them rest for 60 minutes.

5.2.4 Volumetric Swelling

The water uptake capacity of the printed hydrogels was analysed both in static and dynamic conditions, by measuring their volumetric variations upon time, to optimize the shape and size of the hydrogels' contour and their inner microstructures.

Either *Phosphate Buffered Saline Solution* (PBSS) or DMEM cell medium were used. Immediately after printing, samples were rinsed in warmed PBS to remove unreacted polymer and placed at 37ºC to reach the equilibrium swelling. Pictures from the top and lateral side of the gels were taken at different timepoints until reaching the equilibrium swelling, drying first the hydrogels with Kimwipe paper to avoid distortion.

Four critical parameters were defined to determine the proper geometry of the intestinal crypts (see Figure 5.6), being parameter **A** the crypt depth, **a** the width of the crypts in the middle point, **b** the upper aperture of the crypts, and, **c** the distance between consecutive crypts.

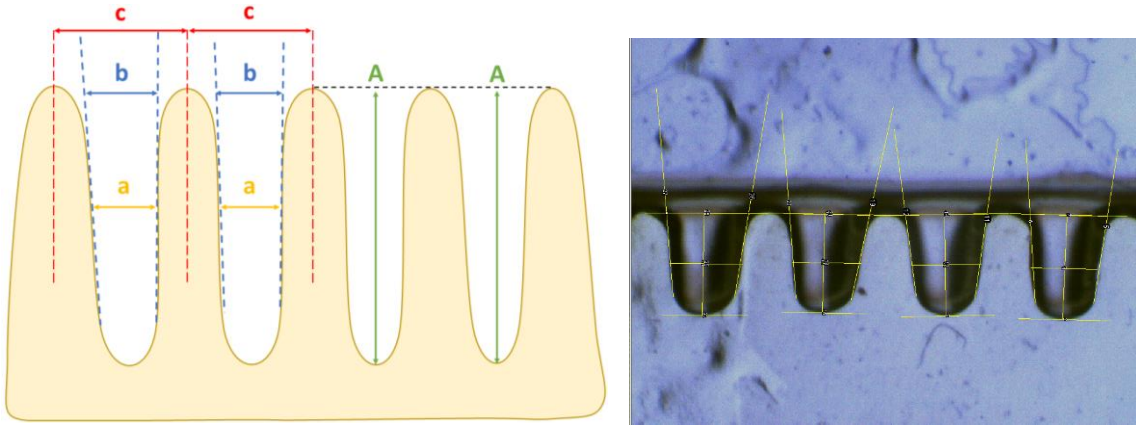

***Figure 5.6**. From left to right: Illustration of the relevant parameters used to quantify the size of the crypts and one example of the method.*

5.2.5 Gut-on-a-chip assembly

The schematic of the assembly of the whole chip is depicted in Figure 5.7. Briefly, the first layer of PDMS was placed in the bottom part of the holder (step 1). In the same way, the 13 mm diameter glass coverslip with the previously printed hydrogel was then placed on top of the PDMS layer (step 2). To guarantee the proper alignment of both parts, a circular allocation was included on the PDMS layer. With the alignment structures, the top layer of PDMS containing some of the microfluidic channels and the inlet and outlet cavities was placed upside down perfectly aligned with the ones

below (step 3). Finally, the cover was placed, on top fitted with some alignment structures and fastened with six screws to press against the PDMS ensuring proper contact all along the surface of the microfluidic chip (steps 4–5). The corresponding tubbing (step 6) and Leuer connectors were added together with a debubble allowing for the application of perfused flow avoiding undesired air bubbles.

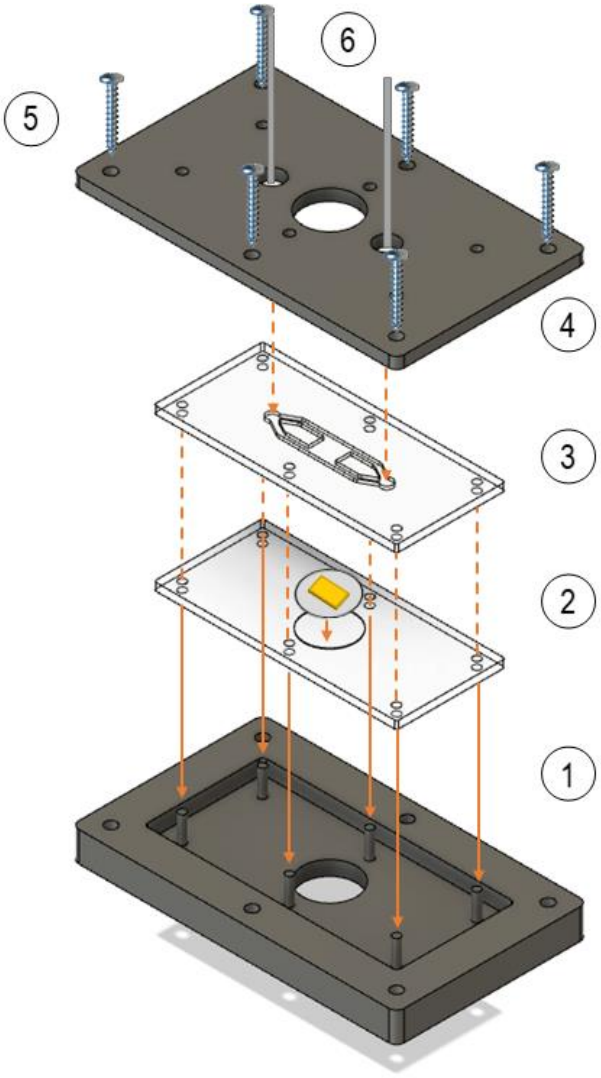

Figure 5.7. *Gut-on-a-chip assembly. This schematic illustrates the steps described in our methodology.*

6. DETAILED ENGINEERING. RESULTS AND DISCUSSION

The results obtained have been organized in four stages that describe the progression of the microfluidic chip design and optimization: from the development of the casing and PDMS layers, to the characterization and selection of the bioink, to the optimization of the 3D structure of the hydrogels, to finally develop the chip assembly.

6.1 Optimization of the structural part of the chip

The gut-on-chip model has been done by integrating the hydrogel into a PDMS structure that will provide a casing for the hydrogel and contain the microfluidic channels of the chip together with the inlet and outlet. To provide structural integrity to the whole system, the PDMS is placed inside hard plastic pieces that will function as outer casing, fastening the whole system and ensuring that no leakages are present (see Figure 6.1). From the casing point of view, the main requirements were:

a) to *integrate* the 3D bioprinted hydrogel containing embedded cells in a faster way once printed
b) to be *perfusable*, so cell medium could flow for oxygen and nutrients exchange
c) to be assembled and disassembled on demand in a **simple** and faster way
d) to contain a *transparent window* to be able to inspect the inner of the channel using optical microscopy
e) to be properly *sterilized* to be compatible with standard cells culture
f) to be **reusable**

It was considered that the best way to achieve the initial objectives was by creating two individual PDMS layers the printed hydrogel could fit in between, with space for the hydrogel and the corresponding microfluidics and an external structure that would allow the correct alignment of the PDMS layers and apply pressure on the PDMS layers to avoid leakage. Figure 6.1 shows the layers of the gut-on-chip from the structural point of view.

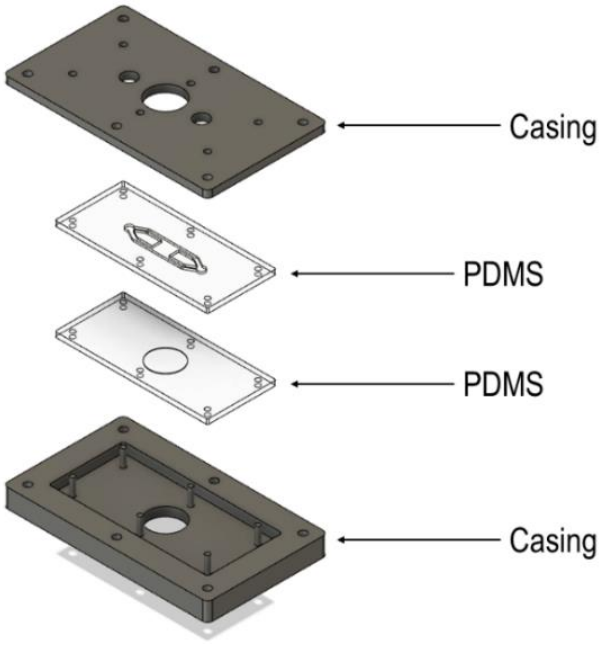

Figure 6.1. *Layers of the gut-on-chip for two-channel.*

6.1.1 External casing

According to the initial objective, different 3D printed casings have been developed to meet the previous requirements. The casing is made up of two different pieces, the lower part (Figure 6.2 left) that has an allocation where the PDMS pieces can be placed and some vertical motifs that will help on the correct alignment of the system. The upper part (Figure 6.2 right) will act as a lid, covering the PDMS and exerting pressure against them to avoid leakage. This is necessary since the two layers of PDMS do not contain any *adhesive* or surface *activation*. Initially, these two parts of the outer casing contained a rectangular central hole that acts as a transparent window for inspection (see Figure 6.2 right)

Additionally, six through-holes were designed both in the cover and in the lower part to be able to place six screws. These screws are intended to seal and press the PDMS layers located at the bottom of the casing.

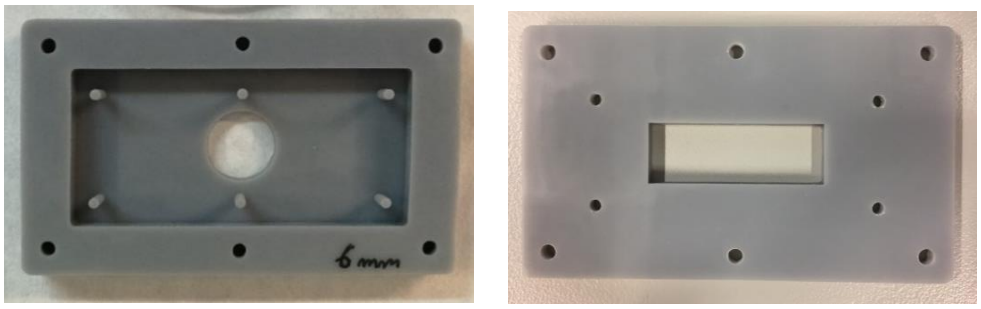

Figure 6.2. *Image of the two sections of the casing. From right to left: Bottom part and cover of the casing.*

After a first trial, results showed that the lid designed was not making the necessary pressure in the central region of the chip to avoid leakage between the two layers of PDMS. Two vertical motifs were added to the lid and bottom to exert more pressure in the hydrogel region (see Figure 6.3 left). Then, the aperture left as the window was too big and some leakage appeared in this region. At that point, a third lid was designed to reduce the inspection area, covering more surface to make a better and more homogeneous pressure (see Figure 6.3 right). In this case, the transparent window cover both the inlet and outlet of the chip, the channel and the region above the hydrogel.

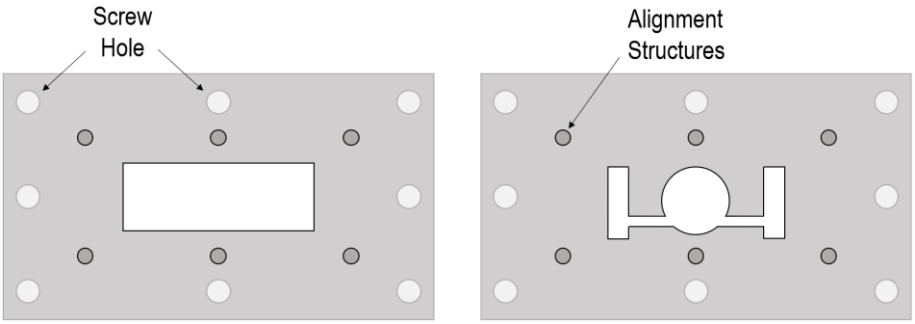

Figure 6.3. *From left to right: Illustration of the initial lid and the improvement made.*

Even the leakage was reduced in this third design, it was still present since the regions between the central window and the inlet and outlet cavities were not robust enough to ensure the desired pressure and bent upwards. The final design that was considered the best solution was the one in the figure below, in which the entire surface was covered except for the inlet and outlet openings and the area of the small central region where the hydrogel is placed (Figure 6.4).

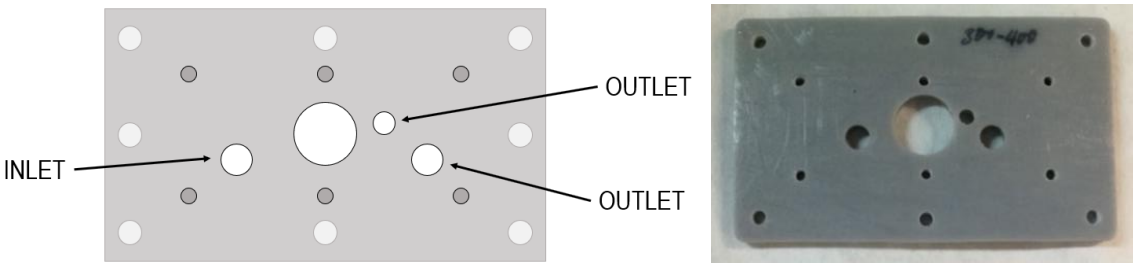

Figure 6.4. Schematic and image of the final lid implemented on the gut-on-chip.

In the same way, for the design of the two-channel lid, a design like the one in Figure 6.4 was made. The lid covered the entire surface except for the inlet and outlet openings and the central region.

6.1.2 PDMS layers

Polydimethylsiloxane (PDMS) is a polymer widely used for the fabrication and prototyping of microfluidic chips for its excellent properties. After the cross-linking process, PDMS becomes a hydrophobic and transparent material at optical frequencies, it is inexpensive, easy to cast, is considered biocompatible and has a low autofluorescence [71,72].

PDMS is the key structure that will locate the hydrogel with the embedded cells and will create the microfluidic channel. As explained above (see Figure 6.1) the microfluidic chip is composed of two layers of PDMS. The bottom layer was designed with a cavity to allocate the circular glass coverslip in which the hydrogel is printed, avoiding any possible gap between the hydrogel and the channel that could alter the flow when introducing the fluid through the channel. Both the size and the thickness of this cavity were optimized considering the dimensions of the glass. The top layer presents the motive of the channel and the allocation for the hydrogel.

All the PDMS layers present six orifices along the longitudinal sides (three on each side) and the allocation for the roundish cover glass in the centre (see Figure 6.5 and Figure 6.6). These holes are used as alignment marks, to perfectly fit the two layers of PDMS onto the external casing, avoiding mismatches. The designs of the casing and the PDMS were optimized to ensure that these orifices coincide with the casing axis (see the assembly layout in Figure 5.7).

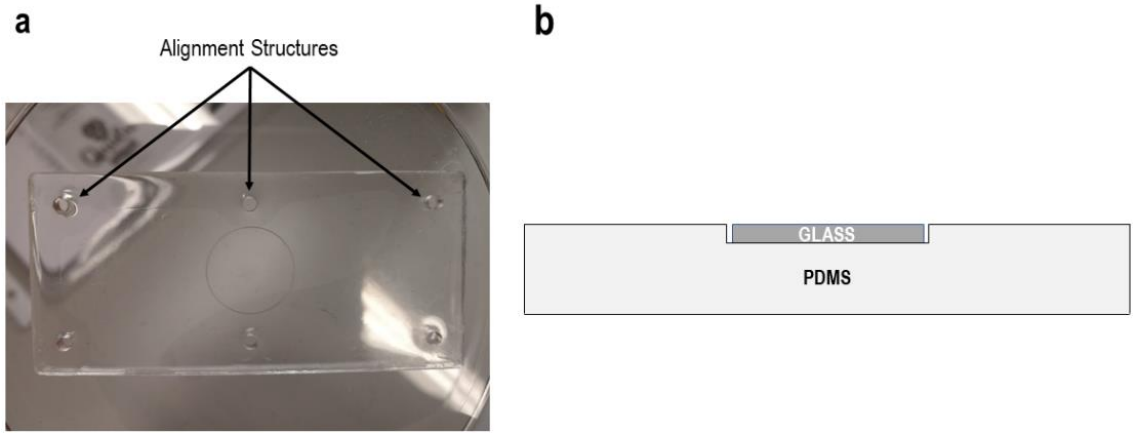

Figure 6.5. A) Image of one PDMS bottom layer. B) Illustration of the PDMS layer from a side view.

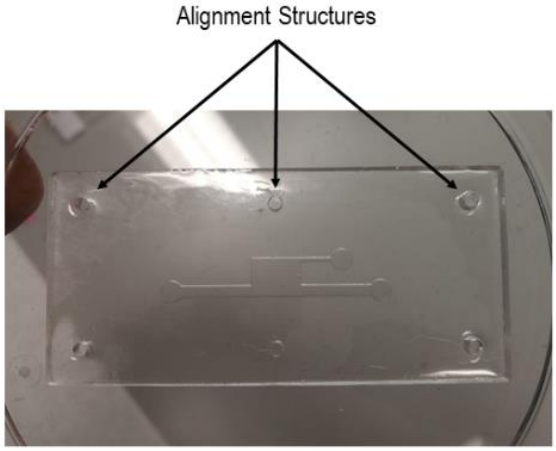

Figure 6.6. *Image of one PDMS top layer.*

During the project, different types of photocurable resins were used to obtain the 3D moulds from which the PDMS layers were made. Initially, we used a BSA-like resin (*ABS-like grey resin*) sensitive to UV light, polymerized using a Phrozen Shuffle XL 3D printer, equipped with an array of 405 nm wavelength LEDs (see left panel in Figure 6.7). This resin allows for the printing of moulds that can be heated up to 65ºC, so could be potentially used for the curing of PDMS at room temperature or in an oven less than 60ºC. However, it was found that the PDMS pieces obtained were irregular, a bit sticky and partially opaque (see middle panel in Figure 6.7). This was considered not suitable for our application since the PDMS had to be transparent. To solve this issue, the DLP-SLA Solus 3D printer was used, since its photosensitive resin (*SolusProto*) allows reaching temperatures up to 95ºC without deformation, resulting in PDMS replicas with high transparency (see right panel in Figure 6.7).

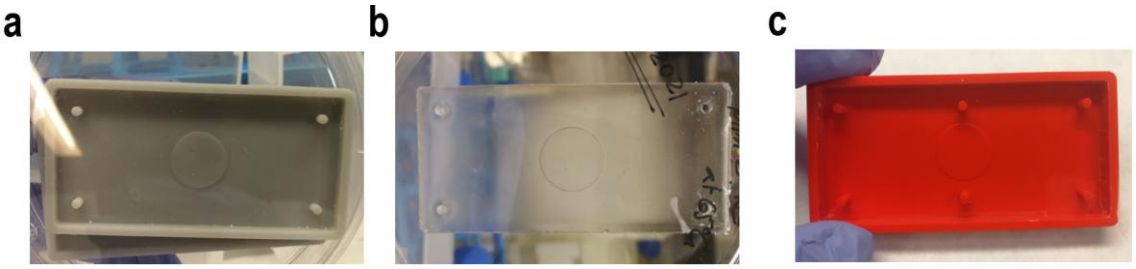

Figure 6.7. *Image of the different moulds used during the project. A) Mould made with the Phrozen printer. B) Replica obtained with the Phrozen moulds. C) Mould made with the Solus printer.*

During the project, two different microfluidic designs were studied and optimized. Initially, a single channel layout (*Figure 6.8-A*) which have one main channel with its corresponding inlet and outlet orifices, so that the hydrogel would only be in direct contact with the liquid from one side. This design also includes an extra channel on the opposite side of the cavity for the allocation of the hydrogel that would act as an outlet for the bubbles. On the other hand, a second layout with two channels was designed and fabricated *(Figure 6.8-B*), including a common inlet and outlet orifices. In this approach, the liquid will flow through both channels reaching the hydrogel from two sides, favouring its proper hydration and the nutrients exchange, especially when cells would be embedded in the gel.

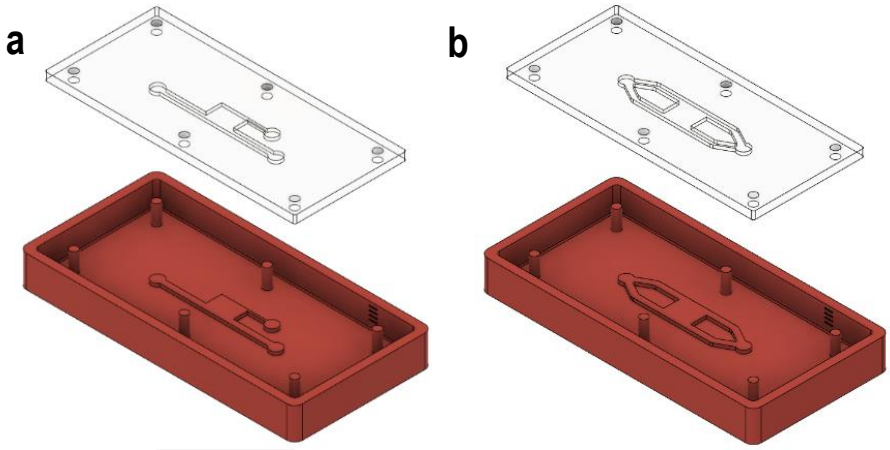

Figure 6.8. *Representation of the PDMS top and the mould used. A) Chip with one channel. B) Chip with two channels.*

When we have the layers of PDMS (Figure 6.8) we should make different holes to place the connections to the infusion pump and the waste. To do this, a 0.75 mm diameter medical punch was used. The syringes through which the cell medium was injected into the chip were placed in these inlets and outlets to facilitate circulation inside the chip.

6.2 Bioink Selection

The appropriate shape and distribution of the microstructures has been proved to be a key parameter for reaching proper cell arrangement and functioning, having a strong impact on the normal intestinal functions, drug absorption and mucus production, among others. [39] Thus, it is very important to include these topographic features in the *in vitro* models to better resemble the native tissue architecture. In this sense, the proper material selection will be of high importance to achieve this goal. As already reviewed in the introductory section, hydrogels are one of the most suitable candidates, since it allows a large variety of combinations and the possibility of tunning their composition on demand, to favour cells attachment and growth. Moreover, they can be microstructured using a large variety of techniques. In previous works, Vila et al. (2020) presented a hydrogel co-network based on **GelMA** and **PEGDA** polymers, and proved to have the required features to mimic the compartments of the intestinal mucosa, providing both structural support and cell-friendly motifs promoting cell adhesion and proliferation [3,73]. Inspired by their results, the composition of this GelMA-PEGDA blend was adapted for bioprinting, leading to a bioink photopolymerizable upon visible-light irradiation with precise control of x-y resolution. This was achieved by two different actions. First, lithium-phenyl-2,4,6-trimethylbenzoylphosphinate (LAP) **photoinitiator** was added. This photoinitiator has a high-water solubility, and an absorption peak around 365 nm, which better matches the spectral range of our 3D bioprinter and the Vivitek projector [46]. Second, a **photoabsorber** was added to the hydrogel composition to control the light penetration into the highly transparent pre-polymer solution. In this case, Tartrazine, a synthetic lemon-yellow dye was chosen [49].

This new bioink allows for (i) a good microstructuring of the hydrogel and (ii) a homogeneous distribution of the cells once trapped within the printed gel.

The concentrations of each of the elements in the pre-polymer solution should be previously studied taking into account cell viability, since the hydrogel will be the scaffold for future cells. Besides having the necessary properties for cells to live and grow on top and inside, the pre-polymer

solution should also be stable allowing the printing of complex 3D structures, such as crypts in the intestine, to mimic better the cellular microenvironment. Table 6.1 summarize the final concentrations of each of the bioink components, that were optimized based on previous studies performed in the laboratory.

Table 6.1. *Composition in percentage of the bioink used to develop the hydrogel.*

GelMA	PEGDA	LAP	Tartrazine
5 %	3 %	0.4 %	0.025 %

6.3 Optimization of the channel design and the printing parameters

As previously described, using the DLP-SLA 3D printing technique, objects are produced via layer-by-layer illumination of the crosslinkable solution. The design of our gut-on-a-chip model was carried out considering only half of the section of the colon, including invaginations in the hydrogel mimicking the large intestinal crypts, leading to a luminal cavity comprised between the printed hydrogel and the PDMS boundaries (see schematics in Figure 6.9).

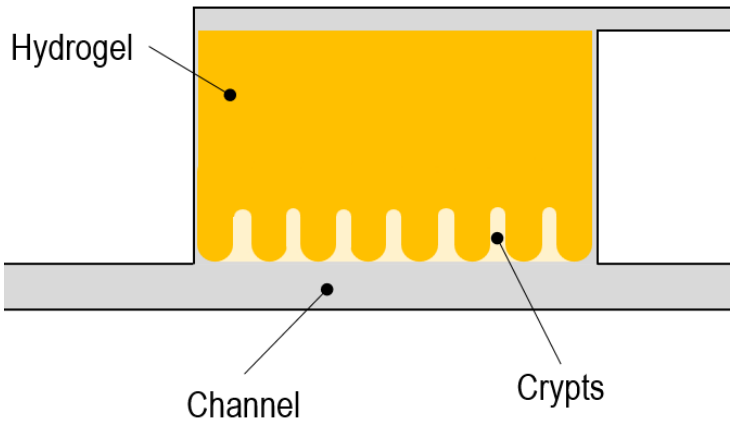

Figure 6.9. *Schematics of the gut-on-a-chip for the hydrogel including crypts and the channel comprised between the printed hydrogel and the PDMS boundaries.*

The fully optimized gut-on-chip model will comprise a central channel surrounded by 3D microstructured hydrogel at both sizes. However, the design was simplified for these initial stages, to focus our attention on optimizing the crypt-like feature sizes and the assembly of the hydrogel with the PDMS layers.

6.3.1 Outer hydrogel dimensions

The final size of the hydrogel has been optimized by performing various experiments. It is important to determine the magnitude of the swelling of our hydrogel due to the absorption of water, considering that PDMS is a stable material that cannot change its shape in case the hydrogel grows. It was also important to achieve almost identical dimensions to those of the designed cavity in the top PDMS layer to prevent the liquid from flowing through other places than the central channel.

So, a first experiment was designed to study the volumetric swelling behaviour of the printed hydrogel to refine the outer dimensions. To do so, rectangular hydrogels with dimensions of 7 millimetres long, 4 millimetres wide and a thickness of 700 microns were printed and kept in PBS

at 37ºC. Measurements of the hydrogels dimensions were performed at different time points to evaluate its change according to the process described above (see *Section 5.2.4, methodology*). Three replicates were evaluated.

In this case, as the geometry of the prints was simple (just a rectangle) without any complex geometric features, the **printing parameters** were not as critical as in the case of the **crypts** optimization process. However, for later comparison when the crypts will be present, these parameters were kept constant, according to previous optimization studies carried out for other laboratory members. Thus, the printing parameters were set to 13 µm for the thickness of each printed layer, 15 seconds for the single layer exposure time for the first printed layers, and 5 seconds for the rest of the layers. The bottom layers should be irradiated for a longer time to ensure a proper attachment of these layers to the glass.

Changes in the dimensions of the hydrogels were measured immediately after printing (t=0) and after 15, 30, 60, 90, 120, 150 and 360 minutes. Figure 6.10 shows the results obtained (tables including all the measurements can be found as supplementary data in the *Annexes* section).

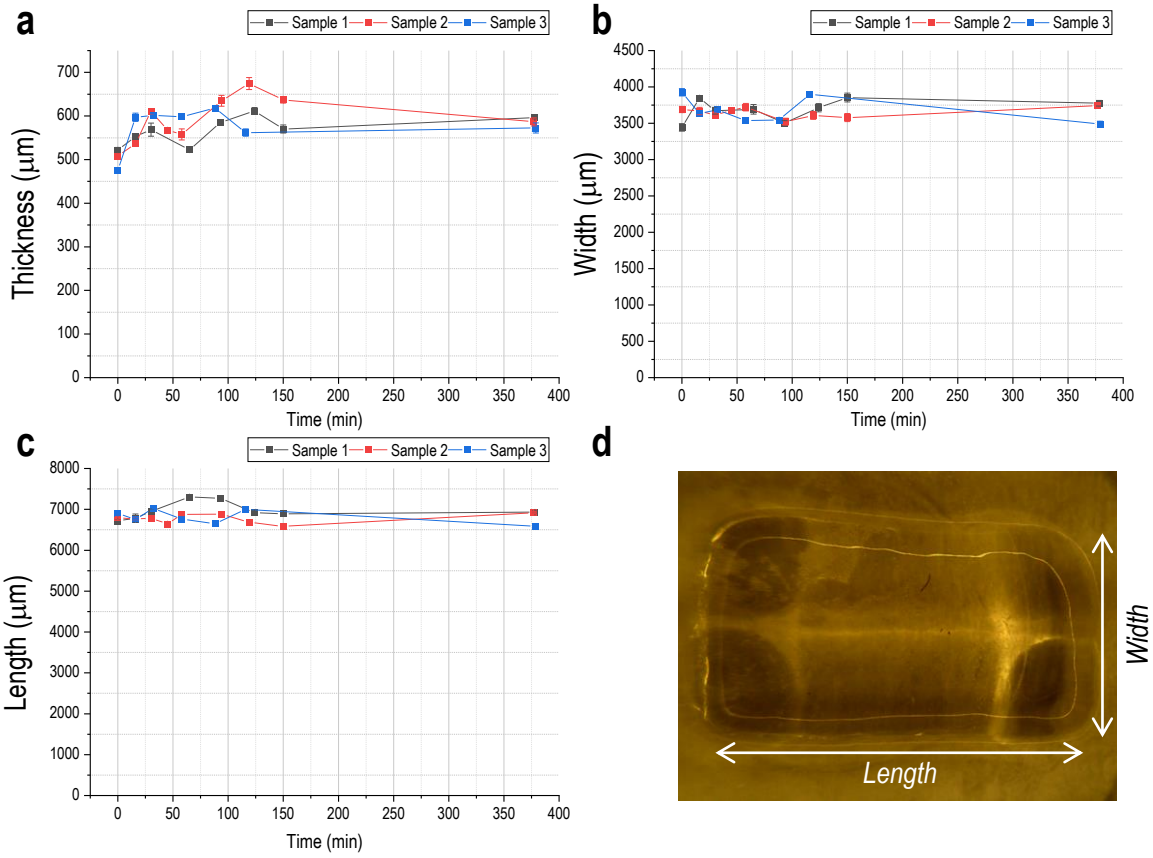

Figure 6.10. *Evolution of the three parameters studied in this experiment and the corresponding error for each measurement. A) Evolution of the thickness for the 3 samples, the x-axis corresponds to the time in minutes and the y-axis to the thickness in micrometres. B) Evolution of the width for the 3 samples, the x-axis corresponds to the time in minutes and the y-axis to the width in micrometres. C) Evolution of the length for the 3 samples, the x-axis corresponds to the time in minutes and the y-axis to the length in micrometres. D) Example of a rectangle hydrogel printed.*

Due to the hydrogel's own polymerization mechanisms, the initial dimensions of the X-Y prints are smaller (6.8 x 3.7 mm^2, instead of 7 x 4 mm^2) and the final dimensions obtained were 585.2 µm +/- 6.9 µm in **thickness**, 3668.5 µm +/- 90.4 µm in **width** and 6811.7 µm +/- 114.9 µm in **length**, values

which represent 16.0%, -0.5% and 0.1% of variation, respectively. Greater growth in width and length was expected, more similar to that found in thickness.

The most significant change occurs in the thickness of our hydrogel and the rest of the dimensions have not changed with respect to the initial measurements (t = 0). The estimation could be improved by carrying out more samples and for a longer time to confirm that in the final time the hydrogel does not grow any more.

The dimensions of the cavity to house the hydrogel to the bottom layer of PDMS are kept at 7 x 4 mm^2, while the height is set at 600 µm, to guarantee an inner contact between the two layers of PDMS. These layers will restrict growth in Z and cause the hydrogel to grow in the XY plane, ensuring final contact between it and the PDMS walls.

6.3.2 Crypts geometry

Once determined the external dimensions of the hydrogel, we focused on the introduction of the **crypts** geometry on one of the long sides (*7 mm*) of the hydrogel (the one in contact with the luminal cavity), to replicate the structure and morphology of the large intestine [74,75] (see Figure 6.11). Taking into account the previous photopolymerization results using the hydrogel composition used in this work, we approach the crypts geometry in the CAD model as regular rectangular grooves all along one of the lateral sides of the hydrogel, keeping a thin layer of hydrogel underneath (Figure 6.11 – A), covering the surface of the glass underneath. In this way, a "u-shaped" crypt section can be obtained after the chip assembly, when the top surface of the 3D printed hydrogel gets in contact with the second PDMS layer (see Figure 6.13 as an example). It is known that cells spread and grew better on top of hard substrates, so covering the bottom part of the crypts we will force them to colonize the hydrogel. Figure 6.11 shows the 3D CAD design of the hydrogel and the crypts used. As previously determined, the outer dimensions of the hydrogel were fixed as 7 x 4 mm^2, with a thickness of 500 µm. The bottom layer mimicking the bottom part of the crypts was set to 250 µm. The length, width and thickness of the hydrogel remained constant throughout the process.

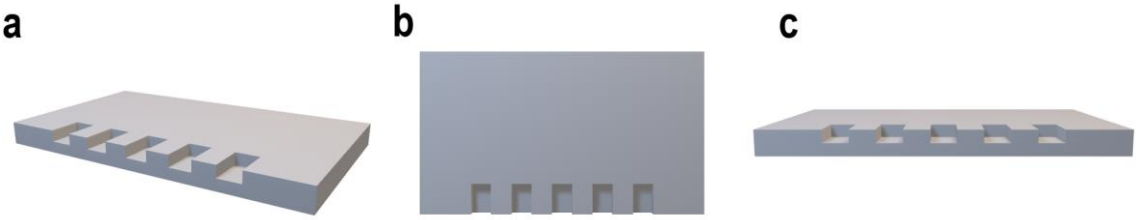

Figure 6.11. *Different views of one of the 3D CAD designs used for printing the hydrogel with crypts: perspective (a), top view (b) and front view (c).*

To determine the dimensions of the crypts some optimization should be performed, varying mainly the following dimensions: the **parameter A**, which corresponds to the *depth* of the crypts and the **parameters B** and **C**, which correspond to the *width* of the crypts and the separation between them, respectively (see Figure 6.12).

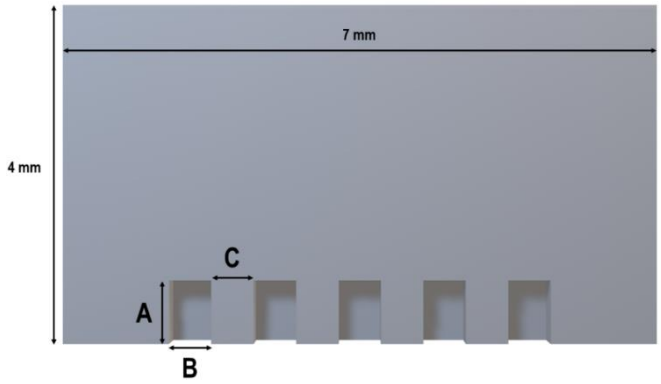

Figure 6.12. *Parameters A, B and C modified in the optimization process.*

As reviewed in the previous sections, the printing methodology is based on illuminating the bioink and the support, where the glass is placed, with enough light to allow the polymerization of the bioink. When working with such small sizes, it is possible that during the printing process, some undesired photopolymerization between the crypts may occur due to the intrinsic nature of the reaction-diffusion mediated photopolymerization [17] and the reduced distance between consecutive crypts. So different 3D CAD models were created to determine the most suitable values for A, B, and C parameters to obtain, after the integration of the hydrogel on the microfluidic chip, proper crypts definition.

The range of values for the three crypt parameters, used for the optimization, are summarized in Table 6.2. Due to the resolution limit of our 3D bioprinter setup and the bioink used, crypts with smaller dimensions could not be obtained.

Table 6.2. *Tested ranges for the parameters A, B and C.*

Parameter	**A**	**B**	**C**
Tested Range (µm)	750 – 850	150 – 500	250 – 400

In particular, two combinations of parameters were of great interest due to the results obtained, achieving a regular crypts distribution, and fixed as possible candidates for the final gut-on-chip design. The first one, with A = 850 µm, B = 150 µm and C = 400 µm (see Figure 6.13), gave rise to large aspect ratio crypts, deeper than wider, resembling more to what can be found *in vivo*. With the second combination, using A = 850 µm, B = 200 µm and C = 400 µm (see Figure 6.14), shorter but wider crypts were obtained, with a smooth variation of the curvature. The printing results were evaluated immediately after printing, after rinsing the hydrogel in warmed PBS to remove the unreacted polymer, and once constrained inside the chip. To better assess the final dimensions of the printed crypts, a 13 mm in diameter glass coverslip was place on top, mimicking the microfluidic chip assembly.

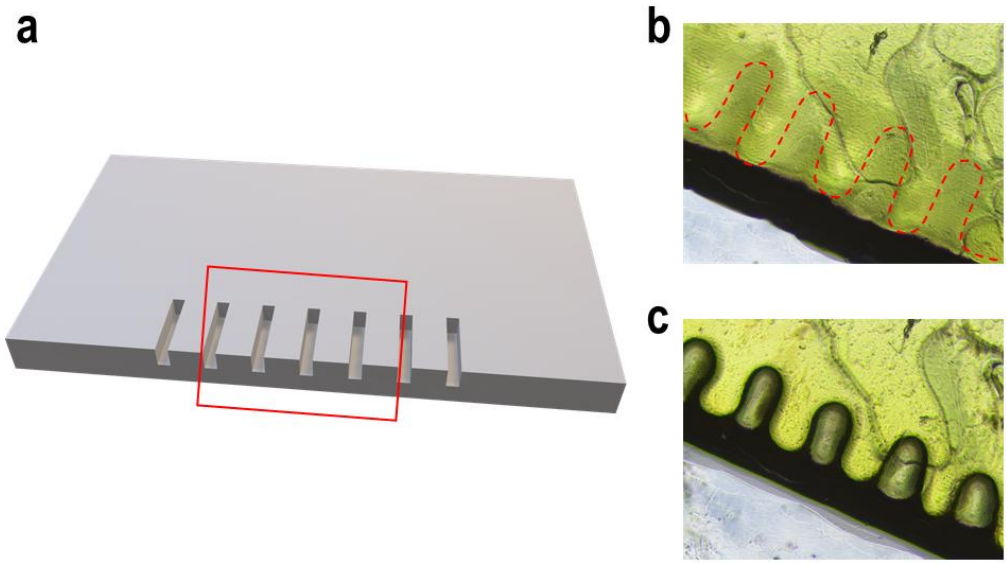

***Figure 6.13**. Printing results for crypts using B = 150 µm. A) Sketch of the 3D CAD model. The highlighted area corresponds to the regions shown in images B and C. B) Crypts immediately after printing with the crypts highlighted. C) Crypts after placing a glass coverslip on top, mimicking the chip assembly.*

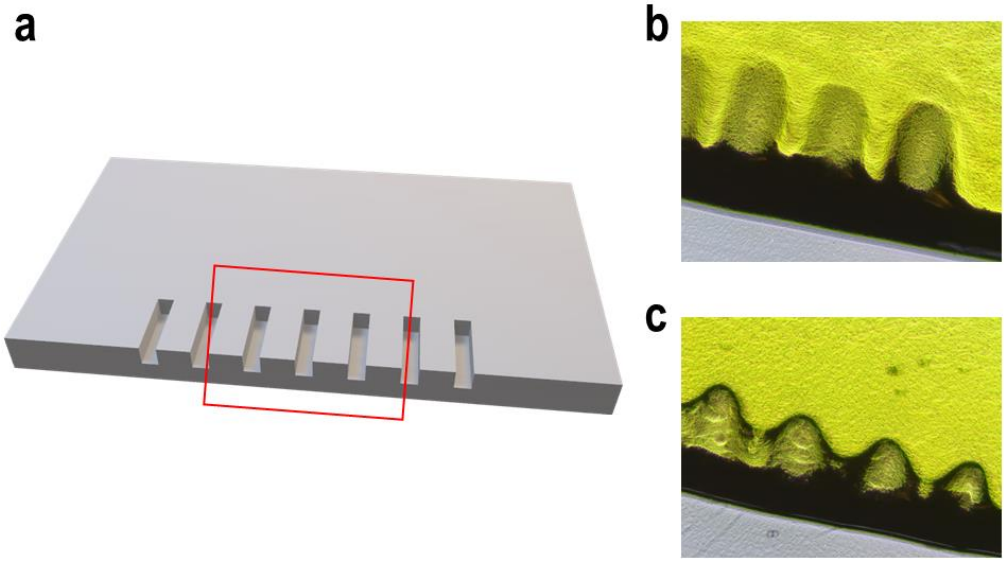

***Figure 6.14.** Printing results for crypts using B = 200 µm. A) Sketch of the 3D CAD model. The highlighted area corresponds to the regions shown in images B and C. B) Crypts immediately after printing. C) Crypts after placing a glass coverslip on top, mimicking the chip assembly.*

In all cases, the **printing parameters** were kept constant, being the same ones as those used for the evaluation of the swelling effect in the hydrogel outer shape: 5 seconds for the layer exposure time, 15 seconds for the exposure time of the initial layers and a layer thickness of 13 µm.

6.3.3 Hydrogel Characterization

Similar to what we performed previously with the outer dimensions of the printed hydrogel; it is very important to evaluate the change in dimensions of the crypts and the hydrogel over time once integrated on the microfluidic chip and covered by cell culture media, due to the swelling phenomenon. Thus, the crypts' dimensions could be adjusted. To determine the swelling in these conditions, hydrogels including both crypts' designs were assembled on chip after printing (see Table 6.3). First, they were washed in warmed PBS and dried to avoid any residue during the

assembly. In this case, casings containing the **two-channels** design were used. To ensure the proper fitting of the hydrogel between the two PDMS layers and that the whole structure, including the outer casing, exerts the correct pressure to leak the channels and the hydrogel cavity, the thickness of the PDMS layers was adjusted. After the assembly, the entire chips were placed in the incubator at 37ºC and continuously perfused with cell culture medium for 96 hours, setting the flow to 2.5 µL/min. This flow rate was previously optimized for other purposes and is in agreement with what can be found in the literature for intestinal models. According to *Bein et. al. 2018*, the flow rate can mimic the dynamic ranges of fluid and associated shear stresses that are observed in the human intestine [2], so it is of great importance to include it in our model, to better replicate the *in vivo* conditions. This fluidic control allows to have a high spatio-temporal regulation on the delivery of nutrients and drug compounds among other factors, to the intestinal epithelium [2]. Figure 6.15 shows, as example, an illustration of the two-channel design and the hydrogel sample 1 once assembled inside the microfluidic chip. The two-channel structure is visible and the hydrogel with the crypts can be clearly distinguished.

Table 6.3 summarizes the crypt parameters and the other rectangular dimensions for both samples tested. As can be observed, the selected parameters for the crypts definition were larger than those previously optimized to be able to correctly examine the growth of the crypts, avoiding their collapse and clogging during the swelling process.

Table 6.3. *Size of the samples printed in the hydrogel characterization.*

	Crypts Parameters			**Outer Geometry**	
	Parameter A (µm)	Parameter B (µm)	Parameter C (µm)	Length (mm)	Width (mm)
Sample 1	850	300	400	7	4
Sample 2	850	500	300	7	4

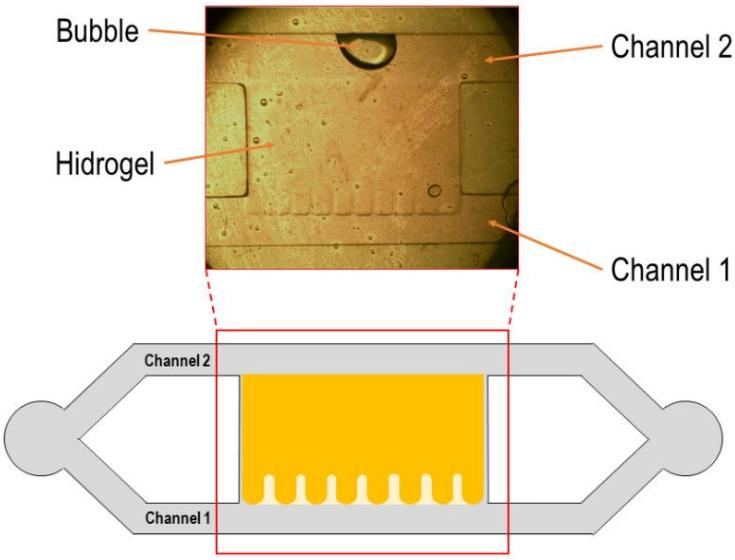

Figure 6.15*. Illustration of the two-channel chip design with the hydrogel after the assembly.*

Graphs in Figure 6.16 show a comparison of the measured hydrogel dimensions for both sample types, just after the assembly (time = 0h) and after 96h. The final dimensions obtained were 7612.3 µm +/- 6.6 µm in length and 4730.1 µm +/- 3.1 µm in width for *sample 1* and 7691.0 µm +/- 26.8 µm in length and 4649.0 µm +/- 5.9 µm in width for *sample 2*. As observed, hydrogels contour grew significantly in both directions, resulting in an increase of 5.3% and 13.6% for **sample 1**, and 4.5% and 10.0% for **sample 2**, in length and width respectively. According to the results obtained, we have the biggest change in the width of the hydrogel since it grows through the channel. On the other hand, the length has varied less since it has PDMS walls which impede growth in that direction. Detailed values for the measurements can be found in the *Annexes*.

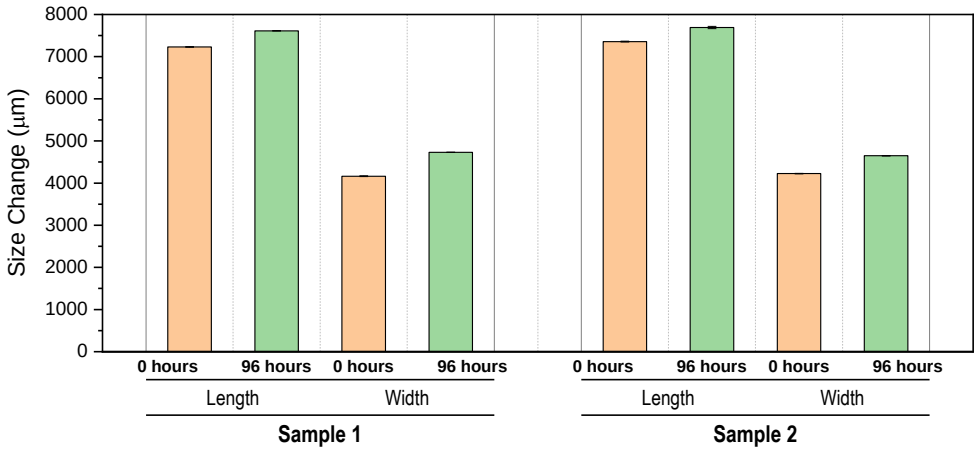

***Figure 6.16**. Change in length and thickness after 96 hours of swelling.*

In the same way, the changes in the dimensions of the **crypts** for both samples were analyzed. Figure 6.18 shows the values obtained for the different parameters analyzed: **A** (which was previously defined in Section 5.2.4), **a**, **b** and **c** (see each parameter in Figure 6.17). These changes were more evident in sample 2, where crypts initially shorter than the ones in sample 1 get closed, reducing dramatically the depth of the evaginations (parameter A).

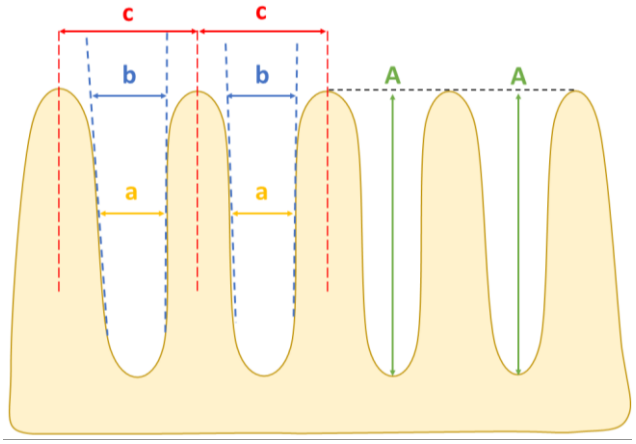

***Figure 6.17.** Schematic of the relevant parameters used to quantify the size of the crypts.*

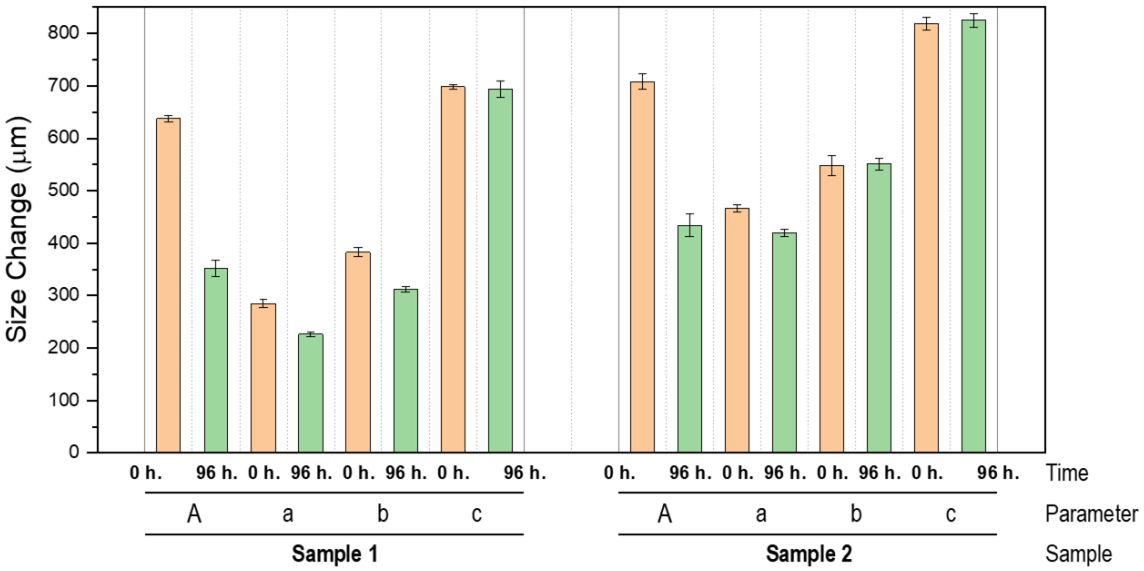

Figure 6.18. Change in crypts size for the two samples.

Most of the crypt parameters have been reduced due to swelling in both samples. Table 6.4 depicts the final dimensions and the corresponding error found in both samples for the four parameters specified in Figure 6.18.

Table 6.4. Dimension changes and errors of each parameter of the crypts after 96 hours.

		Parameter A	Parameter a	Parameter b	Parameter c
Sample 1	Final Dimensions (µm)	352.1	226.4	312.4	693.9
	Error (µm)	± 15.1	± 4.8	± 5.7	± 15.3
	Growth percentage	- 44.8%	- 20.5%	- 18.4%	- 0.6%
Sample 2	Final Dimensions (µm)	434.0	419.1	550.6	825.1
	Error (µm)	± 21.2	± 6.7	± 10.6	± 13.4
	Growth percentage	- 38.7%	- 10.1%	0.4%	0.8%

The *percentage of growth* regarding the initial values at t = 0h, have a negative value since the swelling of the hydrogel has a positive sign and, therefore, the dimensions of the hydrogel are larger causing the dimension of the crypts to be smaller.

Figure 6.19 shows pictures of both samples, sample 1 and sample 2, after 96h of swelling, once disassembled from the microfluidic chip. Here, the changes in dimensions are evident. As obtained from the measurements on-chip, crypts in sample 1 get closed and became shorter, being the parameter A the one that experienced the highest reduction. In sample 2 (*Figure 6.19-B*), however, crypts were more visible even the reduction since initially they were bigger.

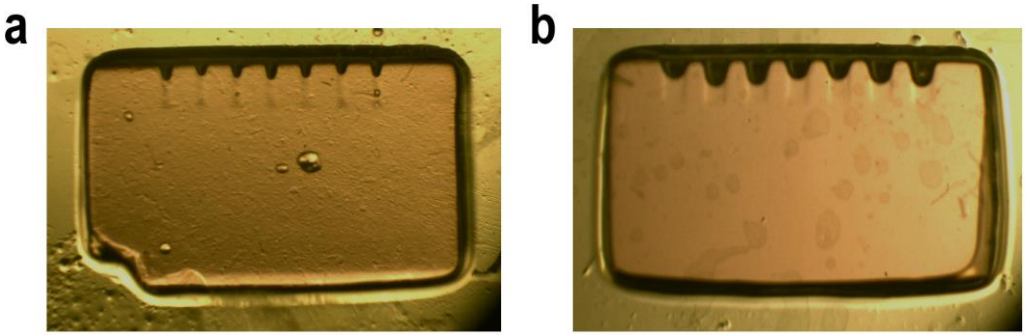

Figure 6.19. *Image of the hydrogel samples once removed from the microfluidic chip after 96 hours. A) Sample 1. B) Sample 2.*

Finally, we can conclude that the swelling of the hydrogel occurs more uniformly when it is inside the chip than when we perform the experiment outside the chip. Also, from the swelling-on-chip, we can deduce that, in percentage, the width of the hydrogel grows more than the length. This may happen because the width can grow more freely by having space with the channels while on both short sides, we have the PDMS walls which difficult the hydrogel to swell in those directions. For crypts, the most affected parameter is A, which is hugely reduced. This was expected since the reduction of parameters b and c, negatively affects this parameter. From Figure 6.19 it can be deduced that after the hydrogel swell, the geometry of the crypts become irregular and unequal in both samples. On one hand, the results obtained make us chose the sample 2 since it replicates better the intestinal crypts and keeps better the geometry of the crypts after swelling, although the parameters of the invaginations can be further optimized taking into account this data. On the other hand, sample 1 shows that the crypts have reduced their depth by 45%, which may indicate that these structures will not correctly replicate the shape and microstructure of the intestinal crypts.

6.4 Gut-on-a-chip model

Once all the components were optimized and integrated into the microfluidic system, there was only one step missing: include the cellular component to the model. Thus, a new set of hydrogels were printed including two of the most representative cell types of the intestine on them: CCD18-Co, which are human colon myofibroblasts, and THP-1 monocytes, as representative cell line of the immune system. The aim of this experiment was to see if the cells embedded in the 3D printed hydrogel could survive once integrated inside the microfluidic chip. For this purpose, four different sets of chips were assembled, two of them with single-channel (see Figure 6.20–A) and two of them with the two-channels design (Figure 6.20–B). The inlet ports of the chip were connected to an infusion pump syringe that introduced complete cell culture medium at a constant *flow rate*. Between the pump and the inlet, we added a **bubble trap**, to avoid air bubbles circulating through the channels and get trapped inside the chip, altering the flow (see Figure 6.21).

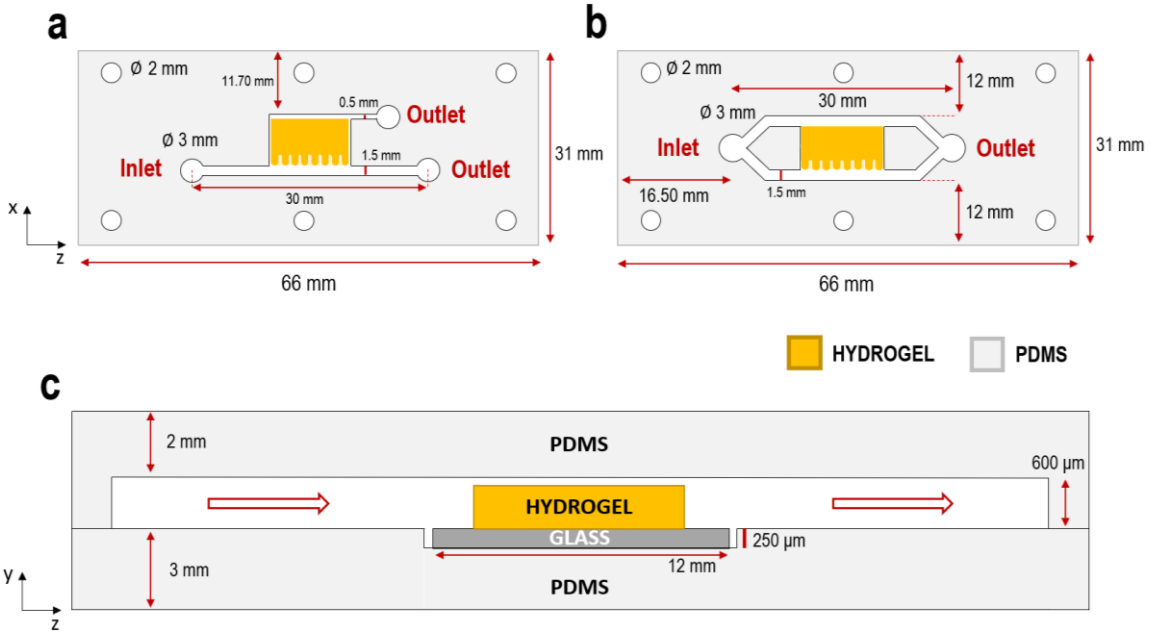

Figure 6.20. A) Illustration of PDMS for 1-Channel layout. B) Illustration of PDMS for 2-Channel layout. C) Side view of the chip in which we can see the channel formed between both PDMS layers and the hydrogel.

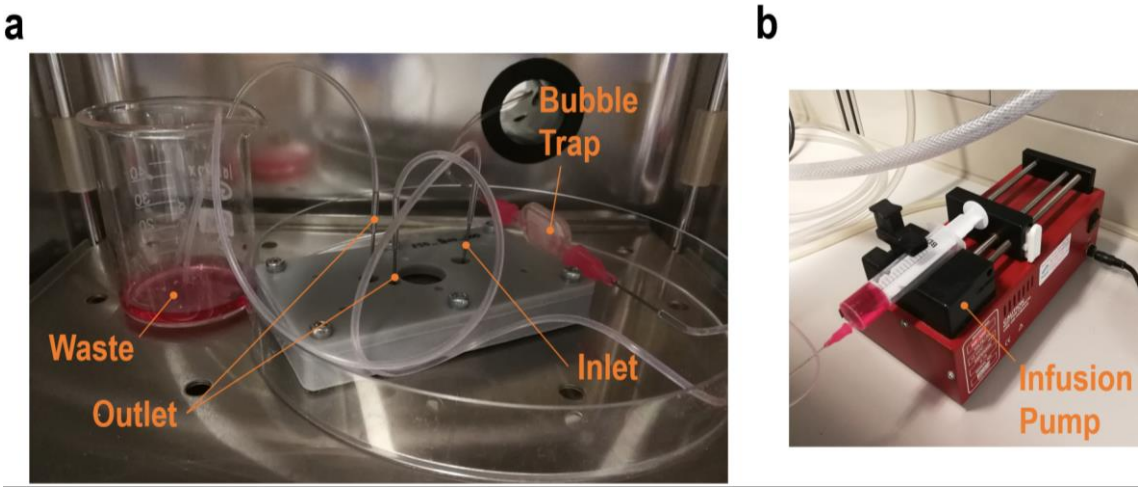

Figure 6.21. A) Chip placed inside the incubator. B) Infusion pump outside the incubator to inject direct current flow.

When the chips were assembled and before the application of the flow, some cell culture media was manually introduced by placing the tip of a needle at one side of the silicone rubber tube, which was directly connected to the bubble trap. The outlet of the bubble trap was directly connected to the inlet of the microfluidic chip. The culture media pumped out from the chip was evacuated from the system directly to a waste container (see Figure 6.21–A). Once the system was completely bled, the inlet of the bubble trap was connected to the infusion pump which started pumping media to the system. For this particular experiment, syringes with a volume of 15 mL were placed in each pump applying a **flow rate** of 2.5 µL/min.

To increase the number of experimental replicates and see if the presence of cells could alter the swelling behaviour of the printed hydrogels, shape measurements were again performed to check the variations on dimensions of the crypts at different time points once assembled inside the microfluidic chip. Table 6.5 summarizes the initial dimensions of the chips and crypts used according to the previous A, a, b and c parameters described (see Figure 6.17). Figure 6.22 shows

the values of the four parameters measured for the crypts (A, a, b and c) just after the assembly (**time = 0h**).

Table 6.5. Design Characteristics of microfluidic chips.

Sample	Number of Channels	Crypts Parameters			Outer Geometry	
		A (µm)	B (µm)	C (µm)	Length (mm)	Width (mm)
Sample 1	1 (*Figure 6.20-A*)	850	300	400	7	4
Sample 2	1 *(Figure 6.20-A)*	850	500	300	7	4
Sample 3	2 *(Figure 6.20-B)*	850	300	400	7	4
Sample 4	2 *(Figure 6.20-B)*	850	500	300	7	4

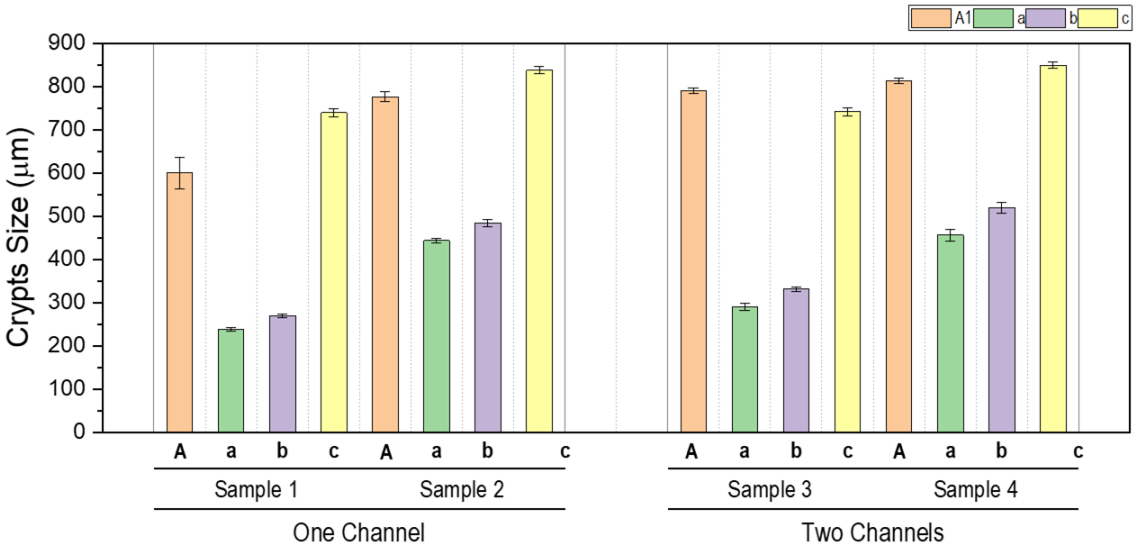

***Figure 6.22**. Dimensions of the four samples at initial time for the parameters A, a, b and c.*

The quantification of the parameters in Figure 6.22 was done with the hydrogel directly assembled on the chip. From these results, it is clear that the dimensions of the crypts at t = 0h differ with respect to the initial measurements made in previous experiments (see Figure 6.18). A possible explanation for this might be that the upper layer of PDMS does not come into contact with the hydrogel. This causes the crypts to not have the characteristic "U-shape" that we had in previous experiments where we made the measurements by placing a glass coverslip on top of the hydrogel. For this reason, the crypts parameters are slightly different compared with previous results. In addition, the variation in **parameters A**, **a** and **b** between samples 1 and 3 (which initially have the same crypts parameters) could be attributed to the absence of contact between the hydrogel and the PDMS which hindered the correct visualization of the crypt geometry.

To monitor the cell activity inside the hydrogel-on-chip, pictures were taken at different timepoints. In particular, cells in **Sample 2** were monitored 72 and 120 hours after bioprinting and chip assembly. **Sample 1** was discarded due to assembly issues, that caused partial dehydration of the hydrogel. Figure 6.23 shows the evolution of the crypts of sample 2 in the three different timepoints. The points that can be seen in Figure 6.23, B and C correspond to the cells previously embedded in the hydrogel.

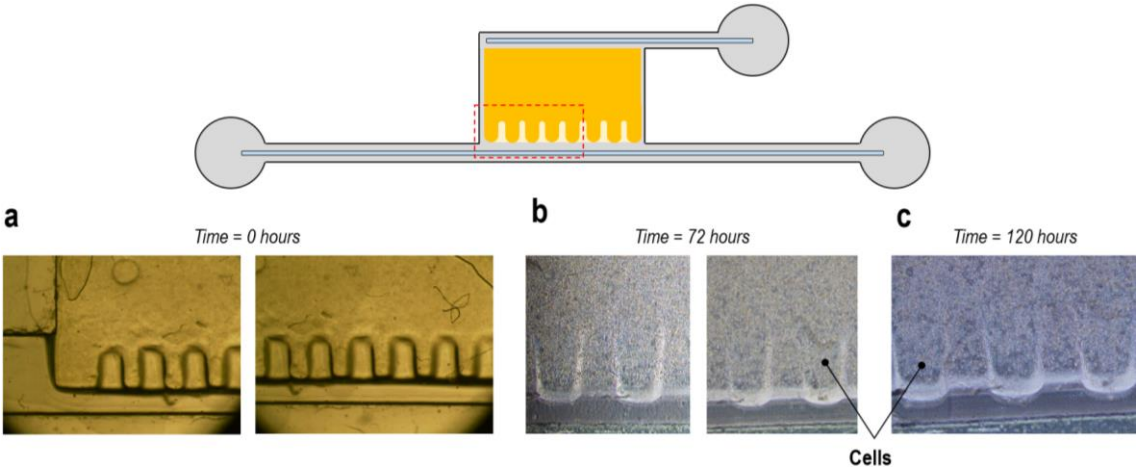

***Figure 6.23**. Design of one channel chip and the crypts at different timepoints (Sample 2). A) Crypts at the initial time, 0 hours after the bioprinting. B) Crypts after 72 hours at the incubator. Images taken with the microscopy; we can visualize embedded cells. C) Crypts after 120 hours at the incubator. Images taken with the microscopy; we can visualize embedded cells.*

For sample 2 most of the parameters have been reduced due to swelling. Table 6.6 depicts the dimensions at 72 hours and at 120 hours and the corresponding error for the four parameters. The *percentage of growth* has been calculated with the initial dimensions at t = 0h and the final dimensions (t = 120h).

***Table 6.6.** Dimension changes and errors of each parameter of the crypts after 72 and 120 hours for the sample 2.*

		Parameter A	**Parameter a**	**Parameter b**	**Parameter c**
72 hours	Dimensions (µm)	752.3	395.4	429.2	876.6
	Error (µm)	13.9	5.0	3.6	11.6
120 hours	Dimensions (µm)	693.4	375.6	433.4	874.4
	Error (µm)	10.6	9.8	6.2	5.7
Growth percentage		-10.7%	-15.4%	-10.5%	4.3%

These values are not comparable to those reviwed in Table 6.4 because all measurements have been made on-chip, unlike the date in Table 6.4 where a glass coverslip was placed on top of the hydrogel. For this reason, the growth percentages differ between the two tables. It remains unclear if the presence of cells could alter the swelling behaviour of the printed hydrogels.

Finally, several images of the chip were taken, specifically of **sample 2** to verify that there was no leakage between the two layers of PDMS and that the hydrogel could be seen correctly from the central circular window (see Figure 6.24).

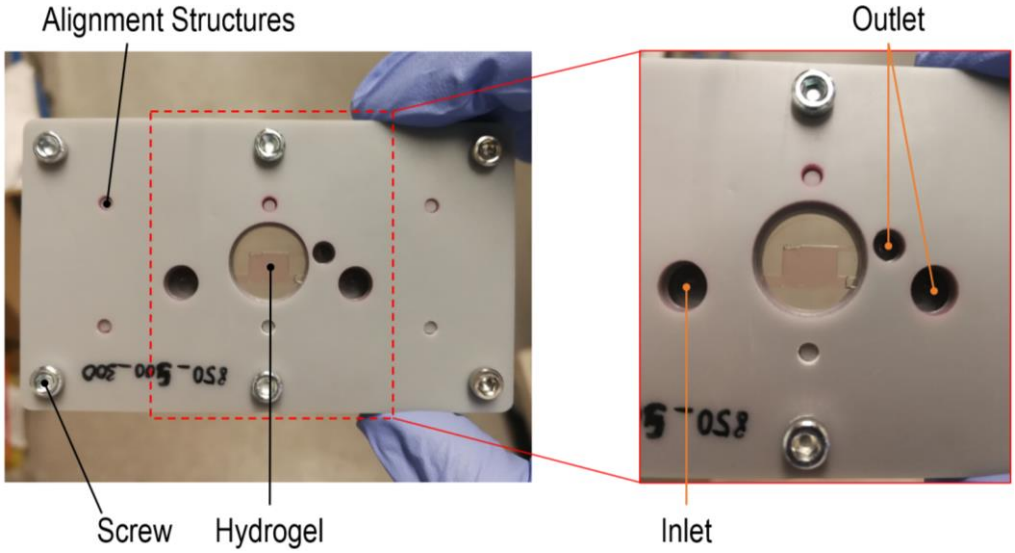

Figure 6.24. *Microfluidic chip with a hydrogel after 120 hours.*

On the other hand, samples 3 and 4 were monitored only up to 2 hours after the bioprinting and assembly since they were used for performing **cell viability analysis** (data not included in this project). Figure 6.25 shows, respectively, examples from samples 3 and 4.

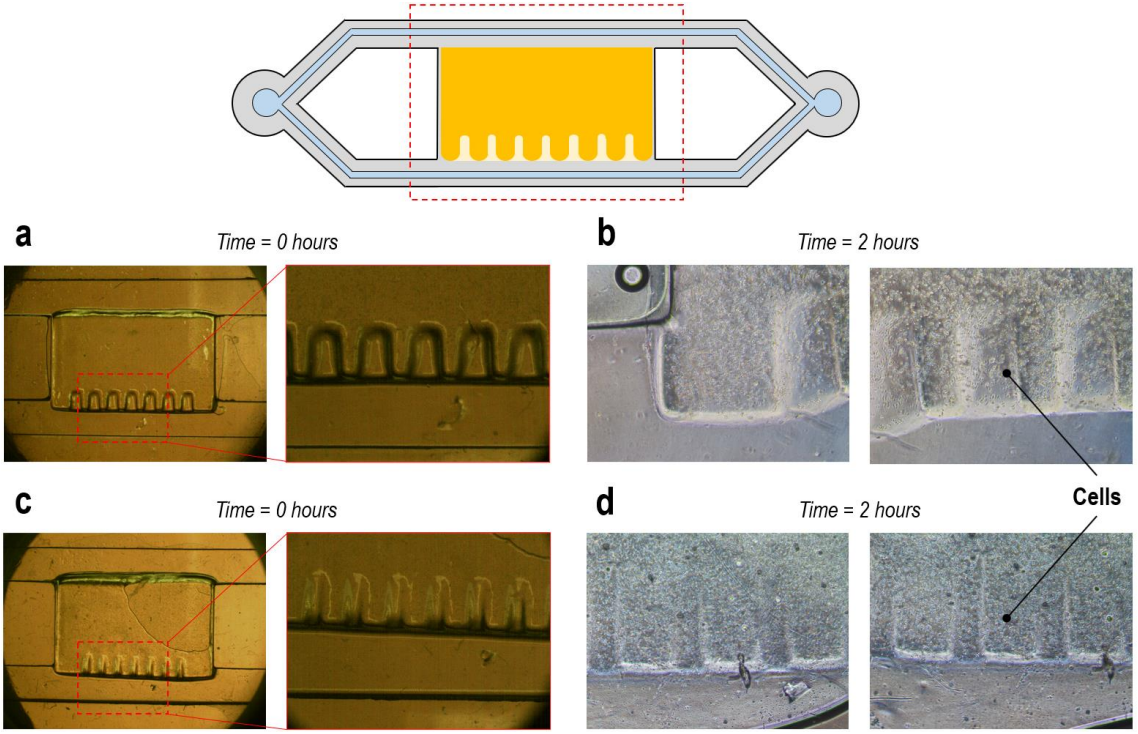

Figure 6.25. *Design of two-channel chip and the crypts at different timepoints for sample 3 (A and B) and sample 4 (C and D). A) Crypts at the initial time, 0 hours after the bioprinting (sample 3). B) Crypts after 2 hours at the incubator. Images taken with the microscopy; we can visualize embedded cells (sample 3). C) Crypts at the initial time, 0 hours after the bioprinting (sample 4). D) Crypts after 2 hours at the incubator. Images taken with the microscopy; we can visualize embedded cells (sample 4).*

To conclude, the results obtained in Figure 6.25 accords with our earlier observations in Figure 6.24, which showed high viability rates of the cells. One interesting finding was that the crypts are still visible in the different samples after swelling (see Figure 6.24 and Figure 6.25). The images acquired from sample 2 were taken at a more advanced time, which provides us information regarding the geometry of the crypts after a swelling of 72 and 120 hours. On the other hand, for

samples 3 and 4 the microstructure was more similar to the initial time as less time has passed. These results further support the idea that embedded cells tend to adapt their shape to the geometry of the crypts as time goes by (such as those cells in sample 2). This study has been unable to demonstrate differences regarding the swelling and cell viability between the two models designed (the one-channel and the two-channel chip).

One concern about the findings of swelling on-chip was that the height of the hydrogel and the PDMS should guarantee a close contact between the two surfaces. Initially, we thought that growth in *Z* of the hydrogel would be enough to get that contact, however, more careful analysis and study of the swelling in the *Z* direction should be done. In addition, one limitation of these methods is that in some cases the close contact between both PDMS surfaces and the pressure exerted by the casing is not enough to avoid leaks, making the chip unviable.

7. IMPLEMENTATION SCHEDULE

7.1 Work-breakdown Structure (WBS)

In this section, we are going to review our Work-breakdown structure or WBS (Figure 7.1). It organizes the work into different manageable sections. In the **Project Management Body of Knowledge**, a set of standard terminologies for project management the WBS is defined as a "hierarchical decomposition of the total scope of work to be carried out by the project team to accomplish the project objectives and create the required deliverables" [76].

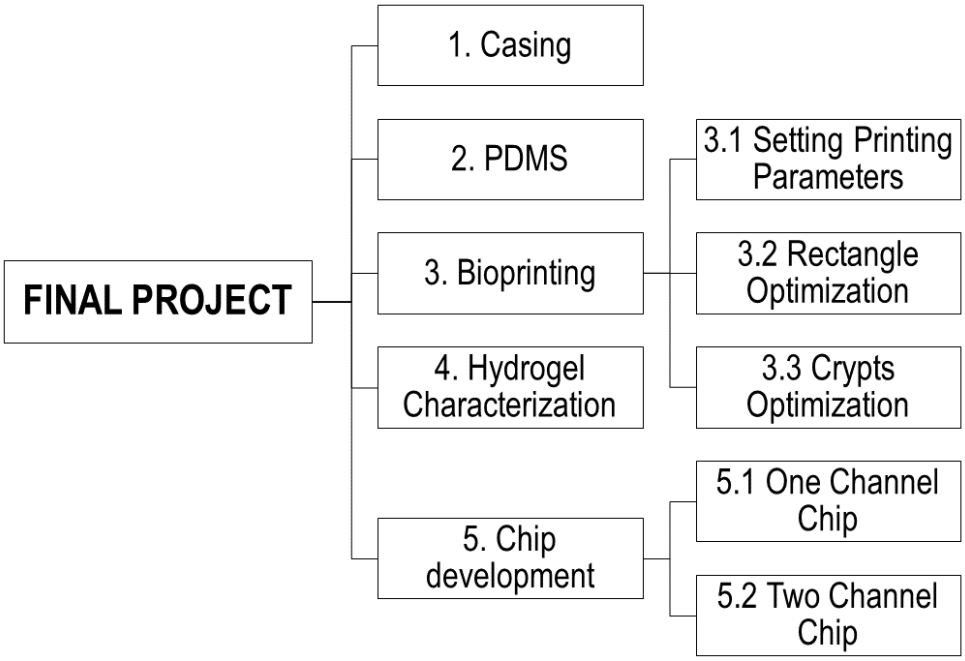

Figure 7.1. *Work-breakdown structure of our project.*

7.1.1 WBS Dictionary

Firstly, we are going to describe each of the activities created in the WBS (see Figure 7.1). In Table 7.1 a brief description of the task that should be developed in each of the activities of the project is presented. In the first column, we can find the number associated with the WBS activity described in section 7.1 and the associated name. The last column corresponds to a concise description of each task.

Table 7.1. *Dictionaries to each of the activities created in the WBS.*

Nº	NAME	DESCRIPTION
1	Casing	Chip casing design and optimization
2	PDMS	Printing the moulds to create the PDMS layers. Familiarization with the creation of PDMS and optimization of the temperature and time that should be in the oven
3	Bioprinting	Adaptation of the Solus 3D printer to print hydrogels and bioink preparation besides performing the subtasks. The total duration of this task corresponds to the sum of the duration of the subtasks

3.1	Setting Printing Parameters	Configuration of the different printing parameters, exposure times and layer thickness.
3.2	Rectangle Optimization	Optimization of the outer geometry of the hydrogel in order to determine the optimal height and width.
3.3	Crypts Optimization	Design and optimization of the geometry of the crypts. Definition of the parameters to be varied and the optimal range for each one. Evaluation of the changes experienced by crypts with respect to the 3D design.
4.	Hydrogel Characterization	Experiment to see the evolution of the crypts and their swelling after a certain time. Familiarization with infusion pumps and the placement of inlets and outlets.
5.	Chip development	Detection of failures or problems in the previous task and flow rate optimization. Measurement of all PDMS layers and printing of new casing with the right dimensions for the following tasks.
5.1	One Channel Chip	Assembly of two chips with a single channel with cells embedded in the hydrogel.
5.2	Two Channel Chip	Assembly of two chips with two channels with cells embedded in the hydrogel.

7.2 Task Sequence Matrix

First, we are going to determine the time associated with each activity (Table 7.2). The first column corresponds to the number of the activity associated with the WBS, the second column the activity sorted in alphabetical order and the next columns corresponds to: *Pessimistic*, *Normal*, *Optimistic* and *Final time*, respectively. Each row is associated with one activity, except tasks number 3 and 5 since the times of these tasks are the sum of the *subtasks*. To determine the final time, we are going to use the next formula:

$$Time_{final} = \frac{T_{optimistic} + T_{pessimistic} + 4 \cdot T_{normal}}{6}$$

Table 7.2. *Data used to calculate the final time of each activity defined in the WBS.*

Nº	ACT.	PREVIOUS TIME	NORMAL TIME	OPTIMISTIC TIME	FINAL TIME
1	A	27	22	18	22
2	B	21	19	18	19
3	-	54	45	37	45
3.1	C	6	3	2	3
3.2	D	20	17	15	17
3.3	E	28	25	20	25
4	F	18	14	12	14
5	-	28	22	18	22

5.1	G	12	9	7	9
5.2	H	16	13	11	13

The ordering of this matrix (Table 7.3) has been done according to the activities in alphabetical order. Each activity has its corresponding numbering, according to the EDT dictionaries, its preceding and consequent activities, and the duration, in days. In addition, the initial and the final dates are also represented in days. Using this matrix, we will obtain the PERT and GANTT diagrams.

Table 7.3. *Task Sequence Matrix, in the first column the number associated with the EDT, in the second column the letter associated with each activity, followed by the preceding, consequent activities and the duration. The last two correspond to the start and end date.*

Nº	NAME	ACT.	PREVIOUS	CONSEQUENT	DURATION	INITIAL	FINAL
1	Casing	A	...	B	22	0	22
2	PDMS	B	A	F	19	22	41
3	Bioprinting	-	-	-	45	0	45
3.1	Setting printing Parameters	C	…	D	3	0	3
3.2	Rectangle Optimization	D	C	E	17	3	20
3.3	Crypts Optimization	E	D	G	25	20	45
4	Hydrogel Characterization	F	B	G	14	41	55
5	Chip Development	-	-	-	22	55	77
5.1	One Channel	G	E,F	H	9	55	64
5.2	Two Channel	H	G	…	13	64	77

7.2.1 PERT Diagram

In this section, the Program (or project) Evaluation and Review Technique (**PERT**) is presented (Figure 7.2). The PERT helps us to estimate and judge how well it is going by calculating the length of time needed for each of the events involved in the project. Each node has an associated number and the *Early* and *Last* time. The lines in red represent the critical path which means that if this path is delayed the whole project will be delayed.

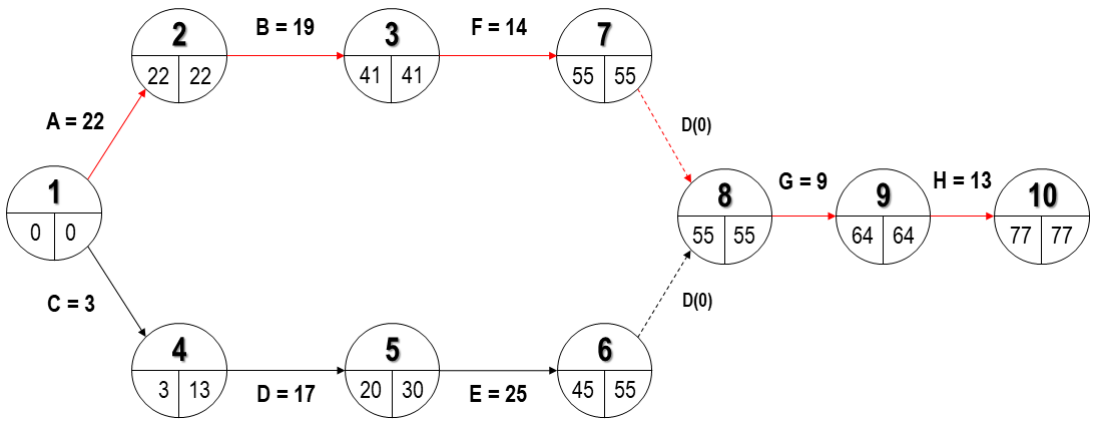

Figure 7.2. *PERT diagram associated with the sequence matrix, with the "Early" and "Last" times indicated in each node and the critical path marked in red.*

7.2.2 GANTT Diagram

The GANTT chart (Figure 7.3) shows the start and finish dates of the tasks and it will help us to monitor specific tasks. This diagram has been made considering the PERT diagram and the task sequence matrix. A total time of 77 *working days* has been obtained to perform the different tasks of the project. Figure 7.3 shows that *Bioprinting* has a duration equal to the sum of subtasks 3.1, 3.2 and 3.3, in the same way as the task of *Chip Development* with the subtasks 5.1 and 5.2.

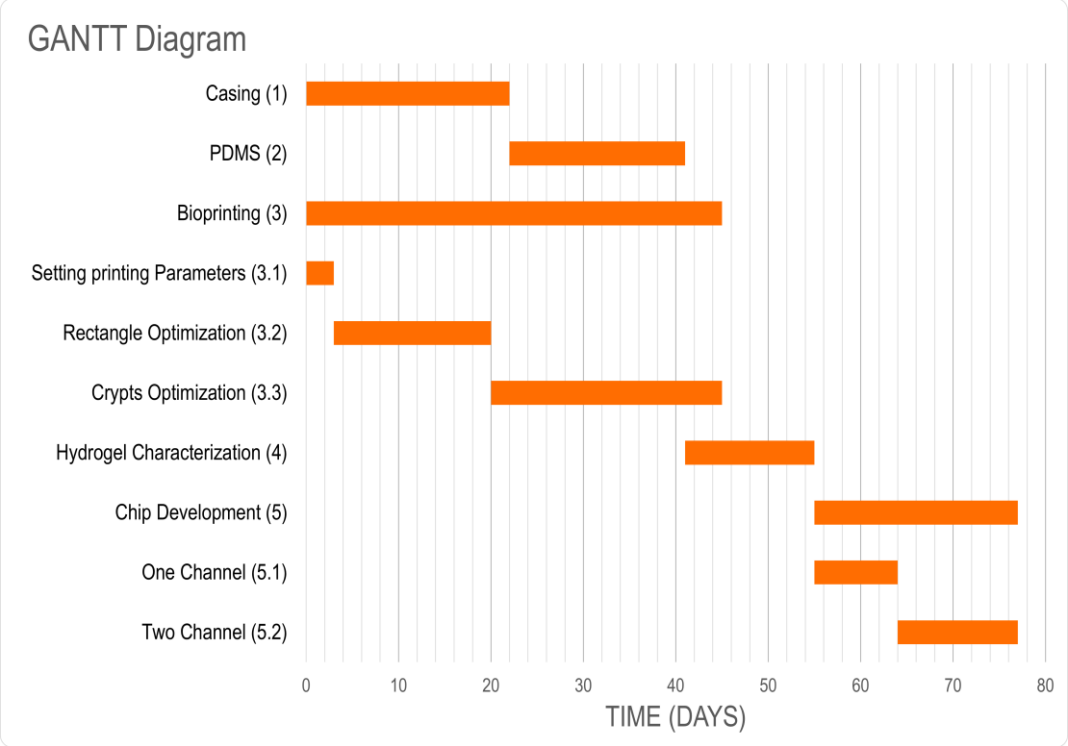

Figure 7.3. *GANTT diagram of our project.*

Considering that the calculated times (third column of Table 7.4) correspond to *working days*, we have calculated each activity's start and end date. In these calculations, it has been considered that the project will be carried out on working days and weekends are excluded. Table 7.4 shows the start and end date, and the total days that we will spend on each activity. The experimental part of the project will end on May 19, 2021.

Table 7.4. *Table considering the working days.*

Nº	ACT.	WORKING DAYS	TOTAL DAYS	START DATE	END DATE
1	A	22	30	01/02/2021	03/03/2021
2	B	19	27	03/03/2021	30/03/2021
3	-	45	63	01/02/2021	05/04/2021
3.1	C	3	3	01/02/2021	04/02/2021
3.2	D	17	25	04/02/2021	01/03/2021
3.3	E	25	35	01/03/2021	05/04/2021
4	F	14	20	30/03/2021	19/04/2021
5	-	22	30	19/04/2021	19/05/2021
5.1	G	9	11	19/04/2021	30/04/2021
5.2	H	13	19	30/04/2021	19/05/2021

8. TECHNICAL PREVIABILITY

The project has been developed at IBEC and therefore all the equipment and facilities have been obtained from there.

8.1 Technical Challenges

8.1.1 Bioprinting

The development of bioprinting is an emerging technology with many advantages but, also has many technical challenges that need to be overcome soon. On one hand, the correct selection of the *bioink* is essential. An ideal bioink should possess proper mechanical, chemical and biological characteristics. Nowadays, some biomaterials used such as collagen or fibrin gel are not developed for bioprinting which makes it a bioink with low physical and biological conditions. One alternative to avoid these limitations is the creation of *hydrogel-based* bioink, which has numerous advantages such as cell attachment, spreading, growth and differentiation [49].

IBEC developed a new hydrogel-based bioink before explained which provides the required features for cells to attach and grow, improving the biological and physical conditions of the current standard *in vitro* models for the small intestinal mucosa [3]. In particular, the designed hydrogel allows mimicking both the epithelial and the stromal compartments, providing a cell microenvironment that favours interactions between both cellular compartments [3]. To create this hydrogel, the synthesis and characterization of GelMA is needed. Then a photo-polymerization reaction using an ultraviolet (UV) of 365 nm of wavelength and co-networks should be performed between the GelMA and the PEGDA (*Figure 8.1*) [3].

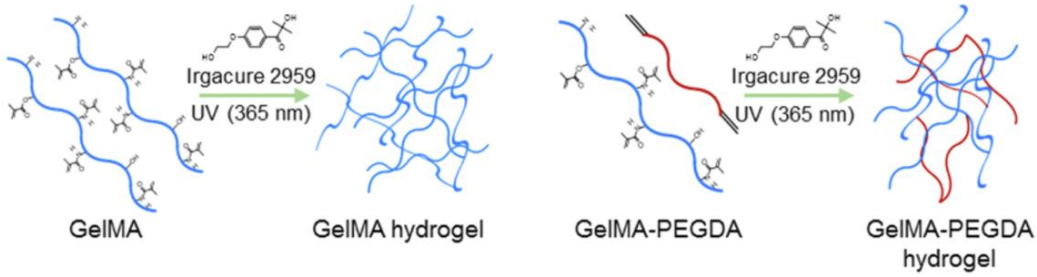

Figure 8.1. *Schematic adapted from Vila et. al. 2020, of the GelMA and GelMA-PEGDA photo-polymerization reaction and co-networks formed. [3]*

Even though the bioprinting technology presents a unique opportunity to produce biomimetic cellular structures the current capacity to produce 3D structures using multiple types of cells, biomaterials, and biomolecules is limited [77]. The lack of the capability to produce structures that completely mimic the tissue structure might cause that the phenotypes and responses of the human intestine do not reproduce as accurately. The incorporation of limited components and limited type of cells of the intestinal compartments, and their associated features, might play a significant role in some disorders [2]. If these technical challenges are overcome, bioprinting will likely be a way to produce OoC systems in the near future, helping to develop better disease models and achieve personalized medicine.

8.1.2 PDMS

The chosen material to create the microfluidic channel and which will contain the hydrogel had to be (i) transparent, to enable the continuous monitoring and analysis of the hydrogel, (ii)

biocompatible and (iii) should be fabricated with a simple method but allowing a high resolution to replicate small structures. PDMS provides a few advantageous features for our microfluidic chip in front of other materials such as glass. As we have reviewed in previous sections, PDMS can be easily fabricated through a moulding process, is a transparent, soft and a flexible material and is commonly used due to its low cost. A technical challenge that we have found during the chip development are the leaks. The system developed is based on two layers of PDMS without any treatment or adhesive. The system has a casing that is responsible for exerting pressure at the two layers to prevent leakage. This is done to be able to disassemble the chip and get back the printed hydrogel in addition to being able to reuse the PDMS. This could be complicated in case of treatment on its surface or using adhesives.

The main problem of not performing any process is that the layers of PDMS may have leakage that may depend on many factors, including if the pieces are clean, the speed at which the liquid is introduced in the chip, if both surfaces are completely flat or the pressure exerted to join both layers during assembly, among others.

8.2 SWOT Analysis

The SWOT analysis is a strategic planning technique that helps to identify the strengths, weaknesses, opportunities, and threats of a project. In this case, the SWOT Analysis is done in Table 8.1.

Table 8.1. *SWOT Analysis of the 3D bioprinting technique developed in this project.*

Strengths	**Weakness**
- 3D bioprinting of microstructures - High resolution - Could *replace* animal experiments - Wide range of bioprinters and methods of bioprinting - Biocompatible Bioink - Chip *easy* to assemble and disassemble	- Quality of the printed gut - Low maturity of the bioprinting technique - Slow maturation of the field - The bioprinting process is still long and slow - Difficult to completely replicate the desired structures - *Leakage* between the layers of PDMS
Opportunities	**Threats**
- Huge market potential - Search for alternatives to animal experiments - Starting to become more affordable - Increasing demand	- Early-stage technology - Validation systems are crucial to its adoption to a regulatory process - High initial cost

8.2.1 Internal Analysis

Some of the strengths of the project are the ability to print *microstructures* with 3D technology with a high resolution, with a solution (*bioink*) that is **biocompatible** for cells and with a printing method

that allows you to print the cells embedded in the hydrogel and print a specific design. In addition, the hydrogel is set on a device which is easy to assemble and disassemble and the introduction of fluid is simple through syringes. Finally, the method of manufacturing the chips is cheap and simple, using 3D printers to perform the casing and moulds and PDMS for the microfluidic channel.

On the other hand, there are also some weaknesses that should be overcome. Firstly, the printing process is still long and slow and some parameters such as humidity or temperature need to be studied to determine if they can affect the printing process and thus, its reproducibility. In addition, leaks are a weakness that should be solved to have a functional chip and that allows to study the evolution of the hydrogel and the embedded cells.

8.2.2 External Analysis

Some of the opportunities of the project are the demand from pharmaceutical industries and regulatory companies to adapt the OoC technology in drug development, safety screening and disease modelling [54], which is clearly increasing. According to the results obtained from the **ORCHID program** [54,61], the OoC's represent the fast-growing multidisciplinary field in the last decades in lab-on-chip, stem cell, microfluidics and biosensors development technology. Moreover, the efforts already obtained in standardization can lay the foundation for the standardization and qualification of OoC systems [54].

On the other hand, the OoC presents some threats such as, the systems are complex multi-parametric implementations that try to answer the complex networked responses of the biological tissue. Also, not in all the OoC technology or process are currently efforts to standardize [54]. Finally, the comparison of the data obtained with OoC with the current animal models might interrupt the fast adaptation of OoC's by stakeholders, and thus slow down standardization [54,57].

9. Economic Previability

In this section, the total economic costs of the project are reviewed. Since it is a previous project, the costs have been approximated using the information proportioned by IBEC. The total cost of the project includes the cost of developing a gut-on-a-chip, and also the salary of the workers. In Table 9.1 is reviewed the material and the workers needed to develop the whole project. To develop it we need people formed in distinct areas such as: biomedical or industrial engineering, biology and chemistry. To compound this cost estimation, it has been considered the length of the project (commented in Section 7) and the number of hours that would work each employee, since no all would take part in the same developmental stages of the project, and some would work jointly.

The necessary workers to develop the project are: two Biomedical Engineers one focused on the cellular part and the other focused on the bioprinting process. Also, a Chemist to develop the *GelMA-PEDGA* and a Biologist specialized in *cell culture* are needed. Since the duration of the creation of the hydrogel and the cell culture required are different, each specialist's time will be different. In addition, an industrial engineer is required to optimize all 3D printing processes, he would be in charge of the control and maintenance of the printers and give support in these aspects.

The equipment and software needed to develop the project is the Solus 3D printer, reviewed in previous Sections, the software of the company and the Phrozen Shuffle XL 3D printer. In addition, a computer to connect the printers and download the software is needed. The light source used to solidify the liquid polymer layer by layer in the Solus printer will be a Vivitek 1080P DLP Projector. Furthermore, other material costs for the chip development, the creation of the PDMS and the hydrogel will be required. Additionally, for the development of the project, various consumables have been used, which have been given a generic price.

Finally, two types of cells will be used, mouse embryonic fibroblasts and human leukemic monocytes. To obtain a monolayer of epithelial cells to recreate the Colorectal adenocarcinoma disease. In this case, the selected cell lines are frozen and have a Level 1 of *biosafety* [78].

Table 9.1. *Approximation of the total cost of the project.*

CONCEPT	UNITS	UNIT PRICE	TOTAL
WORKERS			
BIOMEDICAL ENGINEER	2	14 €/h (500h)	14000 €
BIOLOGIST	1	14 €/h (400h)	5600 €
CHEMIST	1	14 €/h (250h)	3500 €
INDUSTRIAL ENGINEER	1	14 €/h (400h)	5600 €
EQUIPMENT			
SOLUS 3D PRINTING EQUIPMENT	1	3173 €	3173 €
PHROZEN SHUFFLE XL 3D	1	1300 €	1300 €
COMPUTER	1	500 €	500 €
DLP PROJECTOR	1	1000 €	1000 €

MATERIALS			
PDMS ELASTOMERIC KIT	1	313 €	313 €
PEGDA	1	165 €	165 €
LAP	1	125 €	125 €
TARTRAZINE	1	35 €	35 €
TRICHLOROFLUORO-SILANE	1	92 €	92 €
OTHER REAGENTS	1	150 €	150 €
PHROZEN RESIN	2	80 €	160 €
SOLUS RESIN	2	200 €	400 €
SCREWS AND TOOLS	1	200 €	200€
CONSUMABLES			
SYRINGES MICROFLUIDIC CONNECTIONS AND TUBES PIPETTE TIPS PETRI DISHES GLASS COVERSLIPS	1	350 €	350 €
SOFTWARE			
SOLUS SOFTWARE	1	91 €	91 €
PHROZEN SOFTWARE	1	-	-
IMAGE J	1	-	-
FREECAD	1	-	-
AUTODESK FUSION 360	2	- (*)	- (*)
CELLS			
NIH-3T3 MOUSE EMBRYONIC FIBROBLASTS (CELL LINE)	1	451 €	451 €
THP-1 HUMAN LEUKEMIC MONOCYTES (CELL LINE)	1	595 €	595 €
TOTAL			37800 €

***Note**: (*) Student Licence.*

According to the GANTT and PERT Diagram, the chemist will be doing the first task, creating the *GelMA-PEGDA*, this task can be supported by one of the biomedical engineers. The second part, the cell culture of both populations will be done by the Biologist, also supported by one of the

engineers. During the process of cell culture, the design of the 3D structure, the optimization of the printer parameters and the design of the casing should be done by one of the biomedical engineers together with the industrial engineer. On the other hand, one of the biomedical engineers should optimize the process of creation of PDMS and the chip. Finally, the process of bioprinting, optimization and microfluidics should be done by both biomedical engineers.

10. Conclusions

In this project, we reviewed the recently developed microfluidic gut-on-chip model and described the advantages that the proposed model offers with respect to commonly used 2D *in vitro* culture systems, including its ability to emulate more closely the 3D microstructure and function of the living human intestine. In addition, we have reviewed and compared various bioprinting techniques to polymerize and obtain this characteristic 3D microstructure of the intestine using photo-crosslinkable materials such as hydrogels.

The purpose of this research was to determine the feasibility of a microfluidic chip to mimic the intestinal mucosa. The study carried out has been able to confirm that the printing method selected to perform the project, based on stereolithography combined with digital light projector (SLA-DLP) 3D printing, together with a proper bioink selection, are suitable to create 3D microstructures on hydrogels, resembling the human large intestinal crypts. Furthermore, it has been observed high compatibility of hydrogels and of the printing method, allowing for the printing of hydrogel-based structures with embedded cells, that can grow and populate the hydrogel keeping high viability rates (>90%).

Firstly, for the development of the microfluidic chip, the design and optimization of the casing was carried out. The casing has been designed to store the two PDMS layers which in turn contains the hydrogel. The analysis of the outer part leads to the following conclusions: (i) the optimized casing exerts pressure on the PDMS layers, (ii) for some chips, the pressure exerted by the casing has been adequate to avoid leakage. Considering this, the initial objectives regarding the outer part of the chip have been met, but there are remaining issues subject to leakage that should be overcome.

Next, the PDMS layers moulds containing the hydrogel and form the microfluidic channels were designed. The main conclusions that can be drawn are that an accurate temperature and time to solidify the PDMS were found and that the layers were capable of housing the hydrogel inside. The major limitation of the study was the appearance of leakage between both PDMS layers, this can have various origins and causes the chip to become non-viable. As we have argued elsewhere, the correct placement of the glass coverslip with the printed hydrogel in the bottom layer of PDMS can be a key aspect, as well as the dimensions of the gap where the glass is placed. On the other hand, the hydrogel had to be printed centred on the coverslip glass to match the motifs on the PDMS layer. Otherwise, it was possible for the PDMS to get on top of the hydrogel. The results of this research support the idea that it is necessary to use adhesives or activate the PDMS surfaces to be able to completely avoid leakage.

One of the more significant findings to emerge from this project are the printing parameters optimized to achieve proper 3D microfeatures and the outer hydrogel dimensions. The findings of this study suggest that both aspects are optimum. The research has also shown that the optimized crypts geometry resembles what can be found *in vivo*. Despite having optimized this geometry, the growth of the hydrogel was studied with larger geometry to correctly examine the growth of the crypts and avoid their collapse. The evidence from the swelling data suggests that the crypts geometry must be optimized considering the size changes that occur in the hydrogel due to the swelling. Considerably more work will need to be done to determine the optimal crypt geometry.

Recent research on our microfluidic chip has provided a more complete understanding of the gut-on-a-chip technology. Notwithstanding the limitations, the results indicate that the embedded cells can survive inside the chip for more than 120 hours and are able to adapt to the 3D microstructure of the hydrogel. The findings of this research provide insights on the fluidic conditions which guaranteed adequate micro-environmental conditions within the chip, allowing the exchange of cellular media. Consequently, the results of this project support the idea that there are no significant differences between the design formed by one channel and the design composed by two channels. More studies must be carried out for a longer time and increasing the sample size to be able to determine if there is a real difference between both designs and the cells are in better conditions in one of the two.

10.1 Future work

In future works, it should be considered that for this project only one side of the channel was studied. The formation of the channel was achieved by having the hydrogel on one side and the PDMS wall on the other side. In future research, it could be considered that the hydrogel constitutes both sides of the channel. By having hydrogel on both sides and a central channel, the printing parameters must be adjusted very well to keep the cavity of the channel and the crypts open and with certain dimensions. In addition, the optimization process must consider the dimensions just after the printing and when the hydrogel has swollen. Lastly, a greater focus on the dimensions of the channel size could produce interesting findings. Besides, further work is needed to fully understand their implication in our model.

With the aim of completely mimicking the 3D structure of the crypts, a further approximation can be made. The next step would be to close the crypts both above and below, to generate cavities within the hydrogel, surrounded by material all around as found in tissue *in vivo*.

One of the biggest challenges of the project was to ensure the sealing of the system while designing a device that could be easily assembled and disassembled and to recover the hydrogel without damage it to perform further studies, such as immunostaining of specific markers. In this way, PDMS layers surrounding the hydrogel could not be activated by plasma to enhance the bonding neither adhesive layers could be used, leading to some leakage between both layers. Further research should be carried out to establish the best methodology to prevent leakage which could include, a) the activation of both PDMS surfaces, b) use of adhesives to complete seal both layers, c) changing the microfluidic chip material to meet the new requirements.

Further research might explore including representative cells of the intestinal epithelium that grow on top of the hydrogel and cover it, colonizing the crypts, in this way the model could be completed, at the cellular level. Based on this, there are many studies that can be performed, such as the effect of different flow rates on cell growth, which could facilitate the optimization of the dimensions of the microfluidic channels.

References

1. Huh, D. (2015). A human breathing lung-on-a-chip. *Annals of the American Thoracic Society*, *12*(Supplement 1), S42–S44. https://doi.org/10.1513/AnnalsATS.201410-442MG

2. Bein, A., Shin, W., Jalili-Firoozinezhad, S., Park, M. H., Sontheimer-Phelps, A., Tovaglieri, A., Chalkiadaki, A., Kim, H. J., & Ingber, D. E. (2018). Microfluidic Organ-on-a-Chip Models of Human Intestine. In *CMGH* (Vol. 5, Issue 4, pp. 659–668). Elsevier Inc. https://doi.org/10.1016/j.jcmgh.2017.12.010

3. Vila, A., Torras, N., Castaño, A. G., García-Díaz, M., Comelles, J., Pérez-Berezo, T., Corregidor, C., Óscar, C., Engel, E., Fernández-Majada, V., & Martínez, E. (2020). Hydrogel co-networks of gelatine methacrylate and poly(ethylene glycol) diacrylate sustain 3D functional in vitro models of intestinal mucosa. *Biofabrication*, *12*(2), 025008. https://doi.org/10.1088/1758-5090/ab5f50

4. Luo, Y., Qin, J., & Lin, B. (2009). Methods for pumping fluids on biomedical lab-on-a-chip. *Frontiers in Bioscience*, *14*(10), 3913–3924. https://doi.org/10.2735/3500

5. Park, J. Y., Jang, J., & Kang, H. W. (2018). 3D Bioprinting and its application to organ-on-a-chip. *Microelectronic Engineering*, *200*, 1–11. https://doi.org/10.1016/j.mee.2018.08.004

6. Gu, Z., Fu, J., Lin, H., & He, Y. (2020). Development of 3D bioprinting: From printing methods to biomedical applications. In *Asian Journal of Pharmaceutical Sciences* (Vol. 15, Issue 5, pp. 529–557). Shenyang Pharmaceutical University. https://doi.org/10.1016/j.ajps.2019.11.003

7. Yu, F., & Choudhury, D. (2019). Microfluidic bioprinting for organ-on-a-chip models. In *Drug Discovery Today* (Vol. 24, Issue 6, pp. 1248–1257). Elsevier Ltd. https://doi.org/10.1016/j.drudis.2019.03.025

8. Ng, W. L., Lee, J. M., Zhou, M., Chen, Y. W., Lee, K. X. A., Yeong, W. Y., & Shen, Y. F. (2020). Vat polymerization-based bioprinting - process, materials, applications and regulatory challenges. In *Biofabrication* (Vol. 12, Issue 2, p. 022001). Institute of Physics Publishing. https://doi.org/10.1088/1758-5090/ab6034

9. Ma, J., Wang, Y., & Liu, J. (2018). Bioprinting of 3D tissues/organs combined with microfluidics. In *RSC Advances* (Vol. 8, Issue 39, pp. 21712–21727). Royal Society of Chemistry. https://doi.org/10.1039/c8ra03022g

10. Nieto, D., Marchal Corrales, J. A., Jorge De Mora, A., & Moroni, L. (2020). Fundamentals of light-cell-polymer interactions in photo-cross-linking based bioprinting. In *APL Bioengineering* (Vol. 4, Issue 4, p. 41502). American Institute of Physics Inc. https://doi.org/10.1063/5.0022693

11. Ge, Q., Li, Z., Wang, Z., Kowsari, K., Zhang, W., He, X., Zhou, J., & Fang, N. X. (2020). Projection micro stereolithography based 3D printing and its applications. In *International Journal of Extreme Manufacturing* (Vol. 2, Issue 2, p. 22004). IOP Publishing Ltd. https://doi.org/10.1088/2631-7990/ab8d9a

12. Zhang, J., Hu, Q., Wang, S., Tao, J., & Gou, M. (2020). Digital light processing based three-dimensional printing for medical applications. *International Journal of Bioprinting*, *6*(1), 12–27. https://doi.org/10.18063/ijb.v6i1.242

13. Wang, Y., Ma, M., Wang, J., Zhang, W., Lu, W., Gao, Y., Zhang, B., & Guo, Y. (2018). Development of a photo-crosslinking, biodegradable GelMA/PEGDA hydrogel for guided bone regeneration materials. *Materials*, *11*(8). https://doi.org/10.3390/ma11081345

14. Turner, J. R. (2009). Intestinal mucosal barrier function in health and disease. In *Nature*

Reviews Immunology (Vol. 9, Issue 11, pp. 799–809). Nature Publishing Group. https://doi.org/10.1038/nri2653

15. Giraut, A. V. (2020). Hydrogel co-networks of gelatin methacryloyl and poly(ethylene glycol)diacrylate sustain 3D functional in vitro models of intestinal mucosa. In *TDX (Tesis Doctorals en Xarxa)*. Universitat de Barcelona. http://www.tdx.cat/handle/10803/670921

16. Yu, J., Peng, S., Luo, D., & March, J. C. (2012). In vitro 3D human small intestinal villous model for drug permeability determination. In *Biotechnology and Bioengineering* (Vol. 109, Issue 9, pp. 2173–2178). John Wiley & Sons, Ltd. https://doi.org/10.1002/bit.24518

17. Castaño, A. G., García-Díaz, M., Torras, N., Altay, G., Comelles, J., & Martínez, E. (2019). Dynamic photopolymerization produces complex microstructures on hydrogels in a moldless approach to generate a 3D intestinal tissue model. *Biofabrication*, *11*(2), 025007. https://doi.org/10.1088/1758-5090/ab0478

18. Edmondson, R., Broglie, J. J., Adcock, A. F., & Yang, L. (2014). Three-dimensional cell culture systems and their applications in drug discovery and cell-based biosensors. In *Assay and Drug Development Technologies* (Vol. 12, Issue 4, pp. 207–218). Mary Ann Liebert Inc. https://doi.org/10.1089/adt.2014.573

19. Huh, D., Hamilton, G. A., & Ingber, D. E. (2011). From 3D cell culture to organs-on-chips. In *Trends in Cell Biology* (Vol. 21, Issue 12, pp. 745–754). NIH Public Access. https://doi.org/10.1016/j.tcb.2011.09.005

20. *Human intestine on-a-chip: state-of-the-art and into the future*. (n.d.). Retrieved March 28, 2021, from https://wyss.harvard.edu/news/human-intestine-on-a-chip-state-of-the-art-and-into-the-future/

21. Miri, A. K., Mirzaee, I., Hassan, S., Mesbah Oskui, S., Nieto, D., Khademhosseini, A., & Zhang, Y. S. (2019). Effective bioprinting resolution in tissue model fabrication. *Lab on a Chip*, *19*(11), 2019–2037. https://doi.org/10.1039/c8lc01037d

22. Jodat, Y. A., Kang, M. G., Kiaee, K., Kim, G. J., Martinez, A. F. H., Rosenkranz, A., Bae, H., & Shin, S. R. (2019). Human-Derived Organ-on-a-Chip for Personalized Drug Development. *Current Pharmaceutical Design*, *24*(45), 5471–5486. https://doi.org/10.2174/1381612825666190308150055

23. SUN, W., CHEN, Y. Q., LUO, G. A., ZHANG, M., ZHANG, H. Y., WANG, Y. R., & HU, P. (2016). Organs-on-chips and Its Applications. In *Chinese Journal of Analytical Chemistry* (Vol. 44, Issue 4, pp. 533–541). Chinese Academy of Sciences. https://doi.org/10.1016/S1872-2040(16)60920-9

24. Kasendra, M., & Wells, J. M. (2020). A Window into Your Gut: Biologically Inspired Engineering of Mini-gut Tubes In Vitro. *Developmental Cell*, *55*(5), 522–524. https://doi.org/10.1016/j.devcel.2020.11.015

25. Nikolaev, M., Mitrofanova, O., Broguiere, N., Geraldo, S., Dutta, D., Tabata, Y., Elci, B., Brandenberg, N., Kolotuev, I., Gjorevski, N., Clevers, H., & Lutolf, M. P. (2020). Homeostatic mini-intestines through scaffold-guided organoid morphogenesis. *Nature*, *585*(7826), 574–578. https://doi.org/10.1038/s41586-020-2724-8

26. Yi, H.-G., Kim, H., Kwon, J., Choi, Y.-J., Jang, J., & Cho, D.-W. (2021). Application of 3D bioprinting in the prevention and the therapy for human diseases. *Signal Transduction and Targeted Therapy*, *6*(1), 177. https://doi.org/10.1038/s41392-021-00566-8

27. Amin, R., Knowlton, S., Hart, A., Yenilmez, B., Ghaderinezhad, F., Katebifar, S., Messina, M., Khademhosseini, A., & Tasoglu, S. (2016). 3D-printed microfluidic devices. In *Biofabrication*

(Vol. 8, Issue 2, p. 22001). Institute of Physics Publishing. https://doi.org/10.1088/1758-5090/8/2/022001

28. Quan, Y., Sun, M., Tan, Z., Eijkel, J. C. T., Van Den Berg, A., Van Der Meer, A., & Xie, Y. (2020). Organ-on-a-chip: The next generation platform for risk assessment of radiobiology. In *RSC Advances* (Vol. 10, Issue 65, pp. 39521–39530). Royal Society of Chemistry. https://doi.org/10.1039/d0ra05173j

29. Grandfils, E., & Casquillas, G. V. (2020). Gut-on-chip: keeping up with the technology. *Elveflow*. https://www.elveflow.com/microfluidic-reviews/organs-on-chip-3d-cell-culture/gut-on-chip-microfluidics/

30. Horejs, C. (2021). Organ chips, organoids and the animal testing conundrum. In *Nature Reviews Materials* (Vol. 6, Issue 5, pp. 372–373). Nature Research. https://doi.org/10.1038/s41578-021-00313-z

31. Liu, Y., & Chen, Y.-G. (2018). 2D- and 3D-Based Intestinal Stem Cell Cultures for Personalized Medicine. *Cells*, *7*(12), 225. https://doi.org/10.3390/cells7120225

32. Gijzen, L., Marescotti, D., Raineri, E., Nicolas, A., Lanz, H. L., Guerrera, D., van Vught, R., Joore, J., Vulto, P., Peitsch, M. C., Hoeng, J., Lo Sasso, G., & Kurek, D. (2020). An Intestine-on-a-Chip Model of Plug-and-Play Modularity to Study Inflammatory Processes. *SLAS Technology*, *25*(6), 585–597. https://doi.org/10.1177/2472630320924999

33. Shim, K. Y., Lee, D., Han, J., Nguyen, N. T., Park, S., & Sung, J. H. (2017). Microfluidic gut-on-a-chip with three-dimensional villi structure. *Biomedical Microdevices*, *19*(2), 1–10. https://doi.org/10.1007/s10544-017-0179-y

34. Fois, C. A. M., Le, T. Y. L., Schindeler, A., Naficy, S., McClure, D. D., Read, M. N., Valtchev, P., Khademhosseini, A., & Dehghani, F. (2019). Models of the Gut for Analyzing the Impact of Food and Drugs. *Advanced Healthcare Materials*, *8*(21), 1900968. https://doi.org/10.1002/adhm.201900968

35. Ashammakhi, N., Nasiri, R., Barros, N. R. de, Tebon, P., Thakor, J., Goudie, M., Shamloo, A., Martin, M. G., & Khademhosseni, A. (2020). Gut-on-a-chip: Current progress and future opportunities. In *Biomaterials* (Vol. 255, p. 120196). Elsevier Ltd. https://doi.org/10.1016/j.biomaterials.2020.120196

36. Kim, H. J., Huh, D., Hamilton, G., & Ingber, D. E. (2012). Human gut-on-a-chip inhabited by microbial flora that experiences intestinal peristalsis-like motions and flow. *Lab on a Chip*, *12*(12), 2165–2174. https://doi.org/10.1039/c2lc40074j

37. Vancamelbeke, M., & Vermeire, S. (2017). The intestinal barrier: a fundamental role in health and disease. In *Expert Review of Gastroenterology and Hepatology* (Vol. 11, Issue 9, pp. 821–834). Taylor and Francis Ltd. https://doi.org/10.1080/17474124.2017.1343143

38. De Medina, F. S., Romero-Calvo, I., Mascaraque, C., & Martínez-Augustin, O. (2014). Intestinal inflammation and mucosal barrier function. In *Inflammatory Bowel Diseases* (Vol. 20, Issue 12, pp. 2394–2404). Lippincott Williams and Wilkins. https://doi.org/10.1097/MIB.0000000000000204

39. Sung, J. H., Yu, J., Luo, D., Shuler, M. L., & March, J. C. (2011). Microscale 3-D hydrogel scaffold for biomimetic gastrointestinal (GI) tract model. *Lab on a Chip*, *11*(3), 389–392. https://doi.org/10.1039/c0lc00273a

40. Steinway, S. N., Saleh, J., Koo, B. K., Delacour, D., & Kim, D. H. (2020). Human Microphysiological Models of Intestinal Tissue and Gut Microbiome. In *Frontiers in Bioengineering and Biotechnology* (Vol. 8, p. 725). Frontiers Media S.A.

https://doi.org/10.3389/fbioe.2020.00725

41. Joshi, P. N. (2016). Cells and Organs on Chip—A Revolutionary Platform for Biomedicine. In *Lab-on-a-Chip Fabrication and Application*. InTech. https://doi.org/10.5772/64102

42. Bosman, F. T., De Bruine, A., Flohil, C., Van Der Wurff, A., Ten Kate, J., & Dinjens, W. W. M. (1993). Epithelia-stromal interactions in colon cancer. In *International Journal of Developmental Biology* (Vol. 37, Issue 1, pp. 203–211). UPV/EHU Press. https://doi.org/10.1387/ijdb.8507562

43. Costa, J., & Ahluwalia, A. (2019). Advances and Current Challenges in Intestinal in vitro Model Engineering: A Digest. In *Frontiers in Bioengineering and Biotechnology* (Vol. 7, Issue JUN, p. 144). Frontiers Media S.A. https://doi.org/10.3389/fbioe.2019.00144

44. Torras, N., García-Díaz, M., Fernández-Majada, V., & Martínez, E. (2018). Mimicking epithelial tissues in three-dimensional cell culture models. In *Frontiers in Bioengineering and Biotechnology* (Vol. 6, Issue DEC, p. 197). Frontiers Media S.A. https://doi.org/10.3389/fbioe.2018.00197

45. Ding, C., Chen, X., Kang, Q., & Yan, X. (2020). Biomedical Application of Functional Materials in Organ-on-a-Chip. In *Frontiers in Bioengineering and Biotechnology* (Vol. 8, p. 823). Frontiers Media S.A. https://doi.org/10.3389/fbioe.2020.00823

46. Choi, J. R., Yong, K. W., Choi, J. Y., & Cowie, A. C. (2019). Recent advances in photo-crosslinkable hydrogels for biomedical applications. In *BioTechniques* (Vol. 66, Issue 1, pp. 40–53). Future Science. https://doi.org/10.2144/btn-2018-0083

47. Mancha Sánchez, E., Gómez-Blanco, J. C., López Nieto, E., Casado, J. G., Macías-García, A., Díaz Díez, M. A., Carrasco-Amador, J. P., Torrejón Martín, D., Sánchez-Margallo, F. M., & Pagador, J. B. (2020). Hydrogels for Bioprinting: A Systematic Review of Hydrogels Synthesis, Bioprinting Parameters, and Bioprinted Structures Behavior. *Frontiers in Bioengineering and Biotechnology*, *8*, 776. https://doi.org/10.3389/fbioe.2020.00776

48. Ramiah, P., du Toit, L. C., Choonara, Y. E., Kondiah, P. P. D., & Pillay, V. (2020). Hydrogel-Based Bioinks for 3D Bioprinting in Tissue Regeneration. In *Frontiers in Materials* (Vol. 7, p. 76). Frontiers Media S.A. https://doi.org/10.3389/fmats.2020.00076

49. Gungor-Ozkerim, P. S., Inci, I., Zhang, Y. S., Khademhosseini, A., & Dokmeci, M. R. (2018). Bioinks for 3D bioprinting: An overview. In *Biomaterials Science* (Vol. 6, Issue 5, pp. 915–946). Royal Society of Chemistry. https://doi.org/10.1039/c7bm00765e

50. Mastrangeli, M., Millet, S., Mummery, C., Loskill, P., Braeken, D., Eberle, W., Cipriano, M., Fernandez, L., Graef, M., Gidrol, X., Picollet-D'Hahan, N., Van Meer, B., Ochoa, I., Schutte, M., & Van den Eijnden-van Raaij, J. (2019). Building blocks for a European Organ-on-Chip roadmap. *ALTEX*, *36*(3), 481–492. https://doi.org/10.14573/altex.1905221

51. Zhang, B., & Radisic, M. (2017). Organ-on-A-chip devices advance to market. In *Lab on a Chip* (Vol. 17, Issue 14, pp. 2395–2420). Royal Society of Chemistry. https://doi.org/10.1039/c6lc01554a

52. Wilkinson, M. (2019). The Potential of Organ on Chip Technology for Replacing Animal Testing. In *Animal Experimentation: Working Towards a Paradigm Change* (pp. 639–653). BRILL. https://doi.org/10.1163/9789004391192_027

53. Huh, D., Matthews, B. D., Mammoto, A., Montoya-Zavala, M., Yuan Hsin, H., & Ingber, D. E. (2010). Reconstituting organ-level lung functions on a chip. *Science*, *328*(5986), 1662–1668. https://doi.org/10.1126/science.1188302

54. Mastrangeli, M., Millet, S., & Van Den Eijnden-Van Raaij, J. (2019). *Organ-on-Chip In Development: Towards a roadmap for Organs-on-Chip*. https://doi.org/10.20944/preprints201903.0031.v1

55. Ashammakhi, N. A., & Elzagheid, A. (2018). Organ-on-a-chip: New tool for personalized medicine. In *Journal of Craniofacial Surgery* (Vol. 29, Issue 4, pp. 823–824). Lippincott Williams and Wilkins. https://doi.org/10.1097/SCS.0000000000004604

56. Low, L. A., Mummery, C., Berridge, B. R., Austin, C. P., & Tagle, D. A. (2020). Organs-on-chips: into the next decade. In *Nature Reviews Drug Discovery* (Vol. 20, Issue 5, pp. 345–361). Nature Research. https://doi.org/10.1038/s41573-020-0079-3

57. European Union's Horizon 2020 research and innovation programme. (2019, October 1). *ORCHID | organ-on-chip in development*. https://h2020-orchid.eu/

58. *Organs-On-Chips for Radiation Countermeasures | FDA*. (2019, December 16). https://www.fda.gov/emergency-preparedness-and-response/mcm-regulatory-science/organs-chips-radiation-countermeasures

59. *Organ-on-a-chip Technologies (OOAC)*. (2018, May). https://md.catapult.org.uk/resources/organ-on-a-chip-technologies-ooac-current-status-and-translatability-of-data/

60. Blasimme, A., & Rial-Sebbag, E. (2013). Regulation of Cell-Based Therapies in Europe: Current Challenges and Emerging Issues. *Stem Cells and Development*, *22*(S1), 14–19. https://doi.org/10.1089/scd.2013.0352

61. *Organ on Chip in Development*. (2017, October 1). https://cordis.europa.eu/project/id/766884

62. Franzen, N., van Harten, W. H., Retèl, V. P., Loskill, P., van den Eijnden-van Raaij, J., & IJzerman, M. (2019). Impact of organ-on-a-chip technology on pharmaceutical R&D costs. In *Drug Discovery Today* (Vol. 24, Issue 9, pp. 1720–1724). Elsevier Ltd. https://doi.org/10.1016/j.drudis.2019.06.003

63. Fetah, K., Tebon, P., Goudie, M. J., Eichenbaum, J., Ren, L., Barros, N., Nasiri, R., Ahadian, S., Ashammakhi, N., Dokmeci, M. R., & Khademhosseini, A. (2019). The emergence of 3D bioprinting in organ-on-chip systems. *Progress in Biomedical Engineering*, *1*(1), 012001. https://doi.org/10.1088/2516-1091/ab23df

64. He, Y., Gu, Z., Xie, M., Fu, J., & Lin, H. (2020). Why choose 3D bioprinting? Part II: methods and bioprinters. In *Bio-Design and Manufacturing* (Vol. 3, Issue 1, pp. 1–4). Springer. https://doi.org/10.1007/s42242-020-00064-w

65. Sadi Loai, Benjamin R. Kingston, Zongjie Wang, David N. Philpott, Mingyang Tao, H.-L. M. C. (2019). Clinical Perspectives on 3D Bioprinting Paradigms for Regenerative Medicine. *Regenerative Medicine Frontiers*. https://doi.org/10.20900/rmf20190004

66. Kinstlinger, I. S., Calderon, G. A., Royse, M. K., Means, A. K., Grigoryan, B., & Miller, J. S. (2021). Perfusion and endothelialization of engineered tissues with patterned vascular networks. *Nature Protocols*, 1–25. https://doi.org/10.1038/s41596-021-00533-1

67. Murphy, S. V., & Atala, A. (2014). 3D bioprinting of tissues and organs. In *Nature Biotechnology* (Vol. 32, Issue 8, pp. 773–785). Nature Publishing Group. https://doi.org/10.1038/nbt.2958

68. Ji, S., & Guvendiren, M. (2017). Recent Advances in Bioink Design for 3D Bioprinting of Tissues and Organs. In *Frontiers in Bioengineering and Biotechnology* (Vol. 5, Issue APR). Frontiers Media S.A. https://doi.org/10.3389/fbioe.2017.00023

69. Christian Cavallo. (n.d.). *All About Digital Light Processing 3D Printing*. Retrieved May 22, 2021,

from https://www.thomasnet.com/articles/custom-manufacturing-fabricating/digital-light-processing-dlp-3d-printing/

70. Loessner, D., Meinert, C., Kaemmerer, E., Martine, L. C., Yue, K., Levett, P. A., Klein, T. J., Melchels, F. P. W., Khademhosseini, A., & Hutmacher, D. W. (2016). Functionalization, preparation and use of cell-laden gelatin methacryloyl-based hydrogels as modular tissue culture platforms. *Nature Protocols*, *11*(4), 727–746. https://doi.org/10.1038/nprot.2016.037

71. Piruska, A., Nikcevic, I., Lee, S. H., Ahn, C., Heineman, W. R., Limbach, P. A., & Seliskar, C. J. (2005). The autofluorescence of plastic materials and chips measured under laser irradiation. *Lab on a Chip*, *5*(12), 1348–1354. https://doi.org/10.1039/b508288a

72. Hua, F., Sun, Y., Gaur, A., Meitl, M. A., Bilhaut, L., Rotkina, L., Wang, J., Geil, P., Shim, M., Rogers, J. A., & Shim, A. (2004). Polymer imprint lithography with molecular-scale resolution. *Nano Letters*, *4*(12), 2467–2471. https://doi.org/10.1021/nl048355u

73. Wang, Y., Cao, X., Ma, M., Lu, W., Zhang, B., & Guo, Y. (2020). A GelMA-PEGDA-nHA composite hydrogel for bone tissue engineering. *Materials*, *13*(17). https://doi.org/10.3390/MA13173735

74. Kai, Y. (2021). Intestinal villus structure contributes to even shedding of epithelial cells. *Biophysical Journal*, *120*(4), 699–710. https://doi.org/10.1016/j.bpj.2021.01.003

75. Kastl, A. J., Terry, N. A., Wu, G. D., & Albenberg, L. G. (2020). The Structure and Function of the Human Small Intestinal Microbiota: Current Understanding and Future Directions. In *CMGH* (Vol. 9, Issue 1, pp. 33–45). Elsevier Inc. https://doi.org/10.1016/j.jcmgh.2019.07.006

76. Brotherton, S. A., Fried, R. T., & Norman, E. S. (2008). Applying the work breakdown structure to the project management lifecycle. *PMI (Project Management Institute) - Global Congress 2008*. https://www.pmi.org/learning/library/applying-work-breakdown-structure-project-lifecycle-6979

77. Ashammakhi, N., Ahadian, S., Xu, C., Montazerian, H., Ko, H., Nasiri, R., Barros, N., & Khademhosseini, A. (2019). Bioinks and bioprinting technologies to make heterogeneous and biomimetic tissue constructs. In *Materials Today Bio* (Vol. 1, p. 100008). Elsevier B.V. https://doi.org/10.1016/j.mtbio.2019.100008

78. *Caco-2 [Caco2] ATCC ® HTB-37™ Homo sapiens Colon Colorectal*. (n.d.). ATCC. Retrieved April 3, 2021, from https://www.lgcstandards-atcc.org/products/all/htb-37.aspx?geo_country=es#

11. ANNEXES

Following, complementary information of the project is presented.

11.1 Optimization of the Rectangle

These are the data obtained in the experiment to optimize the size of our hydrogel (*Section 6.3.1*). Each table corresponds to the three printed samples and we have the time at which the measurement was made, the thickness, width and length and the error associated with each measurement.

Table 11.1. *Data of the optimization of the rectangle for the sample 1.*

Sample 1

Time (min)	Thickness (µm)	Error of thickness	Width (µm)	Error of width	Length (µm)	Error of length
0	522.00	5.77	3442.86	51.64	6716.00	35.34
16	552.86	4.19	3848.14	24.92	6784.14	103.21
30	568.71	15.07	3672.57	46.16	6951.29	40.14
65	522.43	4.54	3691.57	66.57	7302.71	23.44
93	585.14	4.75	3502.00	34.31	7273.29	56.95
124	611.86	7.62	3713.71	57.24	6919.00	26.07
150	570.14	9.26	3853.86	60.90	6890.71	22.14
378	596.43	3.00	3774.71	38.55	6934.00	27.64

Table 11.2. *Data of the optimization of the rectangle for the sample 2.*

Sample 2

Time (min)	Thickness (µm)	Error of thickness	Width (µm)	Error of width	Length (µm)	Error of length
0	508.14	3.20	3689.57	42.56	6794.29	30.57
16	536.57	6.50	3667.29	50.81	6760.71	25.69
30	610.86	5.89	3612.43	45.12	6786.00	27.54
45	567.86	5.23	3676.57	38.53	6643.00	26.89
58	557.71	12.80	3721.71	51.47	6877.86	33.35
94	634.86	12.31	3521.71	46.86	6883.71	19.70
119	674.29	13.77	3608.86	54.14	6685.43	60.33
150	637.14	7.30	3578.14	55.82	6582.71	65.02
377	586.57	9.16	3742.14	37.63	6919.00	22.80

Table 11.3. Data of the optimization of the rectangle for the sample 3.

Sample 3

Time (min)	Thickness (µm)	Error of thickness	Width (µm)	Error of width	Length (µm)	Error of length
0	474.86	5.53	3925.86	50.31	6902.57	38.14
16	597.14	9.37	3634.00	34.72	6755.86	19.83
32	601.57	3.72	3685.00	22.84	7022.29	34.86
58	598.29	3.01	3535.57	27.25	6761.57	47.69
88	618.00	3.08	3545.43	17.54	6647.00	31.86
116	562.00	8.24	3898.86	23.96	6999.57	36.75
379	572.57	11.49	3488.57	40.16	6582.00	45.13

11.2 Hydrogel Characterization

Data obtained in the experiment to perform the Hydrogel Characterization (*Section 6.3.3*). We can find the length and width of the hydrogel and the parameters A, a, b and c, before and after the **swelling** and the associated error. The first table corresponds to the ***Sample 1*** and the second to the ***Sample 2***.

Table 11.4. Data of the hydrogel characterization for the sample 1.

	Time 0 (0 hours)		Time 1 (96 hours)	
Parameter	*Measurement (µm)*	*Error*	*Measurement (µm)*	*Error*
Length	7230.04	7.22	7612.29	6.60
Width	4163.74	10.46	4730.14	3.12
A	637.72	6.56	352.14	15.06
a	284.76	7.52	226.43	4.78
b	383.02	8.72	312.43	5.71
c	698.13	3.71	693.86	15.31

Table 11.5. Data of the hydrogel characterization for the sample 2.

	Time 0 (0 hours)		Time 1 (96 hours)	
Parameter	*Measurement (µm)*	*Error*	*Measurement (µm)*	*Error*
Length	7357.39	8.42	7691.00	26.76
Width	4225.30	6.98	4649.00	5.89
A	708.46	15.56	434.00	21.22
a	466.07	6.77	419.14	6.72

b	548.17	18.85	550.57	10.62
c	818.77	11.78	825.14	13.38

11.3 Assembly of the microfluidic chip

Data obtained in the experiment to perform the assembly of the microfluidic chip (*Section 6.4*). We can find the parameters A, a, b and c, at the initial time for four samples and the associated error for each measurement. There are two types of chips of one and two channels.

Table 11.6. *Data of the microfluidic chip assembly for all the samples at initial time (0 hours).*

	Sample	A	Error	a	Error	b	Error	c	Error
One Channel	Sample 1	600.28	36.68	238.64	3.74	269.34	4.08	740.03	10.08
	Sample 2	776.69	11.76	443.96	4.98	484.20	7.57	838.25	8.67
Two Channel	Sample 3	790.96	6.58	290.88	8.94	331.17	5.29	742.72	9.27
	Sample 4	814	6.57	456.46	12.92	519.80	12.35	849.95	7.23